Department of Physics
Indian Institute of Technology Guwahati
Ph.D. Thesis

Self-organized criticality on complex networks: Sandpile model, Scaling and Universality

Himangsu Bhaumik

Supervisor: Prof. S. B. Santra
October, 2017.

Self-organized criticality on complex networks: Sandpile model, Scaling and Universality

A thesis submitted by

Himangsu Bhaumik

to

Indian Institute of Technology Guwahati
in partial fulfillment of the requirements
for the award of the degree of
Doctor of Philosophy in Physics

Department of Physics
Indian Institute of Technology Guwahati
Guwahati - 781039, Assam, India

Statement

The work contained in the thesis entitled "*Self-organized criticality on complex networks: Sandpile model, Scaling and Universality*" has been carried out by me under the supervision of Prof. S. B. Santra, Professor, Department of Physics, Indian Institute of Technology Guwahati. This work has not been submitted elsewhere for the award of any degree.

(Himangsu Bhaumik)
Department of Physics
Indian Institute of Technology Guwahati
Guwahati - 781039

August 28, 2018

Certificate

It is certified that the work contained in the thesis entitled "*Self-organized criticality on complex networks: Sandpile model, Scaling and Universality*" by Mr. Himangsu Bhaumik, a Ph.D. student of the Department of Physics, Indian Institute of Technology Guwahati for the award of Doctor of Philosophy has been carried out under my supervision. This work has not been submitted elsewhere for the award of any degree.

(Prof. S. B. Santra)
Department of Physics
Indian Institute of Technology Guwahati
Guwahati - 781039

August 28, 2018

To my parents...

Acknowledgments

I am grateful to my supervisor Prof. Sitangshu Bikas Santra for his patient guidance, valuable suggestions, constant encouragement and support throughout my research work. I am thankful to him for his assistance to make this thesis possible. His unique insight into various research problems, coupled with the sense of sharp wit was a source of great inspiration during this peroid. I hope to employ the lessons learnt under his tutelage in a constructive fashion in my future academic career. Working with him for this long period will be a wonderful memory for the rest of my life.

I would like to thank my doctoral committee members, Prof. S. Basu, Prof P. K. Padmanabhan and Prof S. Dutta for valuable suggestions and critical comments during the period of my work and especially during the annual review. I am thankful to all other faculty members of Physics department for being helpful in all regards.

I wish to thank Department of Physics, Indian Institute of Technology Guwahati (IITG), to provide me with necessary computational facilities. I thank all the technical staff of the department, specially to Mr. Basab B Purkayastha, for the assistance in several ways during this period. My special thanks goes to my senior Dr. J. A. Ahmed who helped me a lot during the initial stage. I am also grateful to Dr. S. Sinha for discussing many things on various issues, academic as well as other. I would like to thank other seniors of the computational lab, Dr. Sen, Partha, Bishu, Ramesh, Arnab, Tapas, Sudin, KC, Bappa, and all of my colleagues and juniors for their co-operation. Special thanks to Sourav and Ashis for spending beautiful time together in many regards.

I am grateful to IITG for the financial support.

I am deeply indebted to my parents for their unconditional love, immense support

and constant encouragement towards my thesis work. They always support my personal choices. Loving thanks to my syster and other family members. A special thanks to my beloved wife, *Nandita*, for her constant love, caring, and mental support in all conditions. She was always close to me inspite of the geographycal distance.

Himangsu

Abstract

Sandpile is a generic model to study self-organized criticality (SOC) which provides a general mechanism for the emergence of complex behavior in many physio-chemical processes. On the other hand, the topology of many interacting systems can be modeled by complex networks which are usually compact, highly disordered, and maximally heterogeneous structures. The situation gets more intriguing when a complex dynamical process like SOC occurs on the top of a complex network. In order to investigate such situations, various sandpile models have been developed on several complex networks. Starting from the regular lattice small world network (SWN) has been developed adding shortcuts with a certain density. Dissipative versions of both the deterministic and the stochastic sandpile models have been studied on SWN. The steady-state critical properties of these newly developed sandpile models are characterized studying distribution functions of various avalanche properties. Three regimes of SWNs are identified: regular lattice regime (low shortcuts density), small world regime (intermediate shortcuts density), and random network regime (high shortcuts density). In the regular lattice regime, the sandpile dynamics is characterized by the respective scaling behaviour that usually occur on the regular lattice such as, Bak, Tang, and Wiesenfeld (BTW)-type correlated scaling for the deterministic model and the stochastic Manna scaling for the stochastic model. Whereas, in the random network regime the dynamics is characterized by mean-field scaling irrespective of the models. Interestingly, on small world regime, both the scaling behavior are found to coexist. In SWN regime, it is possible to identify certain characteristic size, area or time of avalanches below which the avalanche properties follow usual scaling on regular lattice and above which they obey mean-field scaling. Novel scaling forms of such characteristic properties of avalanches are developed analyzing several geometrical quantities of the toppling surface associated with an avalanche. Though the deterministic sandpile model does not obey finite-size scaling (FSS) on the regular lattice, it is found to obey FSS on the random network with MF exponents. On the other hand, the stochastic model is found to obey FSS

on the regular lattice as well as on the random network with the respective exponents. FFS on random network appears to be an outcome of superdiffusive sand transport and uncorrelated toppling waves. In the SWN regime, however, none of the models obeys FSS because of coexistence of multiple scaling forms. A new coexistence scaling theory for more than one scaling forms on an SWN is developed and numerically verified for both the models. An ensemble of avalanche clusters consists of two types of avalanches, dissipative and nondissipative. If at least one sand grain is dissipated from the system during the evolution of an avalanche it is called a dissipative avalanche otherwise it is a nondissipative avalanche. Classifying the whole ensemble of avalanches into the ensemble of dissipative and nondissipative avalanches, the critical properties of the individual ensembles are determined on the regular lattice, random network, as well as on SWN for both the models. Nontrivial scaling properties, very different from those reported in the literature in the case of boundary dissipation, are obtained for the dissipative and nondissipative avalanches. Such novel critical behaviour is found to useful in determining an appropriate FSS form of the distribution of a property x which needs accurate knowledge of the distribution exponents τ_x and capacity dimension D_x. It seems that distribution exponent τ_x is determined by the scaling of nondissipative avalanches whereas, the capacity dimension D_x is determined by the higher moments of the dissipative avalanches. Though in the thermodynamic limit the appearance of a dissipative avalanche would be a rare event, they mostly contribute to the catastrophic cascading effects and its critical behaviour is expected to play a crucial role in those effects. Coexistence scaling theory is further confirmed for nondissipative and dissipative avalanches in the SWN regime with appropriate exponents. In order to control SOC on the complex network, a two-state sandpile model with preferential sand distribution to nodes of specific degrees is developed on a scale-free network with power-law degree distribution: $P_k \sim k^{-\alpha}$. Upon toppling of a critical node two sand grains are distributed in a preferential manner to the two neighbouring nodes. Keeping the one node fixed to the neighbouring node of lowest possible degree and varying the other adjacent node to the node of highest possible degree, the SOC in this model is studied for a wide range of degree exponent α and different values of ϵ. Though the model follows mean-field theory in the random network regime, $\alpha > 4$, a nontrivial scaling behaviour very different from the mean-field scaling is observed in the scale-free regime, $2 < \alpha < 4$, of the network in contrary to the fact that the stochastic sandpile model exhibits mean-field scaling even in the scale-free regime. Distribution of sands to extreme degrees is found to be an efficient and cost effec-

tive way of controlling self-organization as catastrophic cascades in terms of large avalanches which are found to be confined to certain restricted regions of the network in the scale-free regime. The results obtained in the thesis can be extended to understand various real-world problems that occur in society, infrastructure, finance, and many other fields.

Contents

Chapter 1

Introduction

Complexity is ubiquitous in nature. Emergent phenomena that appear in the form of co-operative behaviour in systems with many interacting degrees of freedom are attributed to complexity. Complexity in that sense appears in systems from widely different disciplines such as biology, social behaviour, finance, infrastructural facilities and many others beside topics of condensed matter and statistical physics. Understanding of such emergent phenomena in systems of multidisciplinary nature is of immense importance. The co-operative behaviour of many interacting entities very often leads to critical phenomena[1–3] in which global or long-range features emerge from local interactions among the constituent entities of the system. Such long-ranged phenomena in many slowly driven physio-chemical systems occurred spontaneously (without fine tuning of any parameter of the system) are known to be "Self-Organized Criticality" (SOC)[4–8]. Complexity in SOC refers to the non-existence of any single characteristic event size, time or length scale which promotes to write a mathematical power-law scaling, the fingerprint of criticality of equilibrium phase transition[1–3], of various measurable physical quantities. The essential condition of a system to have the characteristic of SOC is the separation in time scales between the external driving force and the internal relaxation process. Such difference in time scales ensures the existence of a threshold against the external driving force as well as marginally meta-stable states of the system.

On the other hand, majority of real-world networks such as the Internet, the World Wide Web, social network, cellular network, electrical power grid etc., are complex in nature as their degree distributions are highly skewed and cannot be described by classical random graphs[9,10]. Not only the varied degree distribution but also the networks exhibit strong inhomogeneity and high clustering. The networks are found to be compact, small degree of separation between nodes, and infinite

dimensional small-world[11]. The extreme compactness and complex organization of networks result in nontraditional critical behaviour. Critical phenomena in disordered systems have come out to be one of the most studied fundamental topics of statistical physics from the beginning of 21st century. Complex network imposes a new type of disorder, very different from what is known in condensed matter physics, in terms of strong inhomogeneity in the degree space. A completely new emergent phenomena are found to appear in the form of co-operative behaviour of a large number of interacting nodes with such complex architecture. Though the structural properties of complex network are studied thoroughly, the understanding of emergent complex co-operative behaviour still remains as an open challenge[12–15].

The situation becomes more appealing when a complex dynamical process like SOC is defined on a complex network. The complex properties of networks are found to have a profound impact on the behaviour of equilibrium and nonequilibrium phenomena occurring in various systems. A few such systems to mention are: traffic and congestion on networks[16,17], cellular processes and networks[18], gene regulation and Boolean network[19,20], epidemic spreading in heterogeneous networks[21] and many others. Physicists, mathematicians, epidemiologists, computer and social scientists share a common interest in studying these systems and rely on very similar models for the description of diffusion of a physical entity over a heterogeneous structure. Out of all these processes, the threshold activated systems on complex networks[22–24] took the centre stage in the last decade as the occurrence of avalanches beyond a critical threshold on network is found to be very common in nature. A few examples are: avalanche mode of activity in the neural network of brain[25,26], earthquake dynamics on the network of faults in the crust of the earth[27], rapid rearrangement of coronal magnetic field network[28], propagation of information through a network with a malfunctioning router causing the breakdown of the Internet network[29], etc. Some of the fundamental questions that arise spontaneously are does the dynamical steady state describe self-organized criticality when such processes are defined on networks with extreme heterogeneity? As controlling SOC is difficult because of its complex feedback mechanism, can it be controlled by tuning the heterogeneity or the degree distribution of the underlying network? How the introduction of different length and time scales into the problem through various networks with specific topological properties those are very different from regular Euclidean lattices would impact the critical behaviour of self-organizing systems remains an open question. Because of such wide applications, intriguing complex emergent co-operative behaviour and several open questions, study of the self-organizing criticality on com-

plex network has been made the central theme of the present thesis. In the following, first SOC on regular lattice and its characteristic properties will be described, then introduction to several complex networks will be made and some of their properties will be summarized, finally, the problem will be specified categorically.

1.1 Self-organized criticality and sandpile models

SOC refers to the intrinsic tendency of a wide class of slowly driven systems to evolve spontaneously to a nonequilibrium critical steady state characterized by long-range spatiotemporal correlation[6]. Owing to the such correlation, a small perturbation due to the driving force can result of events of all possible sizes and duration, and consequently the distributions of event size and duration show power-law scaling behavior. The concept of SOC becomes famous and acceptable while it attempts to explain how spatiotemporal correlation emerges in diverse field of science like power-law distribution of intensity of earthquake[30], size and frequency distribution of rainfall[31–33], formation of river network[34,35], energy release in solar flares[28,36–38], etc. The idea of SOC also applied to explain the biological evolution[39,40], neuronal avalanches[26,41,42], the activity of brain[25] or electric breakdown[43]. The features of SOC was observed in the field of physics of materials; for instant, the motion of vortices through superconducting materials[44] or the motion of domain wall in ferromagnets[45–50]. SOC has also been demonstrated with tabletop experiments in laboratory like sandpile experiment by Held *et al.*[51], rice-pile experiment by Oslo group[52], droplet formation experiment by Plourde *et al.*[53] or granular piles experiment with different aspect ratio of grains by Denisov *et al.*[54], etc.

In the seminal paper by Bak, Tang, and Wiesenfeld (BTW)[4] the idea of SOC was introduced and a cellular automaton model, called the sandpile model was proposed which later become a prototypical model to study the SOC. There exists a large number of variants of the sandpile model in the literature such as stochastic sandpile models[55,56], directed sandpile model[57], continuous height model[58], etc. However, the deterministic BTW sandpile model and the stochastic sandpile model are mostly studied. Brief descriptions of the models on two dimensional (2d) square lattice are given below.

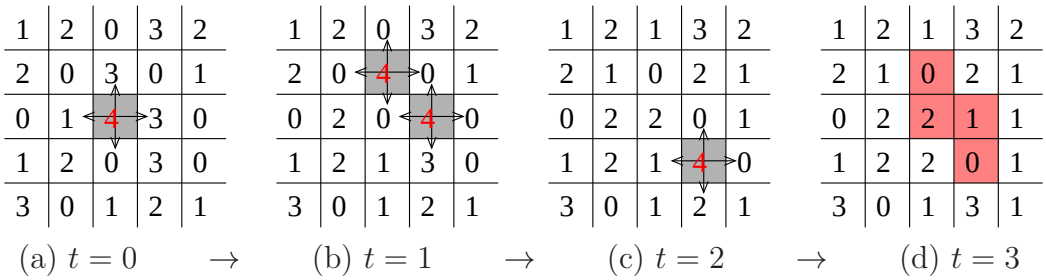

Figure 1.1: An avalanche has been demonstrated following BTW toppling rule on a 5×5 square lattice. The number represents the number of sand at each lattice site. (a) At time $t = 0$ the system is driven by adding one sand at central site, and consequently, the site becomes active (represented by gray colour) and toppling activity starts giving one sand to each nearest neighbour (as shown by arrows). The next parallel updates $t = 1$ and $t = 2$ are given in (b), (c) respectively. (d) At $t = 3$ there is no active site to topple and the avalanche stops having avalanche size $s = 4$ and area $a = 4$ (the pink area).

1.1.1 BTW sandpile model

The BTW sandpile model each lattice site is associated with a non-negative integer variable h representing the height of the 'sand column' at that site. The system is driven by adding sand grains, one at a time, to the randomly chosen lattice sites and the height of the column is increased as $h_i \to h_i + 1$. The sand column at site i becomes unstable or active when it's height h_i exceeds a predefined critical value h_c which is taken as $h_c = 4$ for a square lattice. If $h_i \geq h_c$, the site becomes active and it topples decreasing its height by h_c amount and distributing one sand grain to its each nearest neighbour. The toppling of a single site may make some of the nearest neighbour sites unstable and lead to further toppling activities which result in an avalanche. No sand grain is added during an avalanche to implement the separation of time scales. Propagation of an avalanche stops if all sites of the lattice become under critical. The evolution of an avalanche of BTW model is shown in Fig. 1.1. The avalanche dynamics is generally studied with open boundary condition and sand may dissipate from the system through the boundary. If the model is driven for a sufficiently long time, the model evolves spontaneously to a steady state. The steady state corresponds to the constant average height of the sandpile when the current of the incoming flux (due to the addition of sand) of sand grains is equal to that of the outgoing flux (due to the dissipation of the sand). It is important to note that for BTW model the number of sand grains outgoing from a site after toppling is exactly equal to the number of sand grains incoming to the same site after toppling of its nearest neighbors once each. Therefore, there is a complete toppling balance in BTW toppling rule. The BTW sandpile model is deterministic and abelian, the

final configuration does not depend on the sequence of toppling.

1.1.2 Stochastic sandpile model

Due to irregular shape and size of the sand grain, it may not always possible that the sand grains got distributed equally to its neighbours upon toppling of an active site as in BTW model. A stochastic version of the sandpile model was then introduced by Manna[55] and later modified by Dhar[56] and is found to be another well-studied model for its robust scaling behaviour. In stochastic sandpile model (SSM) the critical height of this model is taken as $h_c = 2$. If $h_i \geq h_c$, the site topples by distributing h_c amount of sand grains randomly. The toppling rule of the ith active node can be given as $h_i \to h_i - h_c$ and $h_j \to h_j + 1$, where $j \in \{j_1, j_2\}$ are two randomly and independently chosen sites out of 4 nearest neighbours. It is found that SSM exhibits a new scaling behaviour and belongs to different universality class (widely known as Manna class) than that of the BTW model.

It should be noted here that, though the above mentioned two models are described on 2d square lattice, one could extend those in higher or lower dimensions with different lattice structure without loss of generality.

1.1.3 Other sandpile models

A few other models to mention are:

Zhang model: A continuous height model was developed by Zhang[58]. In this model at each time instead of adding one sand, a quantum of energy δ $(0 < \delta < 1)$ is added to a randomly chosen site. If the energy of a site is greater than h_c which is generally chosen as 1, the site distributes its "all the energy" equally to its nearest neighbour. It is important to note that though the height variable is a continuous variable, in the dynamical steady state, the stationary height concentrated around discrete values, commonly known as the "emergence of quasi-units". The variants of this model like generalized Zhang model or stochastic Zhang model are also studied[59].

Directed sandpile model: Introducing the preferential direction of sand flow Dhar and Ramaswamy developed a directed sandpile model[57]. Such global directed bias resembles the flow of sand in a real sandpile from top to bottom direction. The model can be easily implemented on 2d square lattice by adding sand to the randomly chosen site at the top edge of the lattice. If the height of the sand column is greater than or equal to the threshold height $h_c = 2$, it topples and distributes two

sand grains by giving one to each of the two downward neighbours. The variants of such directed model is **directed stochastic sandpile model**[60,61]. To study the effect of local bias on the critical steady state of the sandpile model, **rotational sandpile model**[62] is constructed applying a rotational constraint to the toppling rule. The literature of these models is enriched with numerical analysis as well as analytical results.

1.1.4 Characterization of SOC

Equilibrium statistical mechanics provides a well-established method to study the critical behaviour of phase transition[1–3]. In equilibrium critical phenomena, if a suitable parameter is changed continuously, a quantitative change in the system properties occurs at a sharply defined parameter value which is called the critical point. The singular behaviour of various thermodynamic quantities, order parameter, response functions in the vicinity of the critical point is characterized by a set of critical exponents. However, a straightforward prescription to study the systems and estimating critical exponents at out of equilibrium situation is not well defined. Due to the complexity of the system it is not always possible to evaluate the correct Hamiltonian as well as appropriate response functions that could be measured.

In the case of sandpile models, the response of the system to the external drive could be the various properties of an avalanche, such as, the total number of toppling or avalanche size s, the number of distinct sites toppled in an avalanche or the avalanche area a, the number of parallel updates required to die out an avalanche or the lifetime t. In the equilibrium critical phenomena, power-law scaling is the hallmark of criticality which corresponds to the appearance of fluctuation at all possible length scale or clusters of all possible sizes. Since the dynamical system like sandpile model evolves to its own to the nonequilibrium critical steady state, the probability distribution functions of various avalanche properties expected to obey the power-law scaling behaviour in order to demonstrate the criticality of the steady state. The probability distribution of avalanche property x on a finite system size can be given by,

$$P_x(x, x_c) \approx x^{-\tau_x} f_x(x/x_c(L)) \tag{1.1}$$

where $x \in \{s, a, t\}$, τ_x is the critical exponent associated with the avalanche property x, $x_c(L)$ is the system size dependent cutoff value of the avalanche property x, and f_x is a scaling function. In the thermodynamic limit $L \to \infty$, as $x_c(L) \to \infty$, $f(0)$ should be constant and the distributions can be approximated as

$P_x(x,\infty) = P_x(x) \sim x^{-\tau_x}$. Since various avalanche properties are related to each other, conditional expectations among them can be obtained[63]. The conditional expectation of an avalanche property x fixing another property at y can be defined as

$$\langle x(y)\rangle = \int_0^{x_{max}} xP(x|y)dx \tag{1.2}$$

where $P(x,y)$ is the conditional probability to find a property x when the other property is exactly equal to y. In the steady state, the expectation values scale as

$$\langle x(y)\rangle \sim y^{\gamma_{xy}}, \tag{1.3}$$

where γ_{xy} is a critical exponent. Using the identity $\int \langle x(y)\rangle P_y(y)dy = \int \langle x(z)\rangle P_z(z)dz$, a scaling relation

$$\gamma_{xy} = \frac{\tau_y - 1}{\tau_x - 1}. \tag{1.4}$$

can be obtained. Similar to the equilibrium critical phenomena, estimation of the critical exponents, $\tau_x, \tau_y, \gamma_{xy}$ etc., verification of the scaling relations among them could be done. In order to estimate the critical exponent as well as to understand the scaling behaviour of the distribution functions, several different statistical mechanical techniques has been developed. Moment analysis of the distribution functions was found be an useful technique[64,65]. Assuming the cutoff $x_c(L)$ scales with system size as

$$x_c(L) \sim L^{D_x}, \tag{1.5}$$

D_x being the capacity dimension of the avalanche property x, a finite size scaling form of the probability distribution function can be written as

$$P_x(x,L) = x^{-\tau_x} f_x(x/L^{D_x}). \tag{1.6}$$

Consequently, the qth moment of x can be defined as

$$\begin{aligned}\langle x^q\rangle &= \int_0^{x_c} x^q P_x(x,L)dx = \int_0^{x_c} x^{q-\tau_x} f_x(x/L^{D_x})dx \\ &= L^{D_x(q-\tau_x+1)} \int_0^1 z^{q-\tau_x} f_x(z)dz \sim L^{\sigma_x(q)}\end{aligned} \tag{1.7}$$

where, $z = x/L^{D_x}$ is a scaled variable, the value of the integral $\int_0^\infty z^{q-\tau_x} f_x(z)dz$ is a constant, and

$$\sigma_x(q) = D_x(q - \tau_x + 1) \tag{1.8}$$

is the moment scaling function. Estimating the values of $\sigma_x(q)$, the value of D_x can be obtained from the derivative $\partial\sigma_x(q)/\partial q$ in large q limit. Knowing D_x, the exponent τ_x can be estimated from Eq. (1.8). A set of critical exponents then can be obtained for a given sandpile model and the values of the critical exponents define the universality class of that model. The numerical values various critical exponents for the BTW and SSM universality class along with the mean-field (MF) result for various dimensions are given in table 1.1. It could be noted that similar to equilibrium critical phenomena the sandpile universality classes change with the spatial dimension. For both BTW and SSM, the upper critical dimension is found to be $d_c = 4$[66,67] above which the exponents have MF values[68,69].

	τ_s	τ_a	τ_t	γ_{sa}	γ_{st}	D_s	D_a	D_t
BTW(1d)[a]	1	···	1	···	···	2	1	1
BTW(2d)[b]	1.293(9)	1.330(02)	1.48(1)	1.06(1)	1.62(1)	2.50(5)	2	1.52(2)
BTW(3d)[c]	1.333(7)	1.352(20)	1.62(1)*	1.00	1.78	3.00(1)*	3	1.61(1)*
SSM(1d)[d]	1.112(6)	1.25(1)	1.18(2)	2.00(1)	1.48(3)	2.25(1)	1	1.44(1)
SSM(2d)[e]	1.273(2)	1.382(3)	1.49(1)	1.23(1)	1.70(1)	2.750(6)	2	1.53(1)
SSM(3d)[f]	1.407(2)	1.442(12)	1.78(1)	1.07(1)*	1.92(5)*	3.37(1)	3	1.77(1)
MF[g]	3/2	3/2	2	1	2	2	2	1

Table 1.1: Values of various critical exponents for BTW and SSM universality class for one, two, and three dimensions. The mean-field result derived from branching theory is also given for comparison.

[a] The model is defined in Ref. [70] in terms of slope of the and column instead of height. [b] Ref. [64,66,71,72]. [c] Ref. [63,65,66,71]. [d] Ref. [73,74]. [e] Ref. [59,71,74]. [f] Ref. [59,65,67]. [g] Ref. [68,69,75]. * Derived from scaling relation.

It is found that the scaling behaviour of the BTW sandpile model obeys a anomalous multi-scaling whereas SSM follows usual finite size scaling[64,65]. To understand further the avalanche dynamics, a coarse-grained study of sandpile avalanches were performed decomposing the avalanches into waves of toppling[76–78]. The toppling wave time series were found to have a positive auto-correlation in the BTW model whereas the wave time series has no correlation in case of stochastic model[79–81]. It is widely accepted that the presence of correlation in toppling wave time series gives rise the multi-scaling behaviour in the BTW sandpile model[82]. Analysis of avalanches through surface physics approach has been carried out by mapping the avalanches to a surface called toppling surfaces[83], for various models. The Hurst exponents of toppling surfaces of those models reveal the role of underlying symmetry

presents in the models to determine the universality class of these models[83–85].

1.1.5 SOC as absorbing state phase transition

The approach of absorbing state phase transition[86] able to explain the *"path to self-organized criticality"* through the continuous phase transition formalism taking the density of the sand grains ρ as a tuning parameter[87–90]. In this approach, the fixed energy sandpiles are developed where the boundary is closed, and there is no dissipation of sand. Sand grains with density ρ are randomly distributed. The model evolves with the same toppling rule as in ordinary sandpile. If ρ is small enough the toppling activity stops after some time and the system falls into an absorbing state. The density of the sand grains ρ can be tuned from below to a critical value ρ_c, where the toppling activity sustains for an infinitely long time. Thus the system undergoes an active to absorbed phase transition, where the density of active site at long time limit can be treated as the order parameter. In order to characterize such phase transition, various scaling theories are developed at and around the critical point ρ_c[69]. Though recently it has been claimed that the absorbing state phase transition of fixed energy stochastic sandpile model falls under directed percolation universality class[91], the counter studies exist in support of independent Manna universality class[92–94]. An attempt has been made to relate the critical exponents of the absorbing state phase transition in fixed energy sandpile to those of ordinary sandpile model of SOC[95].

Lastly, it could be emphasized here that all those results are mainly obtained on the low dimensional regular lattice.

1.2 Complex networks and its models

A network is a set of objects called node those are connected by another set of connections called link. Networks are everywhere in nature and can be found in vast array of systems. For example, social network like friendship network[96], actor network[97,98], collaboration network[99–102], etc., is a group of people interacting with some certain relationship. In this context, the most significant early work work is Milligram's "small-world" social experiment[103,104] which established the fact "six-degree of separation" among the people. Networks can well describe many biological systems for instant, metabolic networks[105–107], protein interaction network or protein folding network[108–110], genetic regulatory network[111,112], Neural

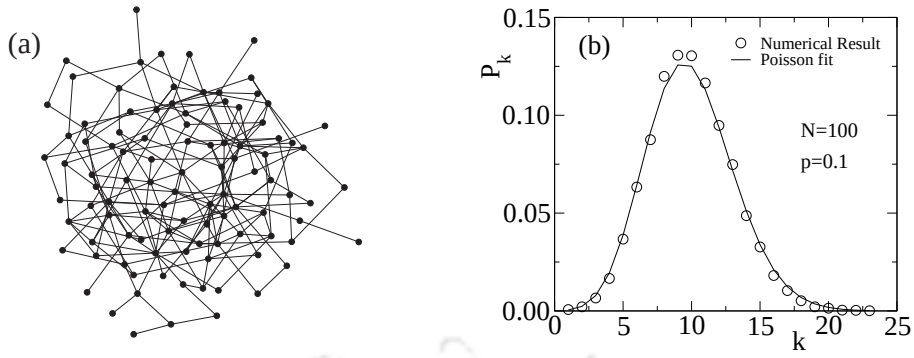

Figure 1.2: (a) A random network of size $N = 100$ generated by ER model for $p = 0.01$. (b) The degree distribution P_k of an ER network generated for $N = 100$, $p = 0.1$ and sampled over 100 realization is shown.

network[113,114]. The technological network such as power grid network[98,115,116], networks of airline[98], road[117], railways[118,119], Internet[120–123], etc., are the man-made network in the civilized society to distribute some commodity or resource. The citation network[124,125], the World Wide Web[126–128], network in the linguistic or semantic network[129,130] are treated as information network where the flow of information makes the virtual network. Besides the appearance of network in the real world, it also appears in the various theory of physics such as the potential energy landscape forms a static scale-free network[131], the conformal space of lattice polymer chain can be mapped into small-world network studied by Scala *et al.*[132], etc.

Considerable research work in last decade on complex networks leads to introduce a large number of different models which are more realistic and can be found in literature[12,133,134]. However, in this section the three pioneer basic models namely, Erdös-Rényi model, small-world model and Barabási-Albert model will be discussed. For each of the model the construction procedure of the network and topological properties of the generated networks which will distinguish them from one another will be mentioned briefly.

1.2.1 Erdös-Rényi model

In 1960 Erdös and Rényi proposed a simple model of random network[135]. Many properties of the random network are exactly solvable in the limit of large network size. Despite the success from the mathematical point of view, real world network can not be described in the framework of random graph model. Nonetheless, the model is important in the sense that this is the first generic model of graph theory

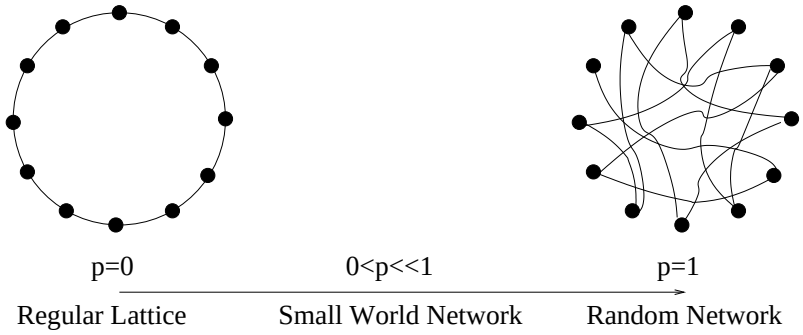

Figure 1.3: Schematic diagram of the generation of small-world network model from 1d linear closed chain. For rewiring probability $p = 0$ the network is a regular lattice whereas for $p = 1$, when all the bonds are rewired, the network behaves as random network. The intermediate region $0 < p << 1$ is called small-world region where the network shows both the high clustering co-efficient and the small average path between any two nodes.

and the basic intuition of the network behaviour, properties etc., comes from the study of this model. In order to generate the network of size N the model says, taking N number of nodes connect each pair of nodes with probability p. This will define a network with N nodes and m links, where $m = pN(N-1)/2$. For ER model the degree distribution P_k (the probability of a node having degree k) can be given by $P_k \simeq \langle k \rangle^k e^{-\langle k \rangle}/k!$ where, $\langle k \rangle = p(N-1) \simeq pN$ is the mean degree. Clearly, the model has a Poisson degree distribution which is shown in Fig. 1.2(b). The average shortest path length between any two nodes $\langle \ell \rangle$ scales with network size N as[136,137] $\langle \ell \rangle \sim \log(N)$ which represents the small-world effect. Clustering co-efficient C is the probability that two neighbouring nodes of a node are also neighbour of each other[12]. Since in ER model the probability of any two nodes are neighbour to each other is simply the connection probability p, hence $C = p = z/(N-1) \simeq z/N$. Clearly, C is vanishingly small for large N.

1.2.2 Small-world networks

Social networks and many other real networks such as, a network of conformations of a lattice polymer chain[98], friendship network[96], etc., have a low average shortest path with high transitivity or clustering co-efficient at the same time. Thus both the property of random graph and regular lattice exist in such networks[133]. To model such networks in 1998 Watts and Strogatz proposed the model of *small-world networks* (SWN) which interpolates between a regular lattice and a random network[116]. In the Watts and Strogatz small-world model, a network is built on a low-dimensional regular lattice by rewiring each link with some certain probability

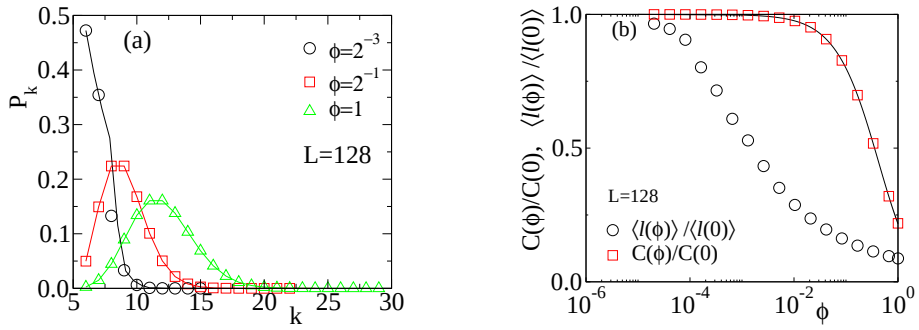

Figure 1.4: (a) Degree distribution for three different shortcut density ϕ of small-world network generated from two dimensional triangular lattice of size $L = 128$ and 64 different realizations. The solid lines are obtained from the Eq. (1.9). (b) Plot of normalized clustering co-efficient and normalized average shortest path between any two node against ϕ for the same network. The solid line through square represents the Eq. (1.12).

p to create "shortcuts" that join remote parts of the lattice to one another. Clearly, for $p = 0$ the lattice will be intact and for $p = 1$ that will generate a random network as shown in Fig. 1.3. The main drawback of this model is during rewiring some part of the network may be disconnected from the rest of the lattice. To overcome this problem as well as for analytical tractability of the model, Newman and Watts[138] proposed that instead of rewiring one can construct a small-world network from a low dimensional lattice by adding shortcut between any two randomly chosen node of the lattice and in this way the underlying lattice will be intact. One can assign a parameter ϕ, the shortcut density which is the number of shortcut added per original bond. Note that both the models are equivalent when the rewiring probability p or the shortcut density ϕ changes in a same way. Hereafter, all the result of small-world network model will be referred to the later version of the model (i.e., of Newman and Watts version).

The degree distribution of the small-world network can be given by[12]

$$P_k = e^{z\phi}\frac{(c\phi)^{k-z}}{(k-z)!} \quad \text{for} \quad k \geq z \tag{1.9}$$

where z is the coordination number of the underlying lattice. P_k of an SWN generated from 2d triangular lattice is shown for different shortcut density in Fig. 1.4(a). It is important to note that, for given shortcut density ϕ, the SWN possesses a characteristic length ξ. Below ξ the SWN behaves as regular lattice and beyond ξ the properties of SWN similar to the random network[139,140]. The average shortest path $\langle \ell \rangle$ in an SWN generated from a d-dimensional lattice of size L can be given

by

$$\langle \ell \rangle = L^d \mathcal{F}(L/\xi) \tag{1.10}$$

where the scaling function $\mathcal{F}(x)$ is a constant for $x \ll 1$ and scales as $\log(x)/x$ for $x \gg 1$ [138,141,142]. With such scaling function form the asymptotic scaling behaviour of $\langle \ell \rangle$ can be retrieved as

$$\langle \ell \rangle \sim \begin{cases} L^d, & \phi \to 0 \\ \log(L), & \phi \to 1 \end{cases} \tag{1.11}$$

Since the clustering co-efficient of the underlying lattice is different for different lattice, the general expression C could be difficult. However, following Ref. [12] the expression of Clustering co-efficient $C(\phi)$ as a function of ϕ can be derived for 2d triangular lattice as

$$C(\phi) = \frac{3}{5 + 12\phi + 6\phi^2} , \tag{1.12}$$

with $C(\phi = 0) = 0.6$. Fig. 1.4(b) illustrates the variation average shortest path $\langle \ell \rangle$ and clustering co-efficient C with shortcut density ϕ of an SWN generated from triangular lattice. It can be seen that for a wide range of ϕ (e.g. $10^{-4} < \phi < 0.10$), $\langle \ell \rangle$ is sufficiently low whereas C remains same as that of a regular lattice. It should be noted that for 2d square lattice a third order clustering co-efficient could not be defined as no triangle exists there. In that case without loss of generality one could modify the definition of C in terms of quadrilaterals (cycle of order four) instead of triangles. For a given node the fourth order clustering co-efficient could be defined as the ratio of all the quadrilaterals passing through the node to the maximum possible number of quadrilaterals it can share[143]. It has been verified that the fourth order clustering co-efficient for SWN generated from 2d square lattice also has a similar variation with ϕ as that of the third order clustering co-efficient (Eq. (1.12)). Note that the SWN does not mimic the degree distribution of the real world network; what it does well is, demonstrate the mean geodesic distance between any two nodes and clustering co-efficient of the real world network.

1.2.3 Barabási-Albert scale-free network

In order to study the growth process of the real networks such as the internet,the World Wide Web or citation network, in which the gradual addition of nodes and links occurs, Barabási and Albert (BA) proposed a model of growing network[144]. In this model, starting a small number of nodes $n0$, at each time one new node is

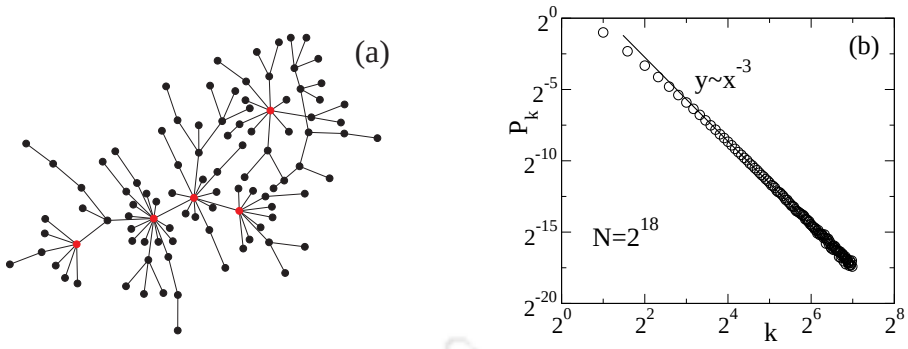

Figure 1.5: (a) A picture of scale-free network generated by BA model with $N = 100$ nodes. Due to power-law degree distribution, few nodes have very large degree compare to others, and those hubs are marked by red dots. (b) Degree distribution of BA scale-free network calculated for $N = 2^{18}$ nodes and sampled over 64 configurations. Clearly, the distribution has power-law behaviour with exponent 3.

added to the network with m ($m < n0$) new links. The links are connected to the other existing nodes with a probability proportional to its existing degree. That is, at jth step, where at each step a new node is introduced, the new node is connected to the existing node i with probability

$$\Pi_i = \frac{d_i}{\sum_{i=1}^{j+n0} d_i}, \tag{1.13}$$

where d_i is the degree of ith node at that time step. At step $N - n0$ the network will consist N nodes with average degree m. A pictorial view of the BA scale-free network is shown in Fig. 1.5(a). The degree distribution of BA model can be solved exactly by master equation approach, and it can be shown that the distribution follows a power-law $P_k \sim k^{-\alpha}$, where α is the degree distribution exponent and equal to 3 for $N \to \infty$[145]. A plot of P_k against k is shown in Fig. 1.5(b) for a network produced by this model for $N = 10^5$ nodes. By a rigorous mathematical proof, Bollabas and Riordan showed that $\langle \ell \rangle$ for BA scale-free network scales with system size N as[146,147] $\langle \ell \rangle \sim \ln(N)/\ln\ln(N)$ for $m \geq 2$. Variant models have been proposed followed by original BA model to generate scale-free networks with generalized degree exponent where the value of α is tunable from 2 to ∞[148,149]. Other models have also been proposed to produce scale-free networks with varied α, for example Configurational model or Reed-Molly model[150], Goh-Kahng-Kim model[151], etc. It should be noted here that, the value of degree exponent α has a significant role to determine the various topological properties of the SFN. Considering the integral $\int_{k_{\max}}^{\infty} P_k dk = 1/N$, the cutoff degree of the network scales as $k_{\max} \sim N^{1/(\alpha-1)}$. Hence, for $\alpha < 2$,

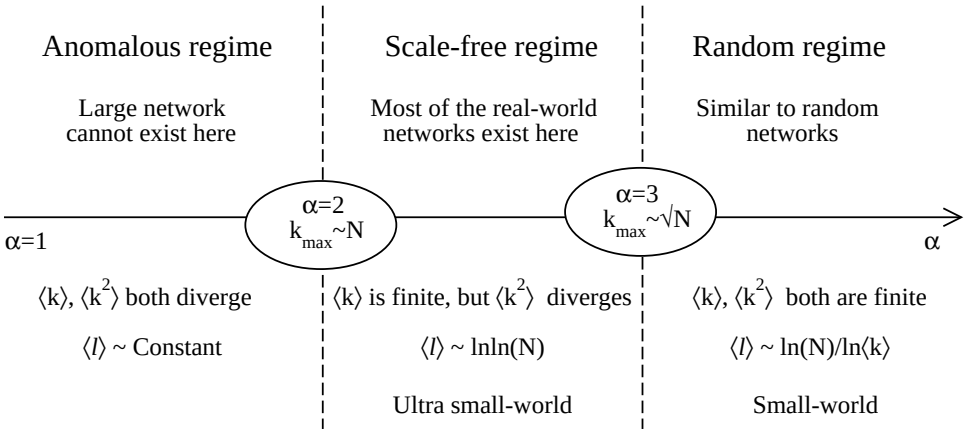

Figure 1.6: Various properties of scale-free networks, such as, cutoff degree $k_{\max}$, average degree $\langle k \rangle$, square average degree $\langle k^2 \rangle$, average shortest path $\langle \ell \rangle$, for different values of α.

$k_{\max}$ grows faster than network size N, and consequently no large network cannot exist in that anomalous regime. In the true scale-free regime ($2 < \alpha < 3$), the network is highly heterogeneous as fluctuation of the degree is a diverging quantity. Since $\langle \ell \rangle \sim \ln \ln(N)$, the networks are ultra small-world [147]. Interestingly, most of the real-world networks fall in this regime [9,10]. On the other hand, for $\alpha > 3$, the networks with small-world property ($\langle \ell \rangle \sim \ln(N)$) and finite characteristic degree, are indistinguishable from the properties of random networks. Various α dependent properties in different regimes are summarized in Fig. 1.6.

Last two decades have witnessed a huge amount of work that explores the statistical and topological features of the large-scale networks [9,10]. However, the study of dynamical phenomena on complex networks have been started recently [11,21,152]. In this thesis, one of the commonly occurred dynamical phenomena on complex networks, the avalanche dynamics, will be investigated on several networks through different sandpile models.

1.3 Sandpile on complex networks

In order to study the effect of heterogeneity, compactness and clustering of a network on the dynamical processes in a simplest possible way, sandpile, the prototypical model to study SOC, defined on regular lattice has been recast on networks. In such a model, diffusion or flow of sand grains on toppling of a node over a heterogeneous network structure will be the underlying principle to follow. The universality class of a statistical model depends strongly on the dimensionality of space on which it is defined or embedded. As the sandpile model is defined on networks several ques-

tions arises naturally. Since the substrate on which the model is defined is changed, the effective dimension of the space is going to be different and the consequences are going to be severe in terms of universality. Not only different networks but also the degree distribution of a given network can be tuned controlling some of the parameters of a network. Different sandpile models, deterministic or stochastic, and their critical behaviour at the steady state poses intriguing questions without answers. Moreover, controlling self-organized criticality is a challenging task because of its complicated feedback mechanism. It could provide an easy way to control SOC of a sandpile model by defining the model on a network and controlling the network structure. Furthermore, since there is no definite boundary in a network, the boundary dissipation in usual lattice models of SOC need to be redefined incorporating bulk dissipation and there is a need of developing generalized sandpile model. The study of SOC on networks via sandpile model has started in the beginning of the 21st century defining a specific sandpile model on a specific network in a specific dimension. For example, sandpile dynamics has been studied on the Erdös-Rényi random network by Bonabeau[153] and later by Christensen[68] and found to follow MF scaling behaviour. The MF behaviour of BTW model on SWN with sufficient addition of extra links was also reported by Lathinen *et al.*[154] in one dimension and by Arcangelis and Herrmann[155] in two dimensions beside their usual behaviour on the regular lattice. Though a few studies were reported on sandpile dynamics on SWN or random network, a detailed study of crossover scaling as the underlying substrate evolves from regular lattice to SWN to random network by tuning the shortcut density found to be missing in the literature. Therefore, in this thesis firstly a thorough study of dynamics of a generalized deterministic sandpile model on SWN will be attempted and the crossover behaviour will be monitored as the SWN evolves from regular lattice to random network. Secondly, as the deterministic model does not obey finite-size scaling on the regular lattice whereas a stochastic model does, a systematic study of a stochastic version of dissipative sandpile model will be studied thoroughly on SWN and new scaling forms will be determined and its crossover will be verified. It is reported in the literature that in the case of boundary dissipation on regular lattice the behaviour of the dissipative avalanches differs considerably from that of the nondissipative avalanches of a stochastic sandpile model[156]. It is then intriguing to characterize the scaling behaviour of dissipative and nondissipative avalanches of both deterministic and stochastic sandpile models with bulk dissipation on SWN. It is considered as the third aspect of the study in this thesis. The study of sandpile model has also been extended to other networks,

for example, on Apollonian networks by Vieira *et al.*[157], on multiplex networks by Lee *et al.*[158], on artificial and real-world directed networks by Christensen and co-workers[159], etc. The dynamics of SOC with coevolution of network structure was studied by Fronczak *et al.*[160]. Out of all those, the scale free network represents a truly heterogeneous complex topology as its degree distribution is represented by a power-law scaling. Hence studying sandpile models on a scale-free network is of special interest. Both the BTW and SSM have been studied on scale-free networks and reported by Goh *et al.*[161] and more recently by Noel *et al.*[162]. It has been shown analytically as well as numerically that, though the SSM shows mean-field result for all values of degree exponent α, the BTW model exhibits new scaling behaviour other that mean-field in the scale-free regime ($\alpha < 3$). Study has also been performed on variants of scale-free network, like optimized network[163], geographically embedded network[164], Barabási-Albert network[165] etc. Finally, in this thesis, a new two-state preferential sandpile model is developed where sand grains after toppling are distributed to preferred nodes. Such preferential sandpile model on scale-free network represents a whole set of new results in context of the controlling self-organizing criticality[166–168]. Implementation of control strategies in self-organizing systems is a challenging task. However, in this model, new control strategies such as tuning of the substrate structure, preferentially distributing sand, changing of the dissipation rate, etc., could be easily implemented to control the SOC dynamics.

The upcoming chapters of the thesis are going to be organized in the following manner. In chapter 2, a deterministic version of dissipative sandpile model will be defined on the small-world networks, and its steady-state critical properties will be characterized by studying probability distribution and expectation values of various avalanche properties. Invoking the network's inherent length scale a new coexistence scaling theory for distribution function as well as a new scaling form of diffusive to super-diffusive sand transport will be developed. Chapter 3 will address the critical behaviour of the stochastic version of sandpile model on small-world networks. The developed scaling forms in the previous chapter will also be verified on the stochastic version of the model. In chapter 4, the effect of dimension, network topology and specific dissipation mode (bulk or boundary) on the steady-state critical properties of nondissipative and dissipative avalanches along with all avalanches are analyzed both for deterministic and stochastic dissipative models. An extensive set of critical exponents for various types of avalanches will be measured by moment analysis technique. Chapter 5 deals with the controlling of SOC on scale-free network intro-

ducing a two-state sandpile model with preferential sand distribution. A detailed study of three different mechanisms of controlling the SOC will be given. Lastly, a summary of the present thesis along with the discussion on the importance of the new results will be presented in chapter 6.

Chapter 2

Dissipative deterministic sandpile model on small-world networks

In this chapter, dissipative version of deterministic (BTW-type) sandpile model will be developed on small-world network (SWN) and its scaling behaviour will be determined. An SWN introduced by Watt and Strogatz[116] is a partially disordered structure interpolating between the regular lattice and the random network. An SWN specified by shortcut density ϕ, number of shortcuts per existing link, is generated adding extra links (or shortcuts) between two randomly chosen sites on the lattice[13]. In this process, $\phi = 0$ corresponds to an regular lattice and $\phi = 1$ corresponds to a random network. A random network is characterized by the Poissonian degree distribution[135,170]. As ϕ increases from 0 there will an onset of small-world behavior around $\phi \approx 1/N$, where N is the number of nodes present in the network[13,138]. The small-world behavior is characterized by the fact that the shortest distance ℓ between any two nodes is as small as that of a random network and at the same time the concept of neighbourhood is preserved as that of a regular lattice[133]. If ϕ is increased further, the small-world behavior will evolve to that of a random network around $\phi \approx 0.1$[13]. There exits a characteristic length $\xi \sim \phi^{-1/d}$ where d is the dimensionality of the lattice, below which SWN belongs to a "large world" regime (regular lattice) and beyond which it behaves as "small world"[139,140]. Depending on the value of ξ, the average shortest distance $\langle \ell \rangle$ scales with the system size L as

$$\langle \ell \rangle = L\mathcal{F}(L/\xi) = L\mathcal{F}(\phi^{1/d}L), \tag{2.1}$$

This chapter is based on the Ref. [169]; H. Bhaumik and S. B. Santra, Phys. Rev. E. 88, 062817 (2013).

where $\mathcal{F}(\phi^{1/d}L)$ is a universal scaling function[138,141] and is given by

$$\mathcal{F}(x) \propto \begin{cases} \text{constant}, & x \ll 1, \\ (\log x)/x, & x \gg 1. \end{cases} \tag{2.2}$$

It can be noted here that the scaling form was exactly determined for one-dimensional SWN by Newman *et al.*[171] except for $x = 1$. Moreover, the effective dimension of the SWN also depends on the length scale at which it is looked at[138]. Below the length scale ξ, the network has the effective dimension as that of the regular lattice from which it is generated, whereas above length scale ξ, the effective dimension increase linearly with the length scale, reminiscent of the behaviour of the multi-fractal[172].

Recently the existence of self-organization on complex structures has triggered studies of SOC dynamics on complex networks[153–155,160,161,163,173,174]. It should be noted that BTW type deterministic sandpile model shows multi-scaling behaviour[64,175] on regular lattice due to its complete toppling balance[82], whereas it shows mean-field (MF) result on random network[153]. It is then intriguing to study such model on SWN for different values of ϕ and see how the scaling behaviour changes as SWN evolves from regular lattice to random network as ϕ increase from 0 to 1. In this chapter, a BTW type generalized dissipative deterministic sandpile model (DDSM) with a variable critical height is developed for a series of SWNs in order to examine the effect of different length scales present in SWNs on the critical behavior of sandpile dynamics as well as that of slowly driven dynamical systems in general.

2.1 The Model: DDSM on SWN

In this model, SWNs are generated by adding shortcuts between two randomly chosen sites of a two-dimensional square lattice of size L. There are L^2 nodes and $2L^2$ bonds present on the two-dimensional square lattice if periodic boundary conditions are assumed. The number of nodes is kept fixed at L^2 throughout the simulation. The regular lattice is modified to an SWN by adding shortcuts between two arbitrary sites of the regular lattice with a specified density ϕ. The sites are chosen uniformly from all over the lattice. The density of extra links per existing

bond of the original lattice is defined as

$$\phi = \frac{N_\phi}{2L^2}, \tag{2.3}$$

where N_ϕ is the number of shortcuts added to the lattice. Care has been taken to avoid more than one link between any two nodes. There is no link which connects a node itself. Each ϕ value corresponds to a particular SWN.

An SWN of a given ϕ is now driven by adding sand grains, one at a time, to randomly chosen nodes. The height of the sand column of each node is stored in an integer variable $h_i, i = 1, 2, \cdots, L^2$. For a given ϕ, the nodes of the SWN will have a particular degree distribution. The critical height or the threshold value for toppling of the ith node is taken to be its degree k_i. If the height of the sand column at any node becomes greater than or equal to the threshold value (k_i), it will be marked as unstable. The corresponding sand column then topples and the height of the sand column is reduced by k_i amount. The node then becomes undercritical. The sand grains flow from the toppled node to its adjacent nodes, which are connected to the toppled node by links. Since no rigid boundary exists for a network, the boundary sites of an regular lattice where sand dissipation used to occur are supposed to be distributed among randomly selected nodes of the network. Dissipation of sand to those nodes is made with an appropriate dissipation factor ϵ_ϕ in an annealed manner. It is realized by dissipating a sand grain with probability ϵ_ϕ in every attempt at sand transport from the critical node. The adjacent nodes are then called sequentially one by one, and every time ϵ_ϕ is compared with a random number r. If $r \leq \epsilon_\phi$, the sand grain is dissipated out from the system and the height of the sand column at the corresponding adjacent node remains the same; otherwise, it is increased by 1 unit. The toppling rule then can be represented as

$$\begin{aligned} & h_i \to h_i - k_i, \\ \text{and} \quad & h_j = \begin{cases} h_j & \text{if } r \leq \epsilon_\phi, \\ h_j + 1 & \text{otherwise,} \end{cases} \end{aligned} \tag{2.4}$$

where $j = 1, 2, 3, \cdots, k_i$. If the toppling of a node causes some of the adjacent nodes to become unstable, subsequent toppling follows on these unstable nodes. The process continues until there is no unstable node present in the system. These toppling activities lead to an avalanche. During an avalanche no sand grain is added to the system.

The critical properties of DDSM are studied on SWNs defined on square lattices

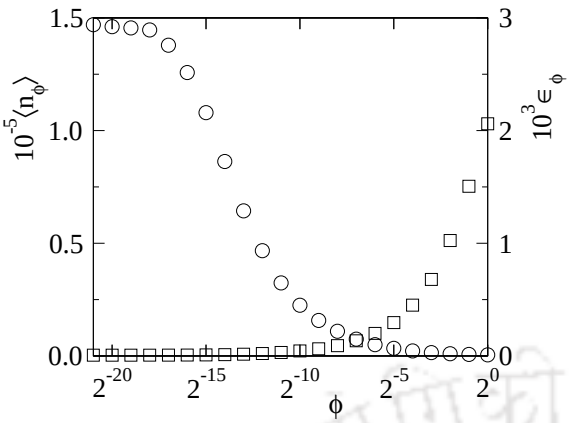

Figure 2.1: Plot of $\langle n_\phi \rangle$ (○) and ϵ_ϕ (□) against ϕ on a log-normal scale for $L = 1024$.

of different sizes varying ϕ from 0 to 1 for each lattice size. It is now essential to determine the dissipation factor ϵ_ϕ for an SWN of given ϕ and system size L.

2.2 Determination of dissipation factor ϵ_ϕ

Malcai *et al.*[176] defined the dissipation factor for a DDSM on regular lattice by the inverse of time steps required for a random walker to reach the lattice boundary starting from an arbitrary site. Such a definition for the dissipation factor on a regular lattice has been extended to the SWN here. The dissipation factor ϵ_ϕ on an SWN corresponding to a given ϕ is then given by

$$\epsilon_\phi = \frac{1}{\langle n_\phi \rangle}, \tag{2.5}$$

where $\langle n_\phi \rangle$ is the average number of steps required for a random walker to reach the lattice boundary starting from an arbitrary node of the SWN. The average number of steps $\langle n_\phi \rangle$ required for such walks is calculated by performing 2×10^6 random walks in 16 different random configurations of every SWN. In performing such walks no periodic boundary condition is applied. In Fig. 2.1, $\langle n_\phi \rangle$ and ϵ_ϕ are plotted against ϕ on a semilogarithmic scale for $L = 1024$. It can be seen that $\langle n_\phi \rangle$ decreases rapidly with increasing ϕ. This is because as ϕ increases the number of shortcuts also increases in the system and consequently the walker needs a lesser number of steps to reach the boundary starting from an arbitrary node. Consequently, ϵ_ϕ increases rapidly as $\phi \to 1$. For the two extreme values of ϕ, the dissipation factors are obtained as $\epsilon_{\phi=0} = 6.7 \times 10^{-6}$ and $\epsilon_{\phi=1} = 0.002$.

Using the estimated ϵ_ϕ, sandpile dynamics now can be studied on SWNs at different values of ϕ on a given L.

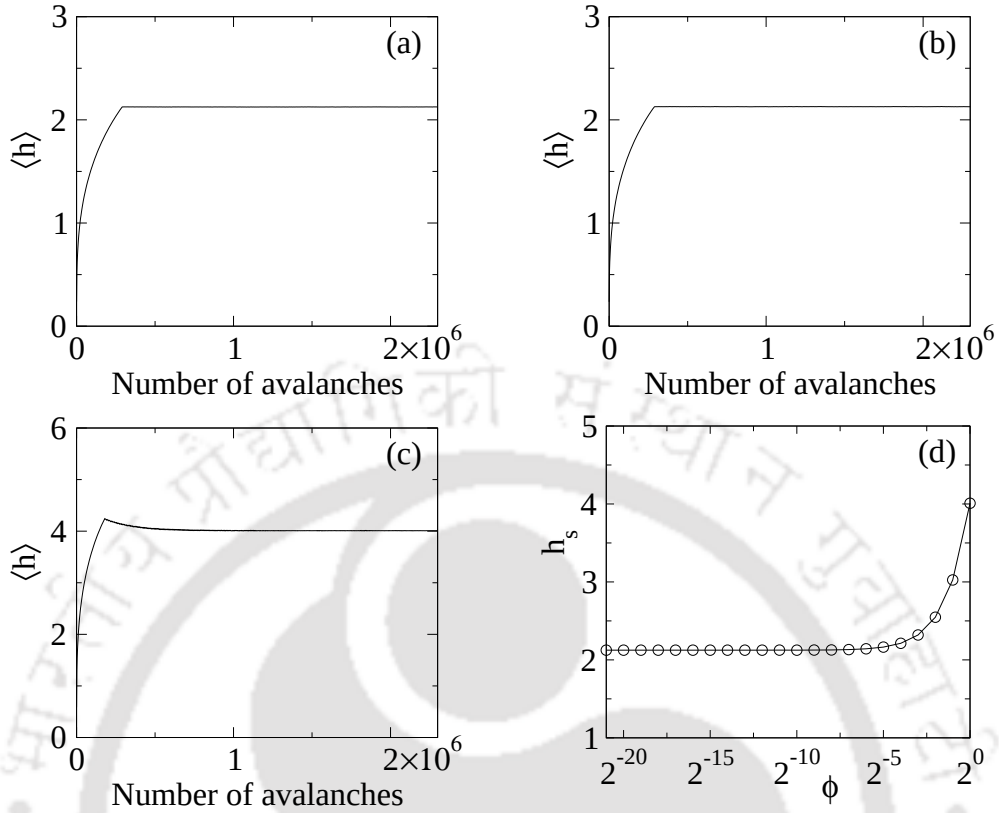

Figure 2.2: Plot of average height $\langle h \rangle$ against number of avalanches of the DDSM on SWNs generated on a square lattice of size $L = 1024$ for (a) $\phi = 0$, (b) $\phi = 2^{-8}$, and (c) $\phi = 1$. (d) Plot of average saturated height h_s against ϕ in log-normal scale.

2.3 Steady state of the DDSM on an SWN

The steady state of the DDSM on an SWN corresponds to a current of the incoming flux of sand grains into the system equal to that of the outgoing flux of sand grains from the system. Thus, under the steady-state conditions the average height $\langle h \rangle$ of the sand columns should remain constant. For L^2 nodes, the average height is defined as

$$\langle h \rangle = \frac{1}{L^2} \sum_{i=1}^{L^2} h_i. \tag{2.6}$$

In Fig. 2.2, $\langle h \rangle$ is plotted against the number of avalanches for SWNs defined on a square lattice of size $L = 1024$ for $\phi = 0$ [2.2(a)], $\phi = 2^{-8}$ [2.2(b)], and $\phi = 1$ [2.2(c)]. It can be seen that the steady state for the DDSM is achieved after the initial 10^6 avalanches in all the SWNs considered. The saturated average height h_s is plotted against ϕ in Fig. 2.2(d). The value of h_s on the regular lattice, $\phi = 0$, is approximately 2.125, as conjectured in the context of the absorbing state phase

transition of the fixed-energy sandpile model on a square lattice[90]. As ϕ increases, the value of h_s remains almost independent of ϕ upto $\phi \approx 2^{-3}$, and beyond this value of ϕ, h_s increases rapidly with ϕ. Since the average critical height of the sandpile model on an SWN is defined by the average degree $\langle k \rangle$ of the network, the variation of h_s with ϕ must be due to the change of $\langle k \rangle$ with ϕ. A simple relationship between $\langle k \rangle$ and ϕ can be obtained as

$$\langle k \rangle = 4 + 2\frac{2L^2\phi}{L^2} = 4(1+\phi), \tag{2.7}$$

where $2L^2\phi$ is the number of shortcuts added and the factor 2 corresponds to an increase in degree by one of two nodes for the addition of each shortcut. Therefore, for $\phi = 0$, $\langle k \rangle = 4$, for $\phi = 1$, $\langle k \rangle = 8$, and for $\phi = 2^{-3}$, $\langle k \rangle = 4.5$. Thus up to $\phi = 2^{-3}$, the increase in $\langle k \rangle$ is small because for $\phi < 0.1$ the network corresponds to the small-world regime and the concept of neighbourhood is preserved. Since $\langle k \rangle$ is small in this region, the change in h_s is expected to be small. For $\phi > 0.1$, $\langle k \rangle$ increases rapidly and hence so does the value of h_s. It is also observed that as ϕ increases, the steady state appears after an initial hump in $\langle h \rangle$. For large ϕ, the dissipation in the system will be mostly through nodes with higher degrees. It takes some time for those nodes to accumulate an appropriate number of sand grains to become critical. During the initial piling up of the sand columns in the higher degree nodes, the average height of the sand columns may increase beyond the saturation value h_s corresponding to the steady state.

Numerical details: To characterize the critical steady state of DDSM, extensive numerical simulations have been performed for various system sizes L and shortcut density ϕ. L is varied from 128 to 1024 in multiple of 2. The value of ϕ is varied from 0 to 1, increasing N_ϕ in multiples of 2. For a given ϕ and L, sixteen SWN configurations are considered . On each SWN, after attaining the steady state 10^6 avalanches are neglected and the next 2×10^6 avalanches are collected. Therefore, a total of 32×10^6 avalanches is taken for data averaging. For each avalanche, different properties like the size s, area a, and lifetime t of an avalanche are measured. The size of an avalanche s is defined as the total number of topplings which occurs in an avalanche, the avalanche area a is equal to the number of distinct sites or nodes toppled in an avalanche, and the lifetime t of an avalanche is the number of parallel updates to make all the nodes (sites) under critical.

2.4 Probability distributions and expectation values

Sandpile dynamics mostly characterize the probability distribution of these avalanche properties and the conditional expectation values $\langle x_\phi(y)\rangle$ of a property x keeping another property y fixed at a certain value[63]. At steady state, the probability distribution functions $P_x(x,\phi)$ on an SWN generated on a large lattice of fixed size with a given ϕ is expected to obey power-law scaling as

$$P_x(x,\phi) \sim x^{-\tau_x(\phi)}, \tag{2.8}$$

where $x \in \{s,a,t\}$ and $\tau_x(\phi)$ is the critical exponent corresponding to the given value of ϕ. The conditional expectation $\langle x_\phi(y)\rangle$ is defined as

$$\langle x_\phi(y)\rangle = \int_0^{x_{max}} x P_{x|y}(x|y)dx, \tag{2.9}$$

where $P_{x|y}(x|y)$ is the conditional probability of property x for a fixed value of y. The quantity $\langle x_\phi(y)\rangle$ is expected to scale with the other property y as

$$\langle x_\phi(y)\rangle \sim y^{\gamma_{xy}(\phi)}, \tag{2.10}$$

where $x \in \{s,a,t\}$ and $\gamma_{xy}(\phi)$ is another ϕ dependent critical exponent. The exponent $\gamma_{xy}(\phi)$ can also be obtained in terms of the distribution exponents $\tau_x(\phi)$ and $\tau_y(\phi)$ as given in[62]:

$$\gamma_{xy}(\phi) = \frac{\tau_y(\phi)-1}{\tau_x(\phi)-1}. \tag{2.11}$$

Before analyzing the probability distributions and the conditional probabilities, one should note that there exists a length scale ξ for a given SWN below which the SWN behaves as a regular lattice and above which it behaves as a network. It is then expected that there should exist a characteristic value x_c of every avalanche property corresponding to the length scale ξ of SWN. For a given ϕ, below and above x_c the probability distributions and the conditional probabilities are then expected to behave differently. In two dimensions, ξ scales with ϕ as $\xi \sim \phi^{-1/2}$ [138]. Therefore, the characteristic area a_c of the avalanches occurring on the regular lattice must be proportional to ξ^2. Hence, the scaling of a_c with ϕ should be given by

$$a_c \sim \phi^{-\alpha_a}, \tag{2.12}$$

with $\alpha_a = 1$. Knowing the scaling of a_c with ϕ, one can find the scaling of s_c and

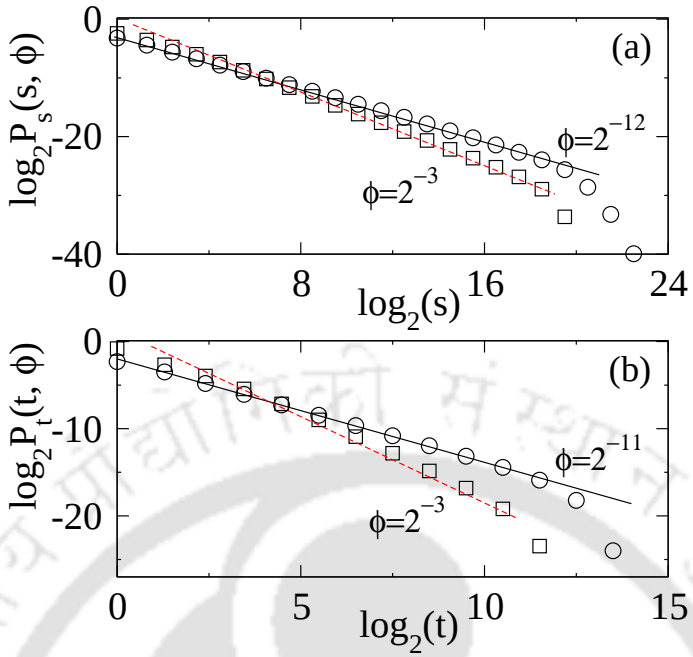

Figure 2.3: (a) Distribution of avalanche size $P_s(s,\phi)$ plotted on a double-logarithmic scale for two values of ϕ: $\phi = 2^{-12}$ (○) and $\phi = 2^{-3}$ (□) for $L = 1024$. Straight lines are fitted through data points. The slope of the solid black line is -1.11 ± 0.01 and that of the dashed red line is -1.50 ± 0.01. (b) Plot of $P_t(t,\phi)$ against t for $L = 1024$. The slope of the solid black line is -1.18 ± 0.01, and the dashed red line has slope -1.98 ± 0.02.

t_c with ϕ as well. From the conditional expectation of avalanche size for a fixed avalanche area one expects $s_c \sim a_c^{\gamma_{sa}}$ on regular lattice. Hence,

$$s_c \sim \phi^{-\gamma_{sa}}. \tag{2.13}$$

Then, $\alpha_s = \gamma_{sa}$. Similarly, $t_c \sim s_c^{\gamma_{ts}}$ or $t_c \sim a_c^{\gamma_{sa}/\gamma_{st}}$. Therefore, one has

$$t_c \sim \phi^{-\gamma_{sa}/\gamma_{st}}. \tag{2.14}$$

Hence, $\alpha_t = \gamma_{sa}/\gamma_{st}$. Since $\gamma_{sa} = 1.06$ and $\gamma_{st} = 1.63$ on a regular lattice[62], the values of α_s and α_t are expected to be 1.06 and 0.65, respectively.

Probability distributions of avalanche size $P_s(s,\phi)$ and those of lifetime $P_t(t,\phi)$ are estimated on SWNs generated for different values of ϕ for a given lattice size. For $\phi = 2^{-12}$ (close to $\phi = 0$) and $\phi = 2^{-3}$ (close to $\phi = 1$), $P_s(s,\phi)$ and $P_t(t,\phi)$ obtained on a lattice of size $L = 1024$ are plotted in Figs. 2.3(a) and 2.3(b), respectively. It can be seen that for both $\phi = 2^{-12}$ and $\phi = 2^{-3}$, $P_s(s,\phi)$ and $P_t(t,\phi)$ show power-law behavior over almost the whole extent of s and t, but with different critical exponents. The scaling behavior at $\phi = 2^{-12}$ is found to be characterized

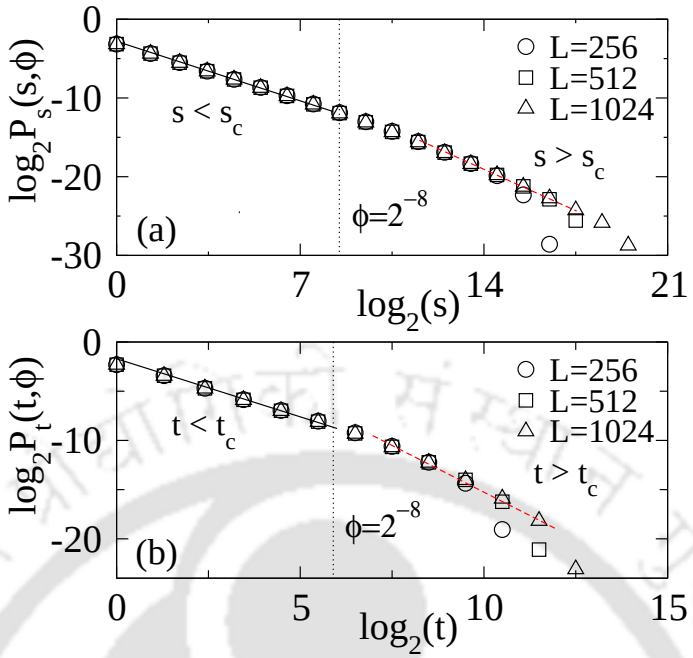

Figure 2.4: (a) Distribution of avalanche size $P_s(s,\phi)$ plotted on a double-logarithmic scale for $\phi = 2^{-8}$ for three system sizes: $L = 256(\bigcirc)$, $512(\square)$, and $1024(\triangle)$. The dotted vertical line at $s = s_c$ separates the two regimes. The slope of the solid black line for $s < s_c$ is -1.11 ± 0.01 and that of the dashed red line for $s > s_c$ is -1.50 ± 0.01. (b) Plot of $P_t(t,\phi)$ versus t. The dotted vertical line at $t = t_c$ separates the two regimes. The solid black line for $t < t_c$ has the slope -1.18 ± 0.01 and the red dashed line for $t > t_c$ has slope -1.98 ± 0.02.

by the avalanche size exponent $\tau_s = 1.11 \pm 0.01$, and avalanche time exponent $\tau_t = 1.18 \pm 0.01$, which are measured by the best-fit straight (black) line through the data points. The value of τ_s for $\phi = 2^{-12}$ is the same as that previously reported for the DDSM on a regular lattice ($\phi = 0$)[176,177]. Note that the value of τ_s in the BTW model (Dhar abelian sandpile model[56,178]) was also reported to be ≈ 1.11 though in the $L \to \infty$ limit it is expected to be ≈ 1.29[65,66,179]. Therefore the BTW-type sandpile dynamics on a regular lattice remains unperturbed when performed on a lattice with an additional $N_\phi = 512$ shortcuts, corresponding to $\phi = 2^{-12}$ on a lattice of size $L = 1024$. On the other hand, the power-law scaling at $\phi = 2^{-3}$ is found to be characterized by critical exponents $\tau_s = 1.5 \pm 0.01$ and $\tau_t = 1.98 \pm 0.02$. The value of τ_s for the DDSM obtained by MF theory for lattices without a spatial structure[68] as well as by the branching process for a random network[68,153] was known to be 3/2 and the exact value of τ_t on a random network obtained by the branching process is 2[153]. Hence, the measured value of $\tau_t = 1.98$ for the random network is close to the exact result. Therefore by the addition of $N_\phi = 2^{18}$ shortcuts

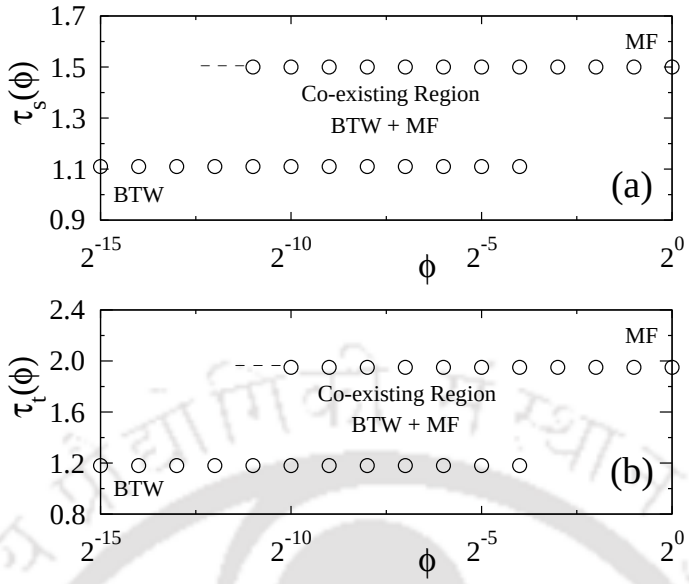

Figure 2.5: (a) Values of the exponent $\tau_s(\phi)$ against ϕ (b) values of $\tau_s(\phi)$ against ϕ. In both cases the exponents are extracted for a system of size $L = 1024$. The extrapolated dashed lines indicate possible exponent values for larger system sizes.

corresponding to $\phi = 2^{-3}$ on a lattice of size $L = 1024$, the regular lattice evolves to a random network and DDSM scaling on it can be described by MF scaling though the critical height is not taken as the mean degree of nodes as in Ref. [68].

For $\phi = 2^{-8}$ (an intermediate value of ϕ), $P_s(s, \phi)$ and $P_t(t, \phi)$ are plotted in Figs. 2.4(a) and 2.4(b), respectively, for different values of system size L. It is interesting to note that for $\phi = 2^{-8}$, the distributions of $P_s(s, \phi)$ and $P_t(t, \phi)$ follow two different power-law scalings at different regimes of s and t, respectively, separated by a characteristic value s_c and t_c as shown by dotted lines in Figs. 2.4(a) and 2.4(b). The values of s_c and t_c are obtained from Eqs. (2.13) and (2.14) respectively. For $s < s_c$, the scaling behavior of $P_s(s, \phi)$ is characterized by $\tau_s = 1.11 \pm 0.01$, whereas for $s > s_c$ it is characterized by $\tau_s = 1.5 \pm 0.01$. Therefore for SWNs corresponding to intermediate values of ϕ, both scaling forms, BTW and MF, of the DDSM coexist. It should also be noted that the characteristic size s_c or characteristic time t_c does not change with the system size L, as the characteristic length scale ξ does not depend on L[138]. The values of the critical exponents $\tau_s(\phi)$ and $\tau_t(\phi)$ obtained for different values of ϕ are shown in Figs. 2.5(a) and 2.5(b). It is important to note that coexistence of both scaling forms persists over a wide range of ϕ values given by $2^{-12} < \phi < 2^{-3}$ for s and $2^{-11} < \phi < 2^{-3}$ for t. The upper limit corresponds to the crossover of SWN to random network at $\phi \approx 0.1$[13]. Though the crossover from regular lattice to SWN occurs at $\phi \approx 1/L^2$[138], for the finite system of size $L = 1024$

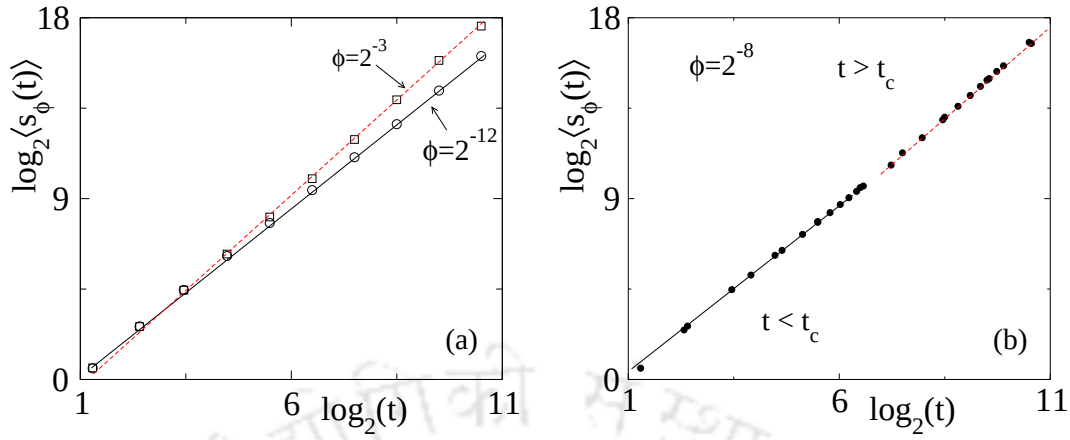

Figure 2.6: (a) Plot of $\langle s_\phi(t)\rangle$ against t for $\phi = 2^{-12}$ (○) and $\phi = 2^{-3}$ (□) with $L = 1024$. Solid lines are the best-fit straight lines having slope 1.62 ± 0.02 (black solid line) for $\phi = 2^{-12}$ and 1.98 ± 0.03 (red dashed line) for $\phi = 2^{-3}$. (b) Plot of $\langle s_\phi(t)\rangle$ against t for $\phi = 2^{-8}$ with $L = 1024$.

the sandpile dynamics is able to recognize such a crossover only at $\phi = 2^{-12}$ (or $\sim 10^{-4}$). If the system size increases, this crossover is expected to appear in the sandpile dynamics for smaller values of ϕ, and it would be possible to measure both exponents in this regime as shown by the dashed line in Fig. 2.3(c). The avalanche area a displays a similar coexistence of scaling behavior over the same range of ϕ. For the regular lattice, τ_a is found 1.12 as per the reported value for the BTW model for finite systems[66]. However, for the random network, it is found that the value of $\tau_a = 1.5$ as does that of τ_s, on the random network. In the SWN regime, both scaling forms are found to coexist. This is also observed in the small-world sandpile model[180,181].

The coexistence of scaling is also verified for the conditional expectation value $\langle s_\phi(t)\rangle$. Its variation against t for $\phi = 2^{-12}$ and 2^{-3} is shown in Fig. 2.6(a) for $L = 1024$. The critical exponents γ_{st} are obtained as 1.62 ± 0.02 and 1.98 ± 0.03 for $\phi = 2^{-12}$ and $\phi = 2^{-3}$, respectively. Since on the regular lattice $\tau_s = 1.11$ and $\tau_t = 1.18$, the expected value of γ_{st} from the scaling relation, Eq. (2.11), is 1.63 on the regular lattice. Similarly for the random network, $\tau_s = 1.5$ and $\tau_t = 2$, the expected values of $\gamma_{st} = 2$ on the random network. The values of the critical exponents γ_{st} are within the error bars of the expected values. In Fig. 2.6(b), $\langle s_\phi(t)\rangle$ for $L = 1024$ is plotted against t for $\phi = 2^{-8}$. Two scalings of $\langle s_\phi(t)\rangle$ with t are shown by the solid back line and dashed red line, respectively, for $t < t_c$ and $t > t_c$. The coexistence scaling of $\langle s_\phi(t)\rangle$ is also observed for the same range of ϕ as observed for the avalanche size distribution.

Recall that in an SWN there exists the concept of neighbourhood, corresponding to a regular lattice, and at the same time, the shortest distance ℓ between two nodes is vanishingly small, corresponding to an random network. Because of the coexistence of the characteristics of a regular lattice as well as those of a random network in an SWN, the sandpile avalanches are segregated, according to their sizes, into two scaling forms. It should be emphasized here that such a coexistence of two scaling behaviors is also observed on SWNs generated by removing the bonds emanating from a site of a square lattice with probability ϕ and rewiring it to a randomly selected lattice site. However, contrary to the present observation, Arcangelis and Hermann[155] obtained a continuous crossover from BTW universality class to MF universality class in the study of a BTW-type sandpile dynamics on SWNs constructed by rewiring a fraction of a bond of a square lattice keeping the critical height the same for all nodes and having dissipation only at the lattice boundary. No coexisting region of both the scaling forms was observed in their study. On the other hand, in a study of the one-dimensional sandpile model on SWNs a transition from noncritical to critical regime was demonstrated by Lahtinen *et al.*[154].

2.5 Scaling of coexisting probability distributions

As per the scaling form of the characteristic avalanche area a_c, size s_c, lifetime t_c [obtained in Eqs. (2.12), (2.13), and (2.14), respectively], a general scaling of the characteristic property x_c with ϕ is assumed as

$$x_c(\phi) \approx \phi^{-\alpha_x}, \tag{2.15}$$

where α_xs corresponds to different characteristic exponents. The values of $x_c(\phi)$ on the regular lattice ($\phi = 0$), must correspond to the cutoff value of the distribution $P_x(x, 0)$ for a given system size L. As the network grows, the distribution $P_x(x, \phi)$ will develop a part corresponding to MF scaling. Consequently, the part representing BTW-type scaling will shrink. Hence, the value of x_c should decrease with increasing ϕ. Eventually, the value of x_c will be the one on the random network when $\phi = 1$. The existence of such a characteristic value of avalanche size as a function of ϕ was noticed in the sandpile dynamics on one-dimensional SWNs[154]. It is now possible to obtain a single probability distribution function for both scaling forms for the whole range of ϕ.

A new scaling form for the distribution functions with respect to the characteristic value $x_c(\phi)$ is now proposed as

$$P_x(x, x_c(\phi)) = \begin{cases} x^{-\tau_{1x}} \mathsf{f}_x\left(\frac{x}{x_c(\phi)}\right) & \text{for } x \leqslant x_c, \\ x^{-\tau_{2x}} \mathsf{g}_x\left(\frac{x}{x_c(\phi)}\right) & \text{for } x \geqslant x_c \ , \end{cases} \tag{2.16}$$

where f_x and g_x are two different scaling functions in two different regions and τ_{1x} and τ_{2x} are the corresponding critical exponents in the respective regions. Since at $x = x_c(\phi)$ the values of $P_x(x, x_c(\phi))$ are the same for both regions, one should have $\mathsf{f}_x(1) = \phi^{-(\tau_{1x}-\tau_{2x})\alpha_x} \mathsf{g}_x(1)$. The probability distribution then can be obtained in terms of a single scaling function, f_x or g_x, as

$$P_x(x, \phi) = \begin{cases} x^{-\tau_{1x}} \mathsf{f}_x(x\phi^{\alpha_x}) & \text{for } x \leqslant x_c, \\ x^{-\tau_{2x}} \phi^{-\Delta_x \alpha_x} \mathsf{f}_x(x\phi^{\alpha_x}) & \text{for } x \geqslant x_c \ , \end{cases} \tag{2.17}$$

where $\Delta_x = (\tau_{2x} - \tau_{1x})$. The ϕ independent scaling form can be obtained by rescaling the probability distribution as

$$P_x(x, \phi)\phi^{-\alpha_x \tau_{1x}} = \begin{cases} z_x^{-\tau_{1x}} \mathsf{f}_x(z_x) & \text{for } z_x \leqslant 1, \\ z_x^{-\tau_{2x}} \mathsf{f}_x(z_x) & \text{for } z_x \geqslant 1 \ , \end{cases} \tag{2.18}$$

where $z_x = x\phi^{\alpha_x}$ is a scaled variable. Such scaling behavior was also observed in the context of anomalous roughening of a fractured surface[182,183].

The above scaling forms are now verified. The rescaled probabilities $P_x(x, \phi)\phi^{-\alpha_x \tau_{1x}}$ are plotted against the scaled variable $z_x = x\phi^{\alpha_x}$ for s and t in Figs. 2.7(a) and 2.7(b), respectively, for the fixed system size $L = 1024$. It can be seen that a good data collapse is obtained for both s and t using $\alpha_s = 1.06$ and $\alpha_t = 0.65$. The critical exponents τ_x corresponding to two different regions are also verified. The straight lines with required slopes in the respective regions are guide for the eye. This confirms the proposed scaling form of the probability distribution functions on SWNs. Such coexistence scaling in the SWN regime has also been verified for a stochastic sandpile model[55,184].

Since the probability distributions are now represented by a single scaling form, the average avalanche properties can also be scaled in a similar fashion. For example, the average cluster size is now expected to scale as

$$\langle s_\phi(t) \rangle = t^{\gamma_{st}} f_{st}(t\phi^{\alpha_t}), \tag{2.19}$$

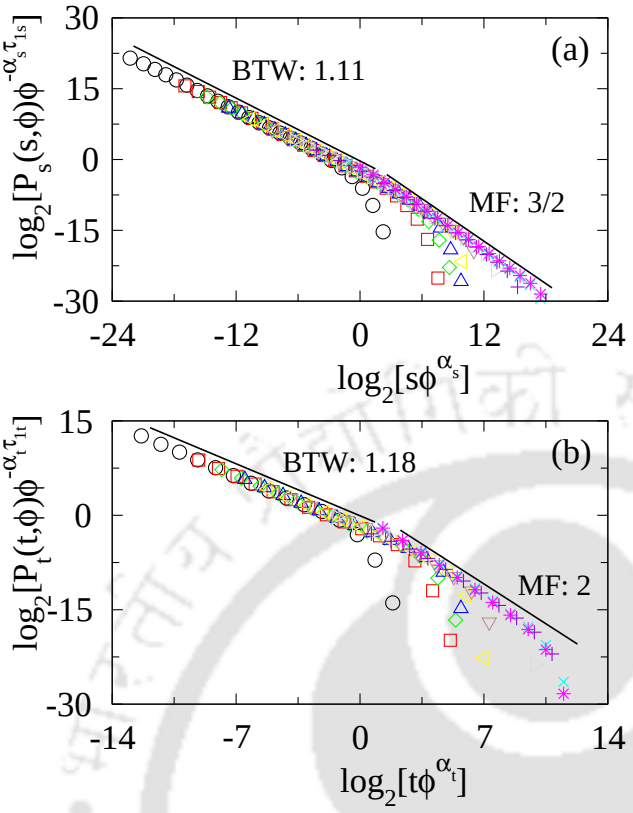

Figure 2.7: (a) Plot of scaled distribution $P_s(s,\phi)\phi^{-\alpha_s\tau_{1s}}$ against a scaled variable $z_s = s\phi^{\alpha_s}$ for $L = 1024$. (b) Plot of $P_t(t,\phi)\phi^{-\alpha_t\tau_{1t}}$ against $z_t = t\phi^{\alpha_t}$ for $L = 1024$. Different symbols correspond to different ϕ values: $\phi = 2^{-21}(\bigcirc)$, $2^{-16}(\square)$, $2^{-14}(\diamond)$, $2^{-12}(\triangle)$,$2^{-10}(\triangleleft)$, $2^{-8}(\triangledown)$, $2^{-6}(\triangleright)$, $2^{-4}(+), 2^{-1}(\times)$, $2^{0}(\divideontimes)$. Reasonable data collapse for both s and t is observed. Solid lines with respective slopes are guides for the eye.

where f_{st} is a new scaling function and the value of γ_{st} corresponds to that on regular lattices. The form of the scaling function is verified by plotting $\langle s_\phi(t)\rangle\phi^{\gamma_{st}\alpha_t}$ against the scaled variable $t\phi^{\alpha_t}$ for $L = 1024$ in Fig. 2.8 taking $\gamma_{st} = 1.63$. It is shown that there is a good data collapse and the scaling function represents two different scaling behaviors with two different exponents, 1.63 and 2, indicated by straight lines with the respective slopes. Such scaling behavior can also be obtained between avalanche size s and area a. Since $\alpha_a = 1$ and $\gamma_{sa} = 1.06$, the change in slope in the scaling function is difficult to observe in the numerical data collected here.

It is now important to understand the origin of coexistence of both critical behaviors of the avalanche properties on an SWN. Since for an avalanche property x there is BTW type scaling for $x < x_c$ and MF type scaling for $x > x_c$, it is intriguing to look into the avalanche cluster morphology for the avalanches following two different scaling behaviors.

2.6 Avalanche cluster morphology

Morphologies of avalanche clusters obtained in the steady state of the DDSM on SWNs corresponding to different ϕ values are shown in Fig. 2.9. These avalanches

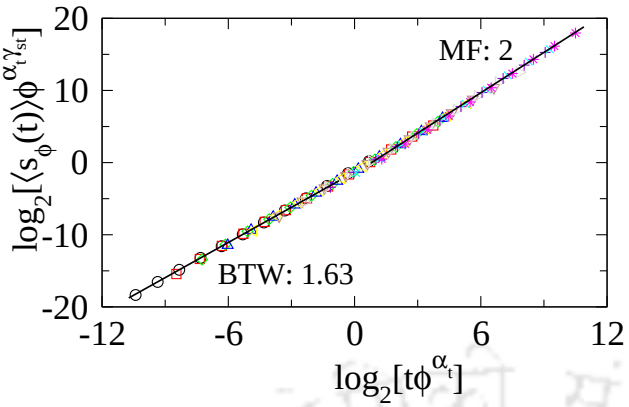

Figure 2.8: Plot of $\langle s_\phi(t)\rangle \phi^{\alpha_t \gamma_{st}}$ against a scaled variable $t\phi^{\alpha_t}$ for $L = 1024$. Symbols are the same as in Fig. 2.7. A good data collapse is observed. The two solid lines having slopes 1.63 and 2, indicating two different scaling forms, are guides for the eye.

are obtained on SWNs defined on a square lattice of size 512×512 for $\phi = 2^{-12}$, $\phi = 2^{-8}$, and $\phi = 2^{-3}$. Different colours correspond to different numbers of topplings of a node. A typical avalanche cluster in the regular lattice regime with $\phi = 2^{-12}$, is shown in Fig. 2.9(a). The avalanche cluster (of size $s = 63774$) is isotropic and mostly compact. It consists of concentric zones of lower and lower numbers of topplings around the node, with the maximum number of topplings (in purple) as expected for a BTW-type avalanche cluster[68,185,186]. A few clusters of compact structure appear here and there because in the presence of a small number of shortcuts in the system a few sand grains are transported to remote parts of the lattice. However, such a small distortion in the morphology of the avalanche cluster with respect to a single compact BTW-type cluster is not able to modify the scaling behavior.

In Fig. 2.9(b), a typical avalanche cluster ($s = 33567$) obtained on a random network corresponding to $\phi = 2^{-3}$ is shown. In this case, the avalanche cluster is completely scattered all over the network. A large number of shortcuts is added to the regular lattice to make it a random network and hence sand grains from a toppled node of a random network are transported to almost all other nodes in the network through the shortcuts. Compact BTW-type clusters are therefore found scattered all over the lattice or the network. Small patches of sites toppled only once are still present. As ϕ approaches 1, the size of these patches decreases.

The morphology of avalanche clusters of the DDSM on an SWN with intermediate ϕ is found to be either that of BTW-type clusters on a regular lattice or that of sparse clusters on a random network. Two such avalanche clusters on an SWN with $\phi = 2^{-8}$ are shown in Figs. 2.9(c) and 2.9(d). It is already seen that the avalanche clusters on SWNs with intermediate ϕ follow two different scaling forms, below and above a characteristic avalanche size s_c. For $\phi = 2^{-8}$, it is given by $s_c = \phi^{-1.06} \approx 360$. A cluster of size 352 ($< s_c$) is shown in Fig. 2.9(c) and a cluster

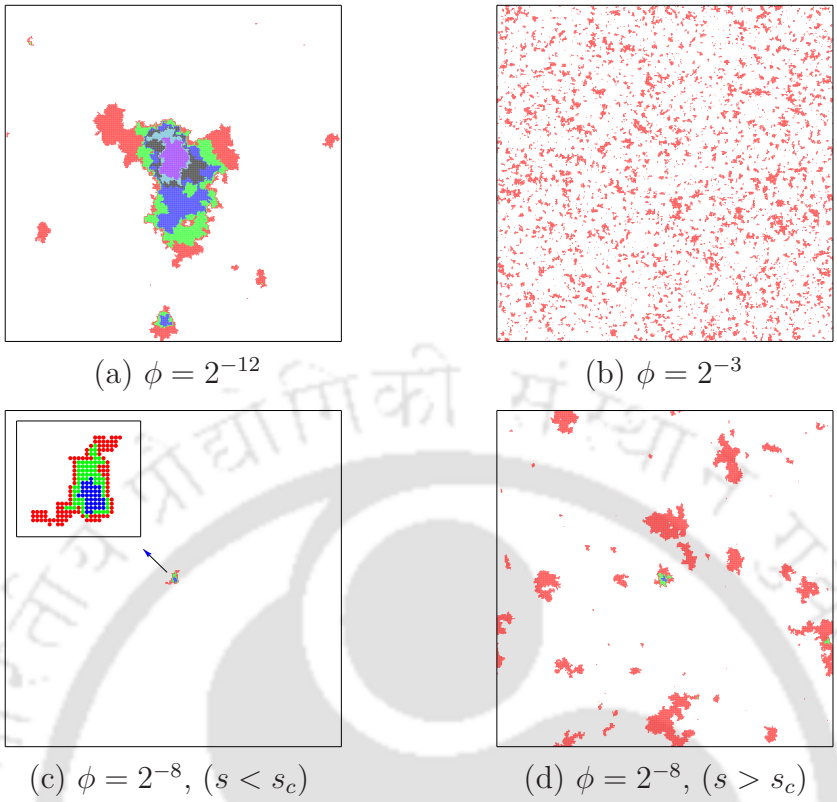

(a) $\phi = 2^{-12}$ (b) $\phi = 2^{-3}$

(c) $\phi = 2^{-8}$, $(s < s_c)$ (d) $\phi = 2^{-8}$, $(s > s_c)$

Figure 2.9: Morphology of avalanche clusters of the DDSM on SWNs generated on an $L = 512$ square lattice for different values of ϕ. (a) For $\phi = 2^{-12}$, almost a BTW-type cluster. (b) For $\phi = 2^{-3}$, an avalanche cluster on an random network completely scattered all over the lattice. (c) For $\phi = 2^{-8}$, a small avalanche cluster of a size (352) less than $s_c(\approx 360)$. Inset: Enlarged version of the same avalanche cluster. (d) For $\phi = 2^{-8}$, a large avalanche cluster [a different realization than (c)] of a size (16872) greater than s_c. Different colours correspond to different numbers of topplings of a node: red for 1, green for 2, blue for 3, black for 4, sky blue for 5, and purple for more than 5 topplings. No colour corresponds to nodes that did not topple at all during the avalanche. The black border represents the lattice boundary.

of size 16872 ($> s_c$) is shown in Fig. 2.9(d). The larger cluster in Fig. 2.9(d) is broken into patches consisting of nodes mostly toppled once and scattered over most of the network, whereas the smaller cluster in Fig. 2.9(c) is still isotropic and compact. An enlarged version of the small cluster is shown in the inset in Fig. 2.9(c). Therefore, on an SWN two types of clusters appear. The smaller compact clusters ($s < s_c$) naturally follow BTW-type scaling and the large sparse clusters ($s > s_c$) follow MF-type scaling. The coexistence of two scaling forms on an SWN is thus due to the presence of both the clusters on the same network. As ϕ decreases (goes toward regular lattice), s_c becomes larger and consequently all clusters are of the BTW type. On the other hand, as ϕ increases to 1 (random network), s_c decreases

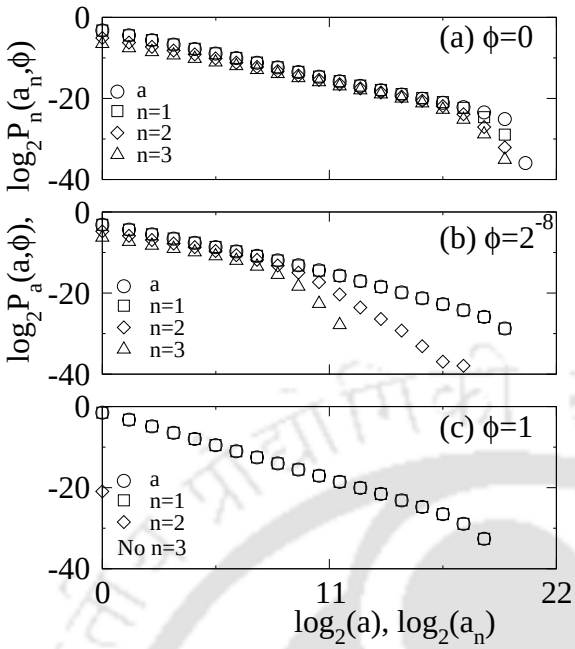

Figure 2.10: Plot of $P_a(a,\phi)$ and $P_n(a_n,\phi)$ for $n = 1, 2, 3$ on a double-logarithmic scale for different values of ϕ: (a) $\phi = 0$, (b) $\phi = 2^{-8}$, and (c) $\phi = 1$ for the system size $L = 1024$.

to 1 and all the clusters are sparse and scattered over all the nodes.

Sandpile dynamics then can be used as a useful tool to probe different length scales present in the underlying structure on which it is performed. Avalanches are expected to display appropriate scaling behaviors corresponding to different length scales.

2.7 Distribution of areas of various toppling sites

From the morphologies of avalanche clusters, it is seen that on regular lattices the avalanches consist of sites toppled multiple times, whereas on random networks they mostly consist of nodes toppled only once. On SWNs with an intermediate ϕ, clusters of both types appear. In order to understand the type of sites present in an avalanche, the distribution of area a_n of sites that are toppled a fixed n number of times should be analyzed. Such area distributions for the BTW model on regular lattices were found to obey power-law scaling with exponents close to that of the total area distribution exponent[187,188]. The idea of studying distributions of a_n is extended here to avalanches obtained on SWNs. The scaling behavior of the number of sites or nodes that toppled n times is then assumed to be

$$P_n(a_n,\phi) \approx a_n^{-\tau_a^{(n)}(\phi)}, \tag{2.20}$$

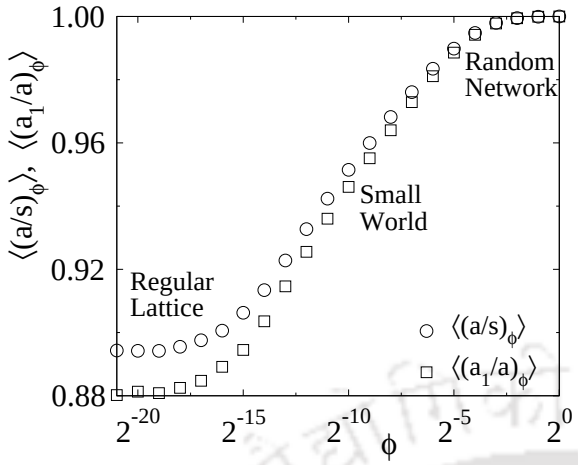

Figure 2.11: Plot of $\langle(a/s)_\phi\rangle$ (○) and $\langle(a_1/a)_\phi\rangle$ (□) against ϕ for the system size $L = 1024$.

where $n = 1, 2, 3, \cdots$ correspond to sites toppled only once, only twice, only three times, etc. In Fig. 2.10, distribution functions $P_n(a_n, \phi)$ corresponding to only one time (a_1), only two times (a_2), and only three times (a_3) are plotted and compared with the distribution of total area a for three values of ϕ: (a) $\phi = 0$, (b) $\phi = 2^{-8}$, and (c) $\phi = 1$ for $L = 1024$. On regular lattices, all three distributions are extended over a long range of a_n, almost as large as the total area a. The distribution of a_1 has an exponent $\tau_a^{(1)} = 1.12 \pm 0.01$, the same as for τ_a. As the network grows to an intermediate regime, say, for $\phi = 2^{-8}$, the distributions of a and a_1 are found to be almost the same for all values of area as shown in Fig. 2.10(b), whereas the distributions of a_2 and a_3 are shrunk toward smaller areas. It can also be noted that the distribution of a or a_1 has two different scaling forms corresponding to two different regimes, as it is seen in the case of the distribution of s and t [Fig. 2.4(a) and Fig. 2.4(b)]. For $\phi = 1$, the distribution of a_1 and that of a become inseparable as shown in Fig. 2.10(c) and they have the same distribution exponent, ≈ 1.5, as does the avalanche size s on a random network. This means that the avalanches consist of singly toppled nodes and the difference between the avalanche area a and the avalanche size s disappears. The distribution of a_2 decreases to a point and there is no node that has toppled three times or more. It can be noted that $a_2 = 1$; i.e., only one node has toppled twice. The probability of the occurrence of such an event is also very low, $P_2(a_2, \phi = 1) \approx 1/2^{20}$. It has already been noted that the possibility of the formation of a loop in a branching process of toppling events on a random network is vanishingly small and usually goes as $1/L^2$, the inverse of the number of nodes[68,153]. Thus the present observation is consistent with the prediction of the branching process.

Not only are the probability distributions of a and s the same, but also the

magnitudes of a and s are found to be same on random networks. This is verified by calculating the ratio $\langle (a/s)_\phi \rangle$ and $\langle (a_1/a)_\phi \rangle$ for several values of ϕ. The variation of $\langle (a/s)_\phi \rangle$ against ϕ is shown in Fig. 2.11 and compared with that of $\langle (a_1/a)_\phi \rangle$. It is shown that for $\phi \geq 0.1$, both ratios are 1. They decrease as ϕ decreases. For $\phi < 0.1$, the ratio $\langle (a/s)_\phi \rangle < 1$ indicates that $s > a$ and the ratio $\langle (a_1/a)_\phi \rangle < 1$ indicates that $a > a_1$. It can also be noted that $\langle (a/s)_\phi \rangle$ and $\langle (a_1/a)_\phi \rangle$ are the same for $\phi \geq 0.1$, whereas for $\phi < 0.1$ they are different.

2.8 Time autocorrelation of toppling waves

A toppling wave is the number of topplings during the propagation of an avalanche starting from a critical site without further toppling at the same site. Each toppling of the critical site creates a new toppling wave. The total number of topplings s in an avalanche can be considered as

$$s = \sum_{k=1}^{m} s_k, \tag{2.21}$$

where s_k is the number of topplings in the kth wave and m is the number of toppling waves in an avalanche. The time evolution of toppling dynamics then can be studied by coarsening the avalanches into a series of toppling waves[76,78]. The toppling waves generated in the BTW model on a regular lattice were found to be correlated[79–81]. As a consequence of this correlation in the toppling waves, it was observed that the model does not obey finite-size scaling (FSS)[82]. It is then interesting to study the time autocorrelation of the toppling waves for the DDSM on SWNs to get a limiting value of ϕ at which FSS would be obeyed for this model. Following Menech and Stella[79–81], a time autocorrelation function for an SWN with a given ϕ is defined as

$$C_\phi(t) = \frac{\langle s_{k+t} s_k \rangle - \langle s_k \rangle^2}{\langle s_k^2 \rangle - \langle s_k \rangle^2}, \tag{2.22}$$

where $t = 1, 2, \cdots$ and $\langle \cdots \rangle$ represents the time average. $C_\phi(t)$ is calculated for four values of ϕ — $\phi = 0$, $\phi = 2^{-13}$, $\phi = 2^{-8}$ and $\phi = 1$ — on a system of size $L = 1024$, generating 2×10^6 toppling waves in the steady state for each ϕ. $C_\phi(t)$ values obtained for the above ϕ values are plotted against t in Fig. 2.12. It can be seen that $C_\phi(t)$ in the DDSM on the original lattice ($\phi = 0$) is positive (shown by the black solid line) and hence, the toppling waves are highly correlated, whereas on random networks ($\phi = 1$), the values of $C_\phi(t)$ is always 0 and hence, toppling waves

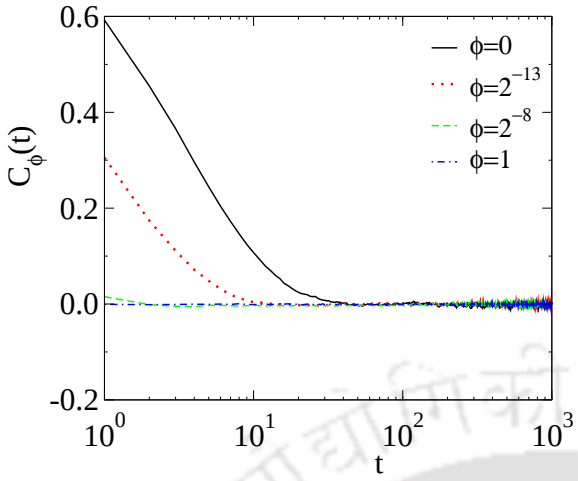

Figure 2.12: Plot of $C_\phi(t)$ against t for different values of ϕ: $\phi = 0$ (solid black line), $\phi = 2^{-13}$ (in dotted red line), $\phi = 2^{-8}$ (in dashed green line), and $\phi = 1$ (in blue dashed dotted line) for $L = 1024$.

are completely uncorrelated [shown by the dashed-dotted blue line]. As ϕ increases from 0 to 1, the strength of the positive correlation decreases, and it vanishes at $\phi \approx 0.1$, corresponding to the onset of a random network. Zero autocorrelation in the toppling waves on a random network is consistent with the fact that the avalanches on such a network consist of nodes mostly toppled only once. Since almost no node in an avalanche toppled twice, an avalanche is thus represented by a single toppling wave. The toppling wave time series then consists of a sequence of toppling numbers of a single toppling wave of independent avalanches. Hence, the toppling waves become uncorrelated. On the other hand, the toppling waves of the DDSM on a regular lattice remain correlated as in the case of the BTW. It should be emphasized here that Karmakar *et al.*[82] showed that the toppling wave correlation in the BTW-type sandpile model on a regular lattice is essentially due to the precise toppling balance. Though in the present model on random networks precise toppling balance is present in the toppling rule, the toppling waves become uncorrelated, because on random networks, the probability of the formation of a loop in the toppling sequence is vanishingly low and hence the concept of precise toppling balance become ineffective.

Since an avalanche cluster on a random network consists of a single toppling wave, the feedback to the original toppled node remains so low that in most cases it never becomes upper critical again. Hence, in the context of information propagation, the critical random network behaves like a one way network. May be due to the fact that the random network already behaves like a one-way network, so the sandpile on a directed SWN[189] is found to belong to the same MF universality class.

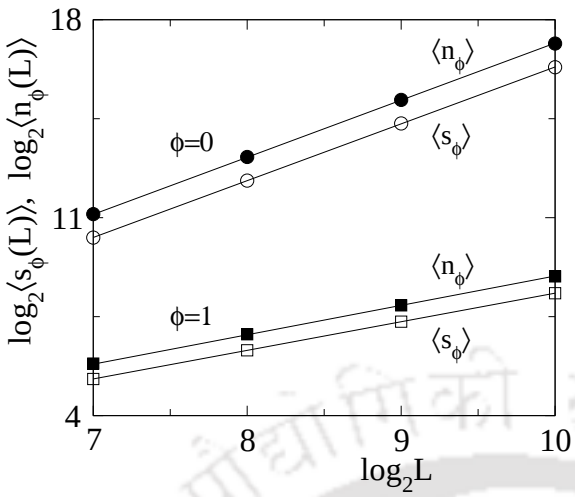

Figure 2.13: Average avalanche size $\langle s_\phi(L)\rangle$ (open symbols) and $\langle n_\phi(L)\rangle$ (filled symbols) plotted against system size L for $\phi = 0$ (circle) and $\phi = 1$ (square). The solid line through the circles has slope 2, and that through the squares has slope 1.

2.9 Diffusive to super diffusive sand transport

The critical behavior of sandpile models on regular lattices is believed to be governed by the diffusive sand transport during avalanches. Since the avalanche size (the total number of topplings) is equivalent to the number of steps required for a random walker starting from an arbitrary site to reach the lattice boundary of a regular lattice[177,190], it is now important to characterize their scaling behavior with lattice size (or number of nodes) on SWNs. For a given ϕ and system size L, the average number of steps $\langle n_\phi(L)\rangle$ required for a random walker to reach the lattice boundary starting from an arbitrary node of an SWN and the average avalanche size can be defined as

$$\langle n_\phi(L)\rangle = \int_0^{n_{max}} nP_{n,\phi}(n,L)dn \tag{2.23}$$

and

$$\langle s_\phi(L)\rangle = \int_0^{s_{max}} sP_{s,\phi}(s,L)ds \tag{2.24}$$

where $P_{n,\phi}(n,L)$ is the probability of finding a random walk with n steps that reaches the lattice boundary starting from an arbitrary node and $P_{s,\phi}(s,L)$ is the probability of having an avalanche of size s for the given ϕ and L. The scaling of $\langle n_\phi(L)\rangle$ and $\langle s_\phi(L)\rangle$ with L is assumed to be

$$\langle n_\phi(L)\rangle \sim L^{\sigma_n(\phi)} \quad \text{and} \quad \langle s_\phi(L)\rangle = L^{\sigma_s(\phi)}, \tag{2.25}$$

where $\sigma_n(\phi)$ and $\sigma_s(\phi)$ are two exponents. In order to verify such a scaling forms for $\langle n_\phi(L)\rangle$ and $\langle s_\phi(L)\rangle$, they are estimated as a function of L for $\phi = 0$ and $\phi = 1$. In Fig. 2.13, $\langle n_\phi(L)\rangle$ and $\langle s_\phi(L)\rangle$ are plotted against L in double logarithmic scale

for both the values of ϕ. The values of the exponents $\sigma_n(\phi)$ and $\sigma_s(\phi)$ are obtained as $\sigma_n = \sigma_s \approx 2$ for $\phi = 0$ and $\sigma_n = \sigma_s \approx 1$ for $\phi = 1$. The solid lines are guides for the eye with the respective slopes. Since at $\phi = 0$, both $\langle n_\phi(L)\rangle$ and $\langle s_\phi(L)\rangle$ scale as $\sim L^2$, the random walk and the sand transport both are of a diffusive nature, whereas at $\phi = 1$ they scale as $\sim L$, therefore they are of a superdiffusive nature. It is observed that the superdiffusive nature is sustained over the whole random network region $\phi \geq 0.1$. But the diffusive nature quickly dies out as the number of shortcuts increases in the system. For intermediate values of $0 < \phi < 0.1$, it was possible to estimate definite values of $\sigma_n(\phi)$ or $\sigma_s(\phi)$ because the data did not represent a linear relationship on the double-logarithmic scale. The curvature in the data is due to the fact that in the intermediate region of ϕ, both scaling forms of $P_s(s, \phi)$ coexist. Therefore a crossover from diffusive to super diffusive sand transport occurs as the regular lattice evolves to a random network. It can be seen that not only the scaling of $\langle n_\phi\rangle$ and $\langle s_\phi\rangle$ are same, but also the magnitude of $\langle n_\phi\rangle$ is just twice that of $\langle s_\phi\rangle$ for both $\phi = 0$ and $\phi = 1$ on a given L. On regular lattices it is already known that $\langle n_\phi\rangle = 2\langle s_\phi\rangle$ [176,177]. Such a relationship is then also valid on random networks. It is also interesting to note that the absolute value of $\langle s_\phi\rangle$ (or $\langle n_\phi\rangle$) is much smaller on random networks than on regular lattices for a given L. It can be recalled that the avalanches on random network consist of nodes that have toppled only once, whereas on regular lattices there exist sites that have toppled multiple times. The cutoff of the distribution $P_s(s, \phi)$ on random networks is much smaller than that on regular lattices (see Fig. 2.3). Therefore, on random networks the occurrence of an avalanche cluster with nodes toppled only once, consists of a single toppling wave, and superdiffusive sand transport during an avalanche all are interconnected phenomena.

Since the shortest distance ℓ between two nodes of an SWN follows two different scaling behaviors, given in Eqs. (2.1) and 2.2, it would be interesting to verify whether or not $\langle n_\phi(L)\rangle$ and $\langle s_\phi(L)\rangle$ follow a similar scaling behavior on SWNs. Following the scaling of $\langle \ell\rangle$ given in Eq. (2.2), general scaling forms of $\langle n_\phi(L)\rangle$ and $\langle s_\phi(L)\rangle$ are proposed as

$$\langle n_\phi(L)\rangle = L^2 \mathcal{G}(\phi^{1/2} L) \tag{2.26}$$

and

$$\langle s_\phi(L)\rangle = \frac{1}{2} L^2 \mathcal{G}(\phi^{1/2} L), \tag{2.27}$$

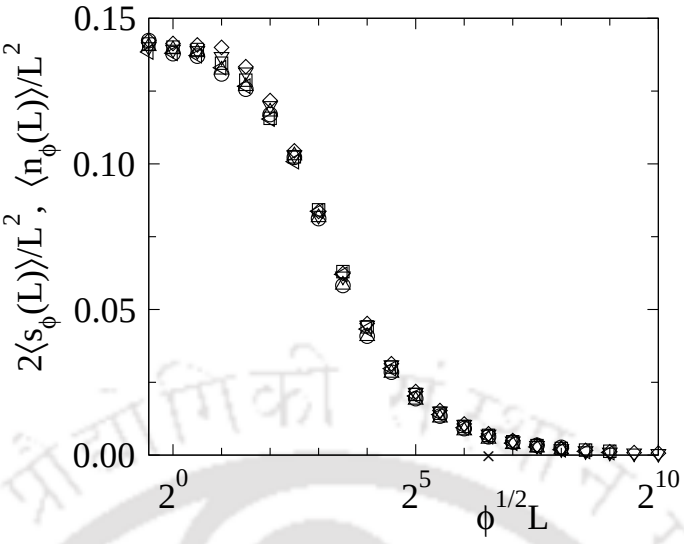

Figure 2.14: Plot of $2\langle s_\phi(L)\rangle/L^2$ and $\langle n_\phi(L)\rangle/L^2$ against the scaled variable $\phi^{1/2}L$. Different symbols for $\langle s_\phi(L)\rangle$ for different system size are: $\bigcirc$ for $L = 256$, $\square$ for 512 and $\diamond$ for 1024. For $\langle n_\phi(L)\rangle$ they are: $\triangle$ for $L = 256$, $\triangleleft$ for 512 and $\triangleright$ for 1024. A reasonable data collapse is observed.

where $\mathcal{G}(x)$ is a universal scaling function given by

$$\mathcal{G}(x) \propto \begin{cases} \text{constant}, & x \ll 1, \\ 1/x, & x \gg 1, \end{cases} \tag{2.28}$$

Verification of the above scaling form is performed by estimating $\langle n_\phi(L)\rangle$ and $\langle s_\phi(L)\rangle$ for different L values for the whole range of ϕ between 0 and 1. In Fig. 2.14, $\langle n_\phi(L)/L^2\rangle$ and $2\langle s_\phi(L)\rangle/L^2$ are plotted against the scaled variable $x = \phi^{1/2}L$. Reasonable data collapses are observed for both $\langle n_\phi(L)\rangle$ and $\langle s_\phi(L)\rangle$. It should be noted here that on a two-dimensional regular square lattice $\langle n_\phi\rangle \approx aL + bL^2$, where $a = 0.56$ and $b = 0.14$ for small L[177]. However, in the limit $L \to \infty$, such a scaling can be approximated as $\langle n_\phi(L)\rangle \approx 0.14L^2$. In the limit $\phi \to 0$, the scaling function approaches 0.14. On the other hand, the $1/x$ scaling would be valid on a random network, i.e., for $\phi \geq 0.1$. For the lowest lattice size the corresponding value of the scaled variable is marked by the cross on the horizontal axis, beyond which $1/x$ scaling is expected to be valid. It should also be noted here that the number of distinct nodes $S(n)$ visited by a random walker in n time steps on a one-dimensional SWN for a fixed L and ϕ represents a crossover in scaling from $S(n) \sim \sqrt{n}$ for $n \ll \xi^2$ to $S(n) \propto n$ for $n \gg \xi^2$[191–193].

2.10 Finite-size scaling of distribution function

Since SWNs are generated on finite systems of size L with a given ϕ, the probability distributions of avalanche quantities should depend on L. The scaling form of the distribution function is assumed to be

$$P_{x,\phi}(x, L) = x^{-\tau_x(\phi)} f_x[x/L^{D_x(\phi)}], \tag{2.29}$$

where $x \in \{s, a, t\}$, f_x is an L dependent scaling function and $D_x(\phi)$ is the capacity dimension of the avalanche property x on an SWN with a given ϕ. It was observed that the avalanche properties like s and t of BTW-type models do not follow the FSS ansatz on regular lattices[64,65,175]. In the following, the FSS analysis is performed for s and t on random networks as well as on SWNs employing moment analysis[64,65,82,175]. The average qth moment of an avalanche property x for a given ϕ can be obtained as

$$\begin{aligned} \langle x^q_\phi(L)\rangle &= \int_0^{x_{max}} x^q P_{x,\phi}(x, L)dx \\ &= \int_0^{x_{max}} x^{q-\tau(\phi)} f_x[x/L^{D_x(\phi)}]dx. \end{aligned} \tag{2.30}$$

Hence, the system size dependences of $\langle s^q_\phi(L)\rangle$ and $\langle t^q_\phi(L)\rangle$ are expected to be

$$\langle s^q_\phi(L)\rangle \sim L^{\sigma_s(q,\phi)} \quad \text{and} \quad \langle t^q_\phi(L)\rangle \sim L^{\sigma_t(q,\phi)}, \tag{2.31}$$

where

$$\sigma_x(q, \phi) = [q + 1 - \tau_x(\phi)]D_x(\phi). \tag{2.32}$$

for $x \in \{s, t\}$ and $q = 1$ corresponds to the average values of the respective avalanche properties such as $\langle s_\phi\rangle$ and $\langle t_\phi\rangle$. For $P_{x,\phi}(x, L)$ to obey FSS for a given ϕ value, the moment exponent $\sigma_x(q, \phi)$ should have a constant gap between two successive values of q, i.e., $\sigma_x(q + 1, \phi) - \sigma_x(q, \phi) = D_x(\phi)$, for the respective ϕ value. For avalanche properties it was usually found that the gap converges to the respective capacity dimension as $q \to \infty$. In order to determine $D_s(\phi)$ and $D_t(\phi)$, sequences of exponents $\sigma_s(q, \phi)$ and $\sigma_t(q, \phi)$ are obtained for 400 equally spaced values of q between 0 and 4 for several ϕ values. The constant gap between two successive $\sigma_x(q, \phi)$s is then verified by estimating the slope $\partial\sigma_x(q, \phi)/\partial q$ using the finite-difference method.

For $\phi < 0.1$, the finite differences $\partial\sigma_s(q, \phi)/\partial q$ and $\partial\sigma_t(q, \phi)/\partial q$ for the sequences of both $\sigma_s(q, \phi)$ and $\sigma_t(q, \phi)$ did not converge to any finite value up to $q = 4$. Hence,

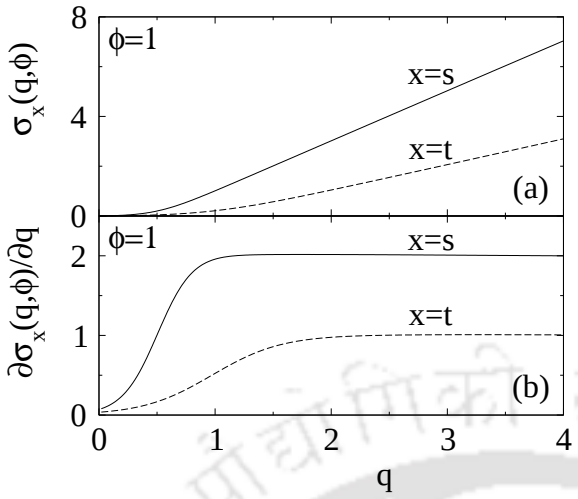

Figure 2.15: (a) $\sigma_x(q,\phi)$ for $x = s$ (solid line) and $x = t$ (dashed line) are plotted against q for $\phi = 1$. (b) $\partial\sigma_x(q,\phi)/\partial q$ plotted against q for $\phi = 1$. It converges to 2 for $x = s$ and to 1 for $x = t$.

$P_{x,\phi}(x, L)$, $x \in \{s, t\}$, does not the follow FSS ansatz in the SWN regime. Note that on SWNs both scaling coexist. Since $P_{x,\phi}(x, L)$ for $x < x_c$ does not follow FSS, the distribution functions for the full range of x are expected not to follow FSS.

For $0.1 \leq \phi \leq 1$, FSS is expected to be valid and it is verified for several values of ϕ in this region. Data for $\phi = 1$ are presented here. The variation of $\sigma_s(q,\phi)$ and $\sigma_t(q,\phi)$ for $\phi = 1$ is plotted against moment q in Fig. 2.15(a) and that of $\partial\sigma_s(q,\phi)/\partial q$ and $\partial\sigma_t(q,\phi)/\partial q$ against moment q are shown in Fig. 2.15(b). It can be seen that for $\phi = 1$ the derivatives saturate to $D_s \approx 2$ and $D_t \approx 1$ for higher values of q. The value of D_s for $\phi = 1$ is expected to be 2 because on random networks all avalanches are constituted of nodes toppled only once; that is, the avalanche area and avalanche size show no difference. On the other hand, the value of D_t for $\phi = 1$ is expected to be 1 because on random networks all avalanches are constituted of single-toppling wave, that is to say the number of parallel updates in a single toppling wave is proportional to the system size L [see Fig. 2.3(b)]. On the regular lattice it was known that $D_s/D_t = \gamma_{st}$. Such a scaling relation is also valid on random networks. Since $D_s = 2$ and $D_t = 1$ for $\phi = 1$, the value of γ_{st} is expected to be 2 as estimated in Sec. V. For $q = 1$ and $\phi = 1$, the scaling relations $\sigma_s = (2 - \tau_s)D_s$ and $\sigma_t = (2 - \tau_t)D_t$ are expected to be satisfied. Since $\tau_s = 3/2$ and $D_s = 2$ for $\phi = 1$, the value of σ_s must be 1 as measured on random networks. Similarly, from the other scaling relation σ_t for $q = 1$ is expected to be 0 because $\tau_t = 2$. Numerically a small finite value of σ_t for $q = 1$ is estimated. However, for $q = 2$, $\sigma_t = 1$ as expected.

Finally, the scaling function forms of $P_{s,\phi}(s, L)$ and $P_{t,\phi}(t, L)$ for $\phi = 1$ on random networks are verified by data collapse. In Fig. 2.16(a), the scaled probability distribution $P_{s,\phi}(s, L)L^{D_s\tau_s}$ for $\phi = 1$ is plotted against the scaled variable s/L^{D_s} taking

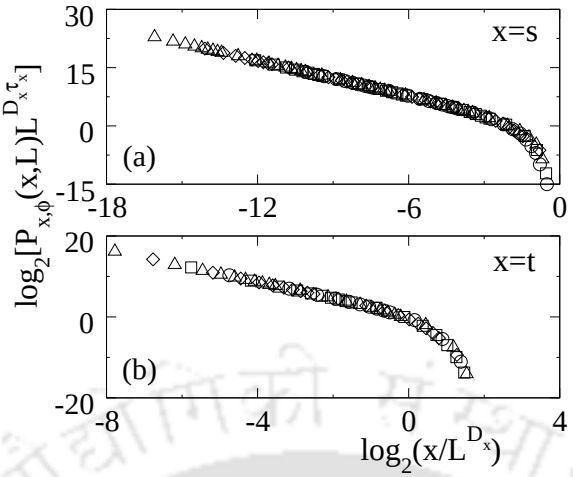

Figure 2.16: Plot of scaled distribution $P_{x,\phi}(x,L)L^{D_x\tau_x}$ against the scaled variable x/L^{D_x} for (a) $\phi = 1$ for $x = s$ and (b) $\phi = 1$ for $x = t$. Different symbols correspond to different system sizes: $L = 128(\bigcirc), 256(\square)$, $512(\diamond)$, and $1024(\triangle)$. A reasonable data collapse is obtained for both s and t.

$\tau_s = 3/2$ and $D_s = 2$ as for the random network. In Fig. 2.16(b), $P_{t,\phi}(t,L)L^{D_t\tau_t}$ for $\phi = 1$ is plotted against the scaled variable t/L^{D_t} taking $\tau_t = 2$ and $D_t = 1$ as for the random network. It is shown that a reasonable data collapse is obtained for random networks generated for four different system sizes, $L = 128, 256, 512$, and 1024. The assumed FSS form of $P_{x,\phi}(x,L)$ on the random network is then rightly chosen. Therefore, FSS would be valid even for a sandpile model with deterministic and conservative toppling rules along with complete toppling balance if it is defined for a system in which the concept of neighbourhood does not exist and there is long distance connectivity.

2.11 Conclusion

The critical properties of a generalized deterministic dissipative sandpile model constructed on SWNs is studied in this chapter. Apart from the BTW-type correlated scaling for $\phi \lesssim 2^{-12}$, two important characteristic features of the DDSM are identified and characterized. First, the DDSM on SWNs ($2^{-12} < \phi < 0.1$) exhibits two scaling behaviors simultaneously. One is BTW-type scaling on regular lattice and the other is MF scaling on random network corresponding to the existence of strong neighbourhoods such as those of regular lattice as well as a vanishingly small shortest distance between two nodes as for random network on an SWN. It was possible to identify a characteristic value of every avalanche property around which a new

coexistence scaling of probability distribution functions is proposed and numerically verified. The avalanche clusters following BTW scaling are found to be compact BTW-type clusters, whereas those following MF scaling are found to be sparse and scattered all over the network. Since avalanche clusters segregate according to the length scales of the SWN, sandpile dynamics can be used as a probe to identify different length scales present in the underlying structure on which it is performed. Second, FSS is found to be valid for the DDSM on random networks ($0.1 \leq \phi \leq 1$), contrary to the fact that the DDSM does not follow FSS on regular lattice or on SWN. The validity of FSS on random network for the DDSM is due to the fact that the avalanches on random network consist of nodes toppled only once. The probability of appearance of a node that has toppled more than once is vanishingly small on random network as the number of nodes $N \to \infty$. As a consequence, precise toppling balance becomes ineffective and toppling waves become uncorrelated. Because of the presence of long-distance connections, sand transport becomes superdiffusive on random network though it is diffusive on regular lattice. Superdiffusive sand transport is found to be essential in order to satisfy FSS relations. BTW-type correlated sandpile models then will also follow FSS if they are studied on systems without a spatial structure and having long distance connections. Therefore, as the shortcut density ϕ is tuned from 0 (regular lattice) to 1 (random network) through a series of SWN structures, the system exhibits a varying self-organizing critical behaviour. This could be considered as a novel technique to control SOC on SWN.

Chapter 3

Dissipative stochastic sandpile model on small-world networks

As small-world network (SWN) is found to have immense impact on the scaling behaviour of a BTW type deterministic model (previous chapter), it is intriguing to develop a dissipative stochastic sandpile model and study its critical behaviour on SWN varying the shortcut density ϕ. Since randomness or stochasticity is inherent in many natural processes, it should be incorporated in a sandpile model keeping realistic sandpile in mind. Introducing stochasticity in the relaxation processes, one of the important sub-classes of sandpile model has been developed which is commonly known as Stochastic sandpile model (SSM) or Manna model[178]. The original model developed by Manna[55] suffers lacking of abelian property as it redistributes all the sand grains to the randomly chosen nearest neighbours from a toppled site. However, abelian property can be restored in Dhar's version of the model[56] where only two particles are distributed to the randomly chosen nearest neighbours from a toppled site. The stochasticity in the relaxation processes eventually breaks the precise toppling balance and the model generates uncorrelated toppling waves[82], and consequently, the model follows finite-size scaling (FSS)[175]. Not only SSM shows robust scaling behaviour than the deterministic BTW model, it is also able to explain certain experimentally observed avalanche behaviour[52]. SSM and its variants (like stochastic parallel Zhang (SPZ) model[195]) are found to be the most studied models in various dimensions in SOC literature[67,74,196]. SPZ model was specially stuied in the contex of neuronal avalanches on the Newman-Watts small-world networks and multiple scaling, stochastic and MF, were reported[197]. However, there

This chapter is based on the Ref. [194]; H. Bhaumik and S. B. Santra, Physica A 511,358 (2018).

are not many studies that report the detail analysis of scaling behaviour of the SSM on a small-world network (SWN) and the effect of dimensionality on the critical behaviour of SSM on SWN. The study of a stochastic sandpile model on SWN and verification of the scaling theory developed in the previous chapter is then important and intriguing. In this chapter a dissipative version of the such a model, dissipative stochastic sandpile model (DSSM) is studied on SWN generated on both one and two dimensional regular lattices. Various scaling forms of such a model are developed and numerically verified. Results are compared with those of the dissipative BTW type model discussed in the previous chapter.

3.1 The Model: DSSM on SWN

SWN is generated both on a one dimension (1d) linear lattice and on a two dimension (2d) square lattice by adding shortcuts between any two randomly chosen lattice sites which will be referred to as nodes later on. The shortcut density ϕ is defined as the number of added shortcuts N_ϕ per existing bond (dL^d bonds are present in a d-dimensional lattice of linear size L with periodic boundary conditions (PBC) and without shortcuts) and is given by $\phi = N_\phi/(dL^d)$. Care has been taken to avoid self-edges of any node and multi-edges between any two nodes. To study sandpile dynamics on an SWN, first an SWN is generated for a particular value of ϕ and it is then driven by adding sand grains, one at a time, to randomly chosen nodes. If the height h_i of the sand column at the ith node becomes greater than or equal to the predefined threshold value h_c, which is equal to 2 here, then the ith node topples and the height of the sand column of the ith node will be reduced by h_c. The sand grains toppled are then distributed among two of its randomly selected adjacent nodes which are connected to the toppled node either by shortcuts or by nearest-neighbour bonds. During distribution of the sand grains PBC is applied. Hence, there is no open boundary in the system where dissipation of sand grains could occur. A dissipation factor ϵ_ϕ is then introduced during transport of a sand grain from one node to another to avoid overloading of the system. The toppling rule of the ith critical node in this DSSM on SWN then can be represented as

$$\begin{aligned} & h_i \to h_i - h_c, \\ \text{and} \quad & h_j = \begin{cases} h_j & \text{if } r \le \epsilon_\phi, \\ h_j + 1 & \text{otherwise} \end{cases} \end{aligned} \tag{3.1}$$

ϕ	ϵ_ϕ	
	$d = 1, L = 8192$	$d = 2, L = 1024$
0	8.94×10^{-8}	6.83×10^{-6}
2^{-9}	5.10×10^{-7}	6.34×10^{-5}
2^{-8}	9.72×10^{-7}	9.12×10^{-5}
2^{-7}	1.81×10^{-6}	1.34×10^{-4}
2^{-6}	3.60×10^{-6}	1.99×10^{-4}
2^{-5}	7.10×10^{-6}	2.96×10^{-4}
1	1.27×10^{-4}	2.06×10^{-3}

Table 3.1: Dissipation factor ϵ_ϕ for selected values of ϕ on 1d lattice of $L = 8192$ and 2d square lattice of size $L = 1024$.

where j is two randomly and independently selected nodes of k_i adjacent nodes of the ith node, and r is a random number uniformly distributed over $[0, 1]$. In this distribution rule, an adjacent node may receive both the sand grains. If the toppling of a node causes some of the adjacent nodes to be unstable, subsequent toppling follows on these unstable nodes. The process continues until there is no unstable node present in the system. These toppling activities lead to an avalanche. During an avalanche no sand grain is added to the system.

For a given SWN, ϵ_ϕ is taken as $1/\langle n_\phi \rangle$, where $\langle n_\phi \rangle$ is the average number of steps required for a random walker to reach the lattice boundary (without PBC) starting from an arbitrary lattice site. There exits a characteristic length $\xi \sim \phi^{-1/d}$ where d is the dimensionality of the lattice, below which SWN belongs to the "large world", the regular lattice regime, and beyond which it behaves as "small world", the random network regime[138–140]. The asymptotic behaviour of $\langle n_\phi \rangle$ with ϕ and L is given by

$$\langle n_\phi \rangle \sim \begin{cases} L^2, & \phi \to 0 \\ L\phi^{-1/d}, & \phi \to 1 \end{cases} \tag{3.2}$$

for a d-dimensional SWN. It has diffusive behaviour for $\phi \to 0$ and super-diffusive behaviour for $\phi \to 1$. The above scaling form is numerically verified in chapter 2. The dissipation factor $\epsilon_\phi = 1/\langle n_\phi \rangle$ for a given ϕ is determined using numerically estimated values of $\langle n_\phi \rangle$. A few values of ϵ_ϕ are listed in Table. 3.1 for 1d and 2d lattices.

3.2 Numerical simulations and steady state

Extensive computer simulations are performed to study the dynamics of DSSM on SWN for various values of ϕ and system sizes L both in 1d and 2d. For 1d, L is varied from 1024 to 8192, whereas for 2d, L is varied from 128 to 1024 in multiples of 2. For a given ϕ, starting from the empty configuration of h_i (i.e., $h_i = 0 \; \forall \; i$), sand grains are added at random positions. The average height of the sand column $\langle h \rangle = \sum_0^{L^d} h_i/L^d$ for three different values of ϕ are plotted against number of avalanches in Figs. 3.1(a) and 3.1(b) for 1d and 2d respectively. It can be observed that after a transient period the system evolves to a steady state which corresponds to equality of current of sand influx (due to adding sand) and current of sand outflux (due to dissipation of sand). Such balance of sand influx and outflux maintains the system in a critical steady state. Critical properties of DSSM on SWN are characterized studying various properties of avalanche like size s (total number of toppling in an avalanche), area a (number of distinct sites toppled in an avalanche), etc., in the steady state at different values of shortcut density ϕ. For a given L and ϕ, data are averaged over 32×10^6 avalanches (collected in the steady state) on 32 different SWN configurations. The information of an avalanche is kept by storing the number of toppling of every node in an array $S_\phi[i], i = 1, \cdots, L^d$ which was set to zero initially. All geometrical properties of an avalanche such as avalanche size s, avalanche area a, etc., can be estimated in terms of $S_\phi[i]$ as

$$s = \sum_{i=1}^{L^d} S_\phi[i], \quad a = \sum_{i=1}^{L^d} 1 \tag{3.3}$$

for all $S_\phi[i] \neq 0$.

3.3 Results and discussion

The critical properties of stochastic sandpile model are already known on regular lattice ($\phi = 0$)[65,67,74] as well as on random networks ($\phi = 1$)[197]. In this chapter, the critical behaviour of DSSM on small world regime ($2^{-12} \leq \phi \leq 0.1$) will be addressed. Limiting behaviour of such result would confirm the results corresponding to $\phi = 0$ and $\phi = 1$. However, a detailed finite- size analysis of the model for extreme values ϕ will be provided in the next chapter.

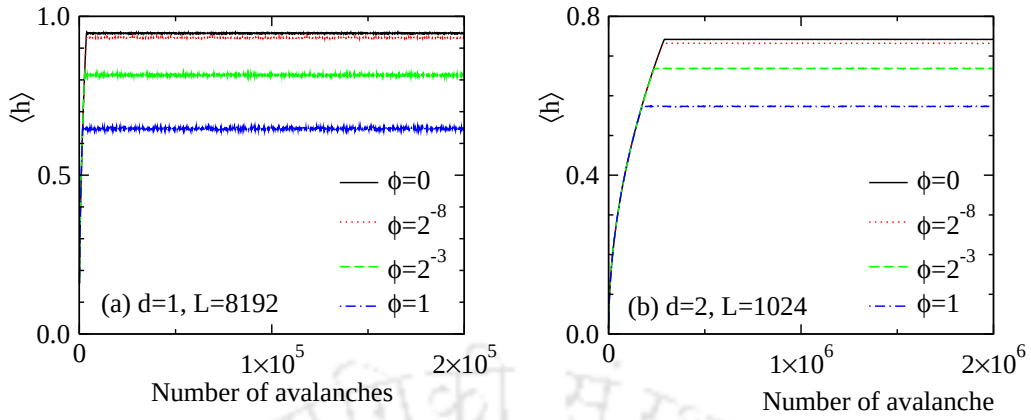

Figure 3.1: Plot of $\langle h \rangle$ against the number of avalanches for different values of ϕ : 0 (solid black line) , 2^{-8} (dotted red line), 2^{-3} (dashed green line), and 1 (blue dotted dashed line) for 1d with $L = 8192$ in (a), and for 2d with $L = 1024$ in (b).

3.3.1 Toppling surface: fragmentation, compactness, and fluctuation

In order to characterize various geometrical properties of avalanche one needs to visualize the avalanche in a suitable parameter space. The values of the toppling number $S_\phi[i]$ of an avalanche at different nodes of SWN define a surface called toppling surface[83] which not only serves as an important quantity to visualize an avalanche but also presents important scaling behaviour of several geometrical properties of the avalanche[85,198]. For an intermediate value of ϕ (SWN regime), the toppling surfaces of DSSM for both 1d and 2d are presented in Fig. 3.2 for various avalanches of different area and sizes. The upper panel corresponds to the toppling surfaces on 1d for $L = 256$ and $\phi = 2^{-6}$, and the lower panel represents those on a 2d square lattice of size $L = 256$ and $\phi = 2^{-8}$. The toppling surfaces are now analyzed mapping them on the underlying RL and ignoring the shortcuts. Since the avalanche clusters are occurring on a network, it might be sparse in the sense that different parts of the same cluster are separated by an Euclidean distance greater than the lattice spacing. A cluster is said to be compact if all the toppled sites are only separated by nearest neighbour lattice spacing. Otherwise the cluster will be called sparse or fragmented. It can be seen that for both 1d and 2d, the avalanches of smaller area are compact as those are confined in a length scale where SWN behaves as a regular lattice. The avalanches of intermediate area and sizes are found to be sparse as those avalanches are exposed to the network. The avalanches of area comparable to system size in 1d are also found compact (see Fig. 3.2(b)) whereas those in 2d still remain sparse (see Fig. 3.2(f)). Hence, not only the characteristic

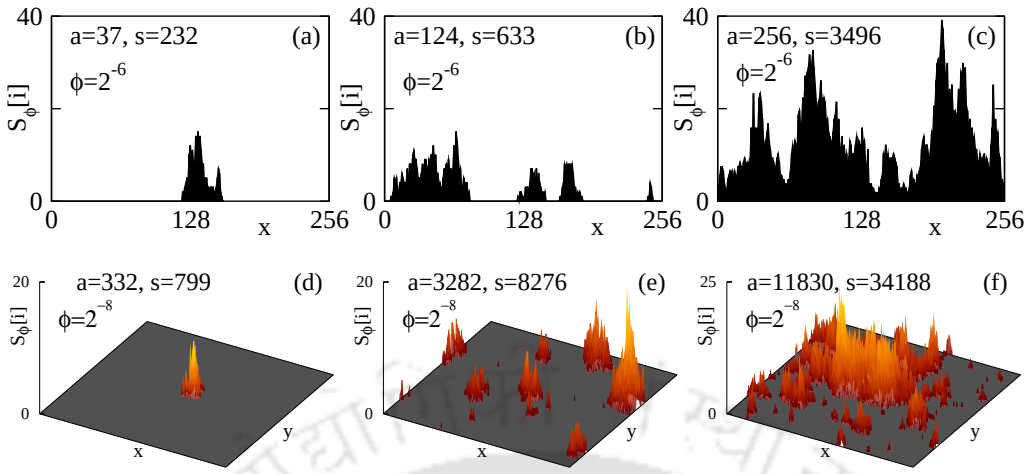

Figure 3.2: Toppling surfaces of various avalanche clusters of different avalanche area (a) and sizes (s) in the SWN regime are shown. Toppling surfaces on 1d lattice of $L = 256$ and $\phi = 2^{-6}$ are presented in the upper panel and those on 2d square lattice of size $L = 256$ and $\phi = 2^{-8}$ are presented in the lower panel. The values of s and a are mentioned as legends in the respective plots.

behaviour of avalanches are different for different values of avalanche size s, but also they differ considerably on different dimensions.

As the avalanches are compact single cluster with no fragmentation on regular lattice and fragmented in several sub-cluster on random network (see Fig. 3.2), the compactness of an avalanche need to be studied. If an avalanche of size s is fragmented into N_f number of fragments with area a_f of the fth fragment, then the compactness C_s and the fluctuation in fragment area, χ_s, can be defined as

$$C_s = \left\langle \frac{1}{N_f} \right\rangle_s , \qquad \chi_s = \left\langle \left[1 - \frac{\langle a_f \rangle^2}{\langle a_f^2 \rangle} \right] \right\rangle_s \tag{3.4}$$

giving $C_s = 1$ and $\chi_s = 0$ for $N_f = 1$ (no fragmentation) and $C_s \to 0$ and $\chi_s \to 1$ for large N_f. For SWN regime, C_s and χ_s are plotted in Figs. 3.3(c) and 3.3(d) for 1d and 2d respectively. It can be seen that there exists three different regimes of avalanche size s in 1d and two such regimes in 2d where both C_s and χ_s display different characteristic behaviour with s. Such regimes are identified by the dashed lines at the tentative crossover sizes s_1 and s_2, marked by crosses in Fig. 3.3, which will be estimated later. Both in 1d and 2d, C_s in the region $s_1 < s < s_2$, is quite low, less than 0.20. Hence an avalanche cluster on an average is fragmented at least into five pieces. These clusters are called sparse. Similarly, χ_s attains a high value and remains more or less constant till $s \approx s_2$. For the avalanches of size $s < s_1$,

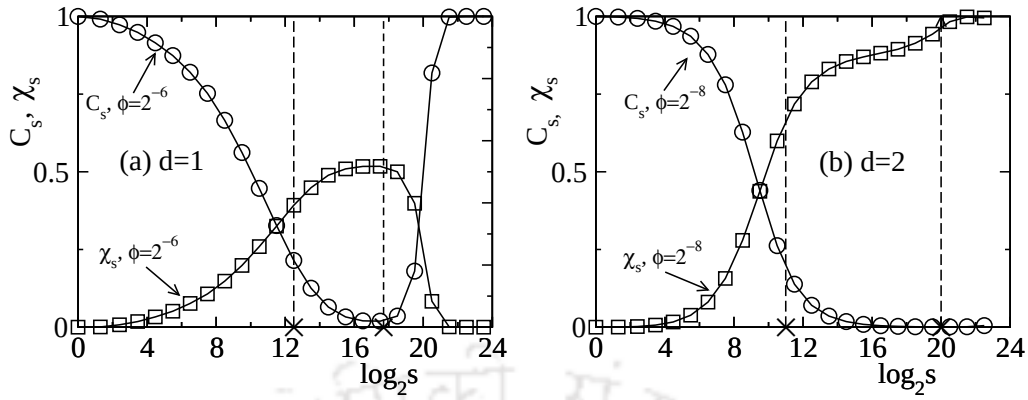

Figure 3.3: Plot of C_s (○) and χ_s (□) against s in semi-logarithmic scale for 1d in (a) and for 2d in (b). Data for 1d are collected for $\phi = 2^{-6}$ on the system size $L = 8192$, whereas, that for 2d are collected for $\phi = 2^{-8}$ and $L = 1024$. Vertical dashed lines in each figure represent tentatively crossover sizes.

C_s is high between 1 and 0.20 indicating a compact avalanche. Consequently, χ_s is small. Whereas for the avalanches of size $s > s_2$, the behaviour of C_s and χ_s are very different in 1d and 2d. For 1d, C_s starts increasing with s and attains 1 and at the same time χ_s goes to zero. The avalanches then become a single compact avalanche again (see, Fig. 3.2(c)) whereas, in 2d, C_s is close to zero and χ_s is almost one. It suggests that in 2d avalanches are not only fragmented but also the fragments have high fluctuation in their masses. These are consistent with the toppling surface presented in Fig. 3.2(f). Usually on regular lattice ($\phi = 0$), the avalanches are trivially found to be compact but on the random network ($\phi = 1$), they are found to be fragmented.

3.3.2 Conditional expectation and scaling

In order to characterize the toppling surface quantitatively, average height S_s and area $\langle a_s \rangle$ of the toppling surfaces are studied as a function of the avalanche size s. The average area $\langle a_s \rangle$ of an avalanche of fixed size s is defined as

$$\langle a_s \rangle = \int a P(a|s) da \sim s^{\gamma_{as}} \tag{3.5}$$

where $P(a|s)$ is the conditional probability for an avalanche of area a and size s to appear[68] and γ_{as} is an exponent. The average height $\langle S_s \rangle$ of a toppling surface is defined as,

$$\langle S_s \rangle = \left\langle \frac{1}{a_s} \sum_{i=1}^{a_s} S_\phi[i] \right\rangle = \frac{s}{\langle a_s \rangle} \sim s^{\gamma_S} \tag{3.6}$$

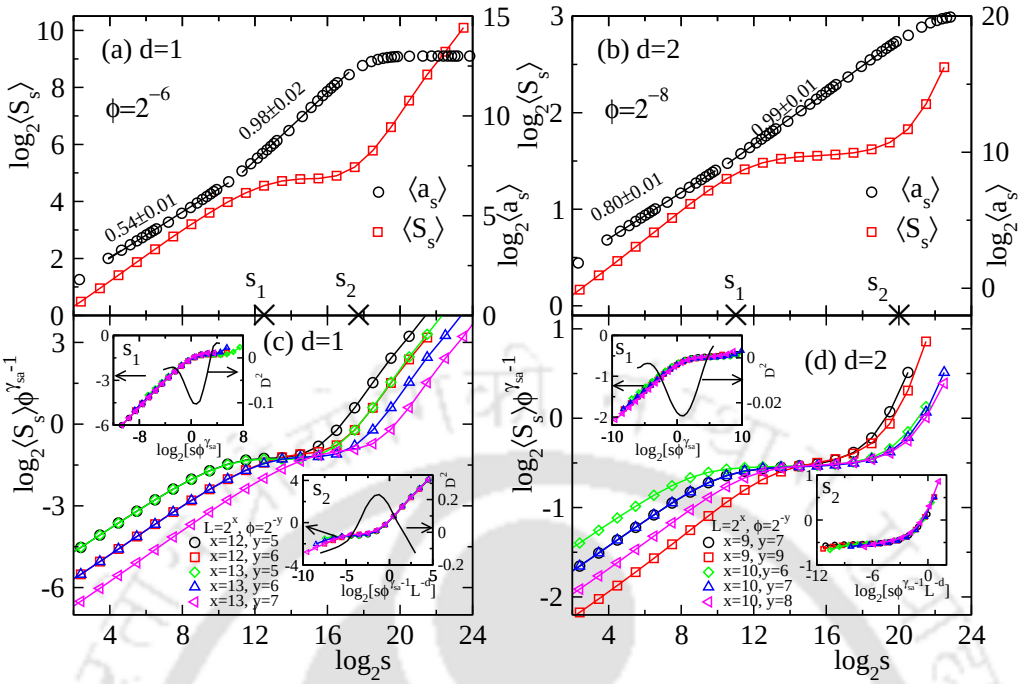

Figure 3.4: Plot of $\langle a_s \rangle$ against s (black circle) and $\langle S_s \rangle$ against s (red square) for 1d in (a) and for 2d in (b). Data for 1d are collected for $\phi = 2^{-6}$ and $L = 8192$, whereas, that for 2d are collected for $\phi = 2^{-8}$ and $L = 1024$. The rescaled S_s, $\langle S_s \rangle \phi^{\gamma_{sa}-1}$ is plotted against s for various values of ϕ and L (see legend) in (c) for 1d and in (d) for 2d. Insets: $S_s \phi^{\gamma_{sa}-1}$ is plotted is plotted against scaled s_1 and s_2. Solid curve in each inset represents the double derivative of the scaled function against its argument.

where $\gamma_S = 1 - \gamma_{as}$ is a new exponent and the average is over different avalanches of fixed size s but of different area a_s for a given ϕ.

In the SWN regime, for a given system size L and shortcut density ϕ, the estimated values of $\langle S_s \rangle$ and $\langle a_s \rangle$ are plotted against s in Figs. 3.4(a) and 3.4(b) for 1d and 2d respectively. The values of γ_{as} are measured by linear least square fit through the data points of $\langle a_s \rangle$ for different region of s. For the avalanches of size $s < s_1$, it is found that $\gamma_{as} = 0.54 \pm 0.01$ in 1d and 0.80 ± 0.01 in 2d in close agreement with the known values of γ_{as} for SSM on regular lattice as $\gamma_{as} = 1/2$[73] in 1d and $\gamma_{as} \approx 0.78$[62,71] in 2d. The scaling exponents of $\langle S_s \rangle$ are found as ≈ 0.5 in 1d and 0.22 in 2d which is consistent with $1 - \gamma_{as}$. The scaling behaviour in this region is thus governed by the properties of the avalanches on regular lattice ($\phi = 0$). For the avalanches of size $s > s_2$, power law scaling of $\langle S_s \rangle$ and $\langle a_s \rangle$ are observed only for 1d and no such scaling behaviour are observed for 2d. In 1d, $\langle a_s \rangle$ saturates in this region though the avalanche size s is increasing indicating $\gamma_{as} = 0$ and $1 - \gamma_{as} = 1$. For the avalanches of intermediate sizes, $s_1 < s < s_2$, $\gamma_{as} \approx 1$, (0.98) in 1d and (0.99) in 2d, as shown in Figs. 3.4(a) and 3.4(b), respectively.

Accordingly, $\langle S_s \rangle$ remains constant against s. Since $\gamma_{as} = 1$ on random network in both 1d and 2d[68], the scaling behaviour in this region is then governed by the properties of the avalanches on random network. The values of s_1 and s_2 can be obtained determining the points of inflections in the plots of $\langle S_s \rangle$ against s. These plots for different ϕ and L are found to be shifted both vertically and horizontally. A scaling form for $\langle S_s \rangle$ as well as for the crossover sizes s_1 and s_2 can be established considering the fact that there exits a characteristic length $\xi \sim \phi^{-1/d}$ where d is the dimensionality of the lattice, below which SWN belongs to "large world", the regular lattice regime and beyond which it behaves as "small world", the random network regime[138–140]. At this length scale, the avalanche area $a \approx \xi^d \sim 1/\phi$ and $\langle S_s \rangle$ can accordingly be obtained as

$$\langle S_s \rangle = \frac{s}{\langle a_s \rangle} \sim \phi^{1-\gamma_{sa}} \tag{3.7}$$

where $\gamma_{sa} = 1/\gamma_{as}$. In Figs. 3.4(c) and 3.4(d), the scaled average height $\langle S_s \rangle \phi^{\gamma_{sa}-1}$ are plotted against s for 1d and 2d respectively for different values of L and ϕ. It can be seen that in the intermediate range of s, the plots in both the figures have a common constant height independent of ϕ and L. The avalanches confined within ξ are expected to have $s < s_1$ whereas the avalanches extend beyond ξ and comparable to L are expected to have $s > s_2$. Hence, two crossover sizes s_1 and s_2 correspond to two length scales, ξ and L, present in this system. The scaling form of s_1 and s_2, the crossover avalanche sizes, are then given by

$$s_1 = \bar{S}\xi^d \sim \phi^{-\gamma_{sa}} \quad \text{and} \quad s_2 = \bar{S}L^d \sim \phi^{1-\gamma_{sa}} L^d \tag{3.8}$$

where $\bar{S}$ is the value of $\langle S_s \rangle$ in the intermediate region. Each data set of $\langle S_s \rangle$ is subdivided into two sets breaking it at the middle of the intermediate region. The scaling forms of s_1 and s_2 are verified independently by data collapse for $\langle S_s \rangle$ in different regions as shown in the insets of Figs. 3.4(c) and 3.4(d). Identifying the point of inflection in the collapsed plots (taking double derivative D^2 with respect to the argument), the values of s_1 and s_2 are found to be $s_1 \approx 2^{12.5}$ and $s_2 \approx 2^{17.7}$ in 1d for $L = 2^{13}$ and $\phi = 2^{-6}$, and $s_1 = 2^{10.97}$ in 2d for $L = 2^{10}$ and $\phi = 2^{-8}$ [199]. The positions of s_1 and s_2 are shown by peaks and dips of D^2 in the respective insets of Figs. 3.4(c) and 3.4(d). No inflection point is found for s_2 in 2d. However, a direct estimation of s_2 from Eq. (3.8), provides $s_2 = 2^{20}$. The values of s_1 and s_2 are marked by crosses in Figs. 3.4(a) and 3.4(b). It has been verified that $\langle S_s \rangle$ of deterministic BTW-type sandpile also exhibits similar scaling behaviour at different

regions of s in the SWN regime.

The ensemble of avalanches that appear in the steady states of these systems then can be classified into three different categories. The avalanches with size $s < s_1$ are mostly fragment less and confined on the large world or regular lattice. The growth of their average height follow different power law scaling with the avalanche size s in 1d and 2d. In the intermediate region $s_1 < s < s_2$, the avalanche clusters are sparse, different parts of the same cluster are connected by the links of the network. These clusters are then appearing on the small world or on the network. Their average height does not grow with their avalanche size as the avalanche cluster becomes sparse both in 1d and 2d. As the size of the avalanches exceed s_2, the avalanche cluster properties are very different in one and two dimensions. In this region, the avalanche clusters become a compact over grown single cluster in 1d whereas in 2d they grow in size but remain sparse.

3.3.3 Avalanche size, area, and lifetime distributions

The exponents associated with the power-law scaling of the probability distributions of avalanche property $x \in \{s, a, t\}$ are generally use to characterize the critical steady state of sandpile model. For a given ϕ, the probability to have an avalanche of property x is given by $P_x(x, \phi) = N_{x,\phi}/N_{\text{tot}}$ where $N_{x,\phi}$ is the number of avalanches having property x out of total number of avalanches N_{tot} generated at the steady state. Since the avalanches occurring on a given SWN (of particular ϕ) exhibits different geometrical properties according to their size s, or area a or lifetime t, a generalized scaling form of $P_x(x, \phi)$ among any two regimes is proposed as

$$P_x(x,\phi) = \begin{cases} x^{-\tau_{x1}} \mathsf{f}_{\mathsf{x}}\left(\frac{x}{x_c(\phi)}\right) & \text{for } x \leqslant x_c \\ x^{-\tau_{x2}} \mathsf{g}_{\mathsf{x}}\left(\frac{x}{x_c(\phi)}\right) & \text{for } x \geqslant x_c \end{cases} \tag{3.9}$$

where x_c is the crossover value of the property x, f_{x} and g_{x} are the respective scaling functions and τ_{x1}, τ_{x2} are the corresponding critical exponents in the respective region. $P_x(x, \phi)$ are estimated on a 1d lattice of size $L = 8192$ for $\phi = 2^{-6}$, and on a 2d square lattice of size $L = 1024$ for $\phi = 2^{-8}$. The values of ϕ is so choosen that the network remains in the SWN regime.

The avalanche size distributions $P_s(s, \phi)$ are presented in Figs. 3.5(a) and 3.5(b) respectively for 1d and 2d lattices. It can be seen that for both the dimensions $P_s(s, \phi)$ do not follow a single power law scaling over the whole range of avalanche sizes. There are three distinct regions of avalanche size s, separated by two crossover

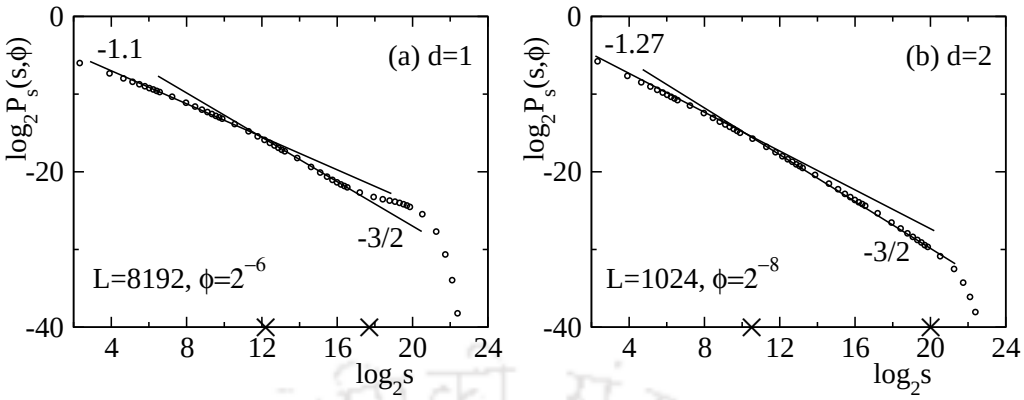

Figure 3.5: Plot of $P_s(s,\phi)$ against s in (a) for 1d for $L = 8192$ and $\phi = 2^{-6}$ and in (b) for 2d for $L = 1024$ and $\phi = 2^{-8}$. The solid lines with required slope (as indicated beside) represent two distinct scaling behaviour in two regimes.

sizes s_1 and s_2 indicated by crosses. Such crossover sizes were already observed in the geometrical aspect of the avalanches presented in the pevious section. $P_s(s,\phi)$ seems to have different scaling exponents in different regions of s. It could be observed that the large avalanches of size $s > s_2$ do not contribute to the power-law scaling. However, such loss of scaling is specific to the choice of ϵ_ϕ. For a smaller ϵ_ϕ than the optimal one choosen for these studies would lead to a hump in the tail of the distribution corresponding to more and more large avalanches. On the other hand, for a larger ϵ_ϕ, the tail of the distribution will shirnk and the scaling of RL will dominate. Hence, the crossover at s_1 and the associated scaling properties will be analyzed in the following. Since the avalanches in the region $s < s_1$ correspond to the avalanches on RL, the scaling behaviour of $P_s(s,\phi)$ should be that of Manna scaling. Whereas, for the region $s > s_1$ the avalanches correspond to those on the random network, and hence the scaling behaviour should follow MF scaling. The size distribution exponent τ_s of SSM on a regular 1d lattice is known to be 1.1[73,87,156,200,201] and that on a regular 2d lattice is ≈ 1.28[65,201]. Whereas the MF value of τ_s is 3/2 on both 1d and 2d. Two straight lines of respective slopes are plotted in Figs. 3.5(a) and 3.5(b) as guide to the eye. It can be noticed that a reasonable portion of data points of $P_s(s,\phi)$ obtained for SWN do follow the respective scaling forms in both the dimensions.

The avalanche area distributions $P_a(a,\phi)$ are presented in Figs. 3.6(a) and 3.6(b) respectively for 1d and 2d lattices. A similar behaviour as that of $P_s(s,\phi)$ is observed for $P_a(a,\phi)$ too. The value of crossover area a_1 associated with crossover size s_1 can be estimated from the conditional expectation relation $a_1 \sim s_1^{\gamma_{as}}$. Taking the respective values of s_1 and γ_{as}, the values of a_1 are estimated as $2^{6.75}$ for 1d and

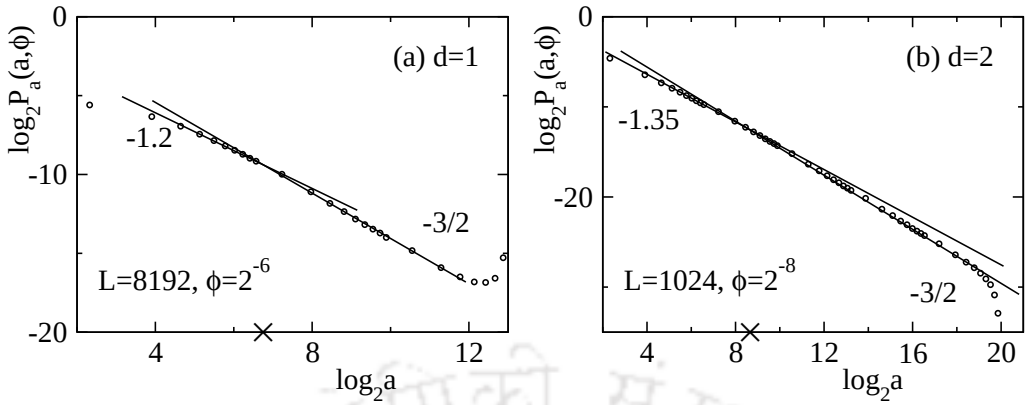

Figure 3.6: Plot of $P_a(a,\phi)$ against a in (a) for 1d and (b) for 2d for same L and ϕ as in Fig. 3.5. The solid lines with required slope (as indicated beside) represent two distinct scaling behaviour in two regimes.

$2^{8.77}$ for 2d and are indicated by crosses in Figs. 3.6(a) and 3.6(b) respectively. The avalanche area distribution exponent τ_a of SSM on a regular 1d lattice is known to be 1.2 and that on a regular 2d lattice is ≈ 1.35[74], whereas the MF value is $\tau_a = 3/2$. It can be seen that data points of $P_a(a,\phi)$ follow SSM scaling in $a < a_1$ regime and MF scaling in $a > a_1$ regime in both the dimensions.

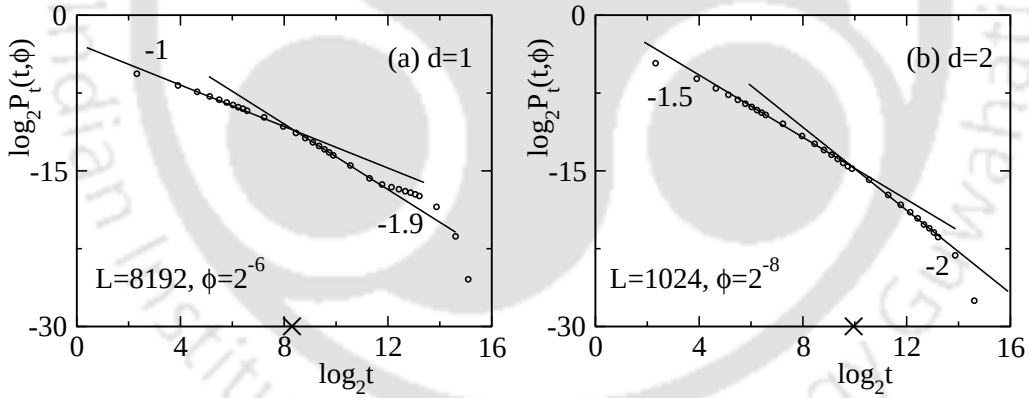

Figure 3.7: Plot of $P_t(t,\phi)$ against t in (a) for 1d and (b) for 2d for same L and ϕ as in Fig. 3.5. The solid lines with required slope (as indicated beside) represent two distinct scaling behaviour in two regimes.

The avalanche lifetime distributions $P_t(t,\phi)$ are presented in Figs. 3.7(a) and 3.7(b) respectively for 1d and 2d lattices. The distributions $P_t(t,\phi)$ found to be similar to that of $P_s(s,\phi)$ as well as $P_a(a,\phi)$. The values of crossover lifetime t_1 indicated by crosses in the respective figures are found to be 2^8 for 1d and 2^{10} for 2d. The avalanche lifetime distribution exponent τ_t of SSM on a regular 1d lattice is known to be 1 and that on a regular 2d lattice is ≈ 1.5[74], whereas the MF value is $\tau_t = 2$. It can be seen that data points of $P_t(t,\phi)$ follow SSM scaling in $t < t_1$

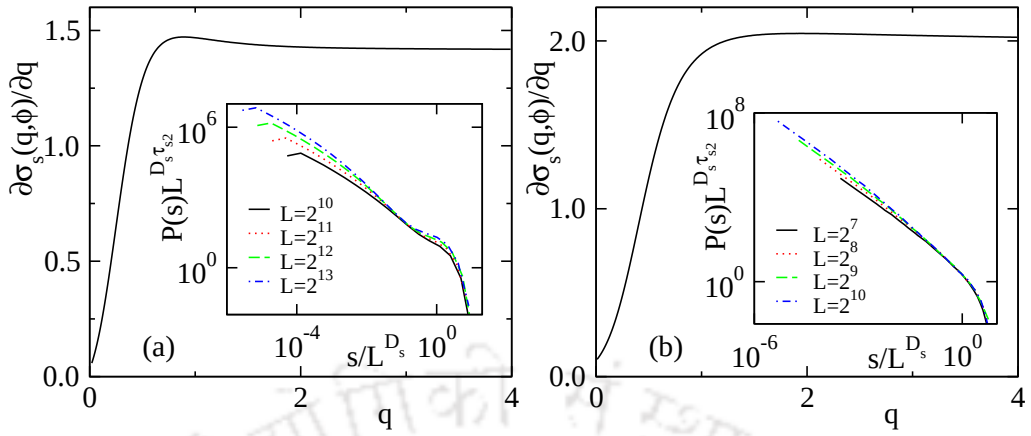

Figure 3.8: Plot of $\partial\sigma_s(q,\phi)/\partial q$ against q in (a) for 1d with $\phi = 2^{-6}$ and in (b) for 2d with $\phi = 2^{-8}$. Inset: Attempt to collapse the data of avalanche size distribution for different system sizes taking $\tau_s = 3/2$, and respective values of D_s.

regime and MF scaling in $t > t_1$ regime in both the dimensions.

It has already been mentioned in chapter 2 that, the probability distributions of various avalanche properties of the deterministic BTW-type sandpile model do not follow FSS in SWN regime ($2^{-12} < \phi < 0.1$). Such a violation of FSS is expected because in SWN regime, both the scaling forms, BTW type correlated scaling on regular lattice (which does not follow FSS) and MF scaling on random networks, coexist together. On the other hand, the distribution functions of stochastic sandpile model follow FSS both on regular lattice ($\phi = 0$) as well as on random network ($\phi = 1$)[175,197]. It is then important to verify whether the probability distributions of DSSM follow FSS or not in the SWN regime. The FSS scaling form of size distribution function for a given fixed ϕ is assumed as $P(s,L) \approx s^{-\tau_s} f(s/L^{D_s})$, where D_s is the capacity dimension. Moment analysis of the avalanche size has been performed for both the dimensions. The moment scaling function $\sigma_s(q,\phi)$ defined in chapter 2 [Eqs. (2.30) and (2.32)], are then calculated and its derivatives with respect to q are plotted against q in Fig. 3.8 (a) for 1d with $\phi = 2^{-6}$ and in Fig. 3.8 (b) for 2d with $\phi = 2^{-8}$. It can be seen that for large q, $\partial\sigma_s(q,\phi)/\partial q$ converges in both the cases and the values of capacity dimension estimated as $D_s \approx 1.42$ and ≈ 2 for 1d and 2d, respectively. It should be noted here that for the given values of ϕ, the distribution functions consist of two scaling forms with exponents τ_{s1} and τ_{s2}. An attempt has been made to collapse the data by plotting the scaled distribution $P(s,\phi)L^{D_s\tau_{s2}}$ against the scaled variable s/L^{D_s} in the respective insets. For both the dimensions, τ_{s2} is taken as $3/2$. Clearly, the collapse does not work for the whole range of s. The deviation is more prominent in the small avalanche

size region where the avalanches follow usual stochastic scaling of the respective dimensions. Therefore in the SWN regime, FSS of the probability distributions of s, a or t can not be verified for the stochastic sandpile model because same scaling form is not valid over the entire range of a parameter. A similar observation is also reported by Benella *et.al.*[202] in a recent study of avalanching systems with long range connectivity. Since FSS fails in the SWN regime, the ϕ dependent coexistence scaling could be useful to verify the scaling form of the probability distribution functions.

3.3.4 Coexistence scaling

Verification of the scaling form given in Eq. (3.9) can be performed for the two regions taking crossover value $x_c = x_1$. At $x_1(\phi)$ the values of $P_x(x,\phi)$ are same for both the regions. Since $s_1 \sim \phi^{-\gamma_{sa}}$, then one should have $\mathsf{f_s}(1) = \phi^{-(\tau_{s1}-\tau_{s2})\gamma_{sa}}\mathsf{g_s}(1)$. Following coexistence scaling developed in section 2.5 of chapter 2, the scaled size distribution can be obtained as

$$P_s(s,\phi)\phi^{-\gamma_{sa}\tau_{s1}} = \begin{cases} (s\phi^{\gamma_{sa}})^{-\tau_{s1}}\,\mathsf{f_s}(s\phi^{\gamma_{sa}}) & \text{for } s \leqslant s_1 \\ (s\phi^{\gamma_{sa}})^{-\tau_{s2}}\,\mathsf{f_s}(s\phi^{\gamma_{sa}}) & \text{for } s \geqslant s_1 \end{cases} \tag{3.10}$$

Similarly considering $a_1 \sim s_1^{\gamma_{as}} \sim \phi^{-1}$ a scaled area distribution can be written as

$$P_a(a,\phi)\phi^{-\tau_{a1}} = \begin{cases} (a\phi)^{-\tau_{a1}}\,\mathsf{f_a}(a\phi) & \text{for } a \leqslant a_1 \\ (a\phi)^{-\tau_{a2}}\,\mathsf{f_a}(a\phi) & \text{for } a \geqslant a_1 \end{cases} \tag{3.11}$$

To verify the scaling forms given in Eqs. (3.10) and (3.11), the scaled distributions are plotted in Fig. 3.9 against their respective scaled variable. Data of size distributions are presented in Figs. 3.9(a) and 3.9(b) for 1d and 2d respectively. It can be seen that a good data collapse is obtained using $\gamma_{sa} = 2$, $\tau_{s1} = 1.11$ for 1d and using $\gamma_{sa} = 1.26$, $\tau_{s1} = 1.27$ for 2d. Similarly Figs. 3.9(c) and 3.9(d) represent the data of scaled area distributions for 1d and 2d respectively. A reasonable collapse is also observed taking $\tau_{a1} = 1.2$ for 1d and $\tau_{a1} = 1.35$ for 2d. The straight lines with required slopes in the respective regions are guide to the eye. A similar coexistence scaling for the lifetime t can also be obtained knowing that the crossover time $t_1 \sim \phi^{-\gamma_{ta}}$ where $\gamma_{ta} = 1/\gamma_{at}$. The values of γ_{at} on the regular lattice is know to be approximately 0.68 and 1.35 in 1d and 2d respectively[71,73]. It has been verified that a good collapse of data can be obtained taking appropriate values of τ_{t1}. Hence, it confirms the validity of the proposed scaling function forms given in Eq. (3.9).

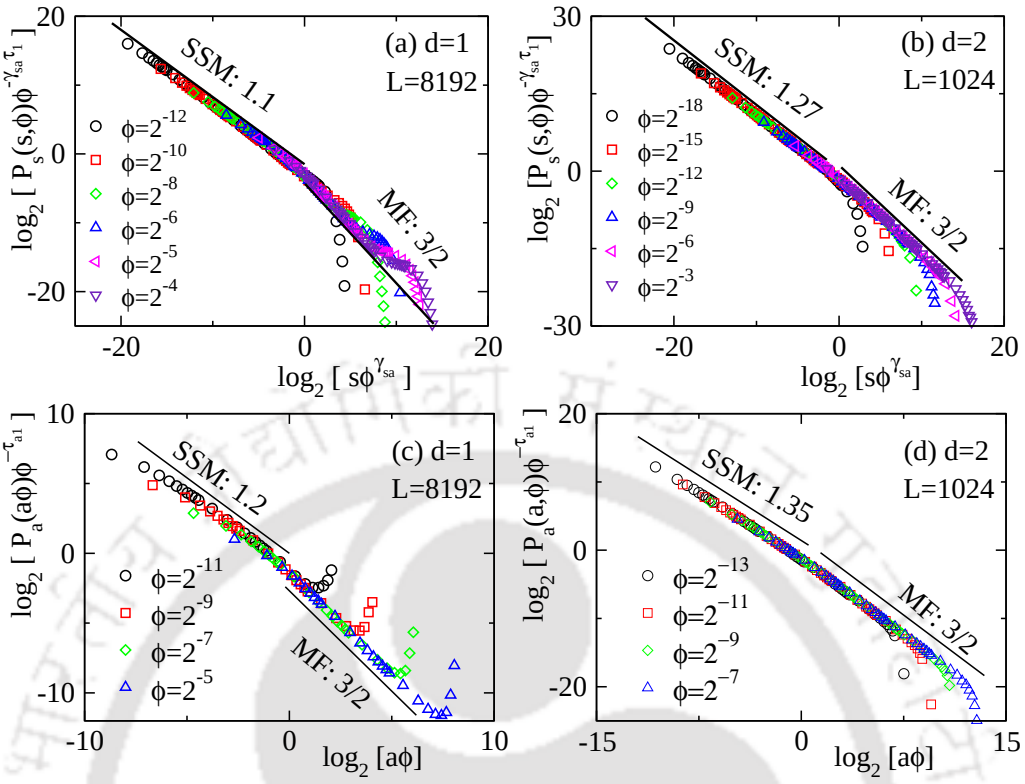

Figure 3.9: Plot of scaled size distributions against scaled variable for selected values of ϕ in (a) for 1d and in (b) for 2d. The scaled area distributions for several values of ϕ is shown in (c) for 1d and in (d) for 2d. The system size considered for 1d is $L = 8192$, and for 2d is $L = 1024$.

It should be noted here that the presence of internal length scale and modification of the scaling forms of avalanche properties may also appear due to parameters pertaining to other forms of disorder in the system such as bulk defects[203], rate of dissipation ϵ_ϕ [204,205], etc. Change in scaling behaviour may occur due to variation of ϵ_ϕ, as observed in other studies[204,205], and in that case a generalized scaling function involving ϵ_ϕ should be obtained.

The coexistence scaling of the average height $\langle S_s \rangle$ around crossover size s_1 and s_2 has already been demonstrated in previous section (Figs. 3.4(c) and 3.4(d)). Another geometrical property of toppling surface, the average area $\langle a_s \rangle$ of a given size s also exhibits multiple scaling forms in different regions of s. A coexistence scaling form of $\langle a_s \rangle$ around the crossover size s_1 can be written as

$$\langle a_s \rangle = \begin{cases} s^{\gamma_{as1}} f_{as}\left(\frac{s}{s_1}\right) & \text{for } s \leqslant s_1 \\ s^{\gamma_{as2}} g_{as}\left(\frac{s}{s_1}\right) & \text{for } s \geqslant s_1 \end{cases} \tag{3.12}$$

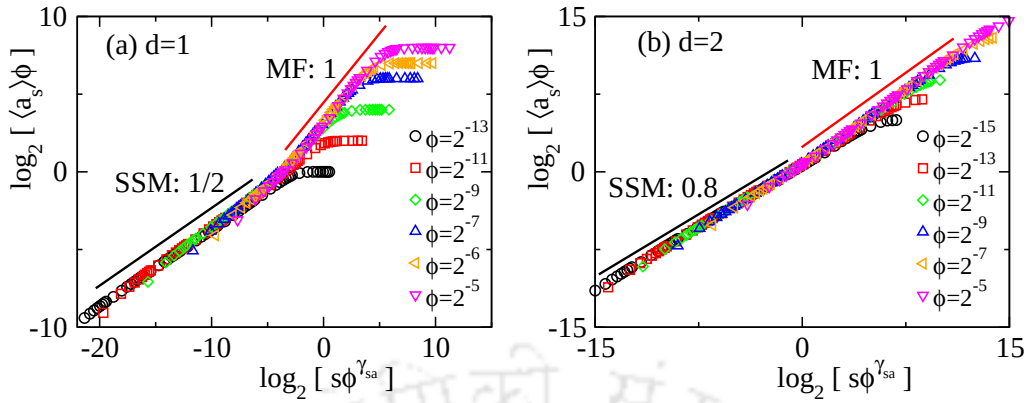

Figure 3.10: Plot of scaled average area against scaled variable for selected values of ϕ in (a) for 1d with $L = 8192$ and (b) for 2d with $L = 1024$. Reasonable data collapse verify the scaling forms given in Eq. (3.12). Straight lines with required slope are guide to the eye.

where, f_{as} and g_{as} are the scaling functions in respective regions and γ_{as1} and γ_{as2} are the exponents in the regime $s \leqslant s_1$ and $s \geqslant s_1$ respectively. Note that at $s = s_1$ the value of $\langle a_s \rangle$ will be same for both the regions and hence $f_{as}(1) = s_1^{\gamma_{as2}-\gamma_{as1}} g_{as}(1)$. Considering $\gamma_{sa} = 1/\gamma_{as}$, Eq. (3.12) can be written in terms of single scaling function as

$$\langle a_s \rangle \phi = \begin{cases} (s\phi^{\gamma_{sa1}})^{\gamma_{as1}} f_{as}\left(s\phi^{\gamma_{sa1}}\right) & \text{for } s \leqslant s_1 \\ (s\phi^{\gamma_{sa1}})^{\gamma_{as2}} f_{as}\left(s\phi^{\gamma_{sa1}}\right) & \text{for } s \geqslant s_1 \end{cases} \tag{3.13}$$

A plot of $\langle a_s \rangle \phi$ against $s\phi^{\gamma_{sa}}$ for different values of ϕ should fall on a single curve. Satisfactory collapse of date are observed as shown in Fig. 3.10(a) for 1d and in Fig. 3.10(b) for 2d. Moreover, the scaling function represents two different scaling behaviour with two different exponents, 1/2 and 1 in 1d and 0.8 and 1 in 2d, as indicated by straight lines with the respective slopes.

Hence it could be rationalized that if a dynamical model like sandpile is studied on SWN, multiple scaling forms of an event size will coexist in the distribution of the event sizes. In other words, SWN can be considered as a segregator of several scaling forms that appear in the event size distribution.

3.3.5 Sand transport: diffusivity and scaling

It is known in the literature that, similar to the deterministic model, the critical properties the stochastic model on regular lattice ($\phi = 0$) also governed by the diffusive nature of the sand transport[73,74], i.e., $r \sim \sqrt{t}$. However, as the SWN evolves to random network ($\phi = 1$), it is expected that the diffusive nature changes

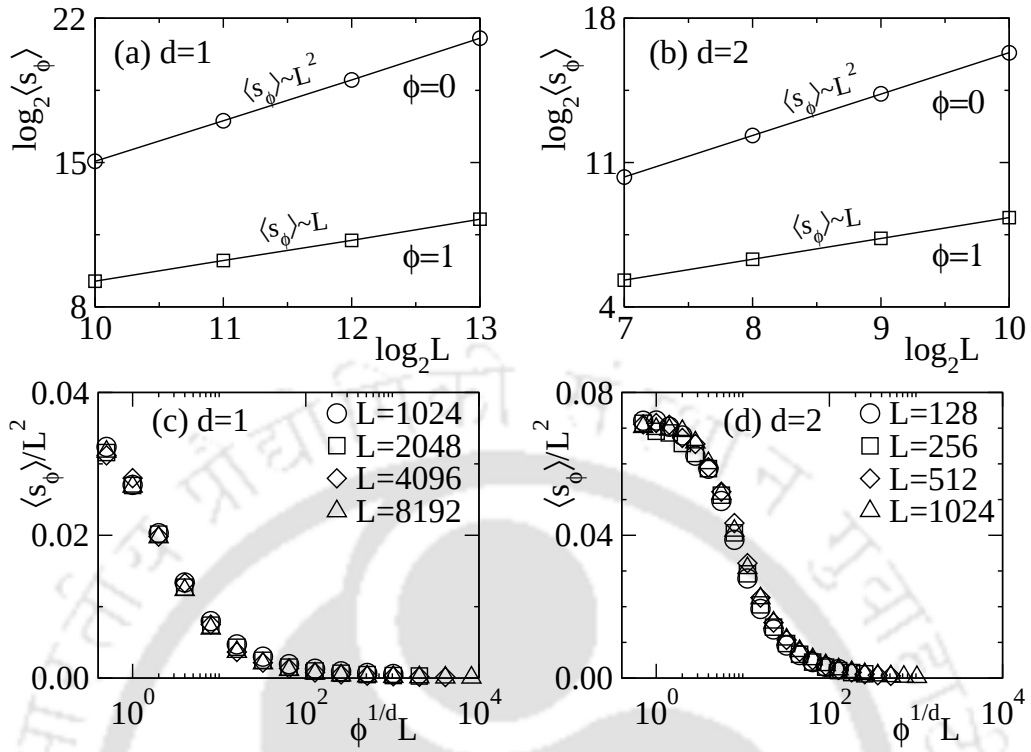

Figure 3.11: Plot of $\langle s_\phi \rangle$ against L for $\phi = 0$ (○) and $\phi = 1$ (□) in (a) for 1d and in (b) for 2d. Plot of scaled average size $\langle s_\phi \rangle / L^2$ against scaled variable $\phi^{1/d} L$ for (c) $d = 1$ and (d) $d = 2$. Different symbols correspond to different system sizes L.

to super-diffusive one i.e., $r \sim t$, as it is already observed for the deterministic model in the previous chapter as well as for other diffusive model studied on network[206]. In order to verify the same, the average avalanche size (time to diffuse) on a given system size L (length to diffuse) for a given ϕ is defined as

$$\langle s_\phi \rangle = \int s P_s(s, \phi) ds. \tag{3.14}$$

and it is evaluated on several system sizes for a given ϕ. In Figs. 3.11(a) and 3.11(b), $\langle s_\phi \rangle$ for the extreme values of ϕ (0 and 1) are plotted against the system size L for 1d and 2d respectively. It can be seen that in both the dimensions, the diffusive behaviour of the model, $\langle s_\phi \rangle \sim L^2$ holds for $\phi = 0$, whereas the behaviour changes to super-diffusive for other extreme value of ϕ i.e., $\langle s_\phi \rangle \sim L$ for $\phi = 1$. It could be recalled that the avalanches on RN consist of nodes that toppled only once whereas on RL there exist sites that toppled multiple times. Hence, because of the presence of long distance shortcuts on RN, the diffusion of sand must be faster than on RL on which it is delayed because of multiple toppling of sites.

It is now important to check the scaling behaviour of $\langle s_\phi \rangle$ with ϕ on SWNs. Ex-

tending the proposed scaling form as developed in chapter 2 for DDSM, a generalized scaling form of $\langle s_\phi \rangle$ can be written as

$$\langle s_\phi \rangle = L^2 \mathcal{G}(\phi^{1/d} L) \tag{3.15}$$

where d is the space dimension. The behaviour of the scaling function $\mathcal{G}(x)$ is given by,

$$\mathcal{G}(x) \propto \begin{cases} \text{constant}, & x \ll 1, \\ 1/x, & x \gg 1, \end{cases} \tag{3.16}$$

In order to verify the above scaling form, $\langle s_\phi \rangle$ is calculated for different system sizes over the full range of ϕ for both 1d and 2d. The scaled average size $\langle s_\phi \rangle / L^2$ is plotted against the scaled variable $\phi^{1/d} L$ in Figs. 3.11(c) and 3.11(d) for 1d and 2d respectively. Taking the respective d values, reasonable collapse of data are observed in both the cases. Note that, for 2d, the limiting values of $\langle s_\phi \rangle / L^2$ as $\phi \to 0$ is found to be 0.7 which is consistence with the relations $2\langle s_\phi \rangle = \langle n_\phi \rangle$ and $\langle n_\phi \rangle \approx 0.14 L^2$, for $L \to \infty$[177]. However, for 1d, $\langle s_\phi \rangle / L^2$ is found to be ≈ 0.031 as $\phi \to 0$.

3.4 Conclusion

A dissipative stochastic sandpile model (DSSM) is constructed and studied on SWN both in 1d and 2d varying the shortcut density ϕ. As ϕ varies from 0 to 1, the regular lattice evolves to random network via a series of SWNs. Two important aspects are addressed in this study, first, the impact of the transformation of a RL to a SWN to the scaling behaviour of avalanches and secondly, the role of dimensionality of the underlying RL. Since the critical behaviour of the stochastic model on the regular lattice as well as on the random network is known, emphasis is given in analyzing the critical properties of the model on SWN regime ($2^{-12} < \phi < 0.1$). Several new geometrical quantities such as toppling surface and its fragmentation, compactness and fluctuation in fragment size are defined and characterized as a function of avalanche size s for a given ϕ, within the SWN regime. Such fragmentation of avalanche cluster is evident in the plots of toppling surfaces. To characterize the toppling surface further, the average height $\langle S_s \rangle$ and average area $\langle a_s \rangle$ of the surface are studied as a function of avalanche size s. It is found that there exist three regimes of avalanche size s, separated by two crossover sizes s_1 and s_2 ($s_1 < s_2$). Below s_1, the avalanches are found to be compact as on regular lattice. For $s_1 < s < s_2$, the avalanches are

fragmented in many sub-clusters those are connected by long-ranged links of the network. Novel scaling forms of s_1 and s_2 as well as that of $\langle S_s \rangle$ are developed and numerically verified. Distributions of avalanche size s and area a are also found to exhibit two scaling forms about the crossover size s_1. Below s_1 it is Manna scaling on regular lattice whereas above s_1 it is MF scaling on random network. Since two scaling forms appear simultaneously in the SWN regime, the probability distributions of various avalanche properties of DSSM do not follow the usual FSS in contrary to the fact that stochastic sandpile model follow FSS on regular lattice. Around the crossover a coexistence scaling form of the distributions and the expectation value are developed and numerically verified. The sand transport behaviour in DSSM is found to change from diffusive to super diffusive nature as SWN evolve from regular lattice to random network, similar to the deterministic model. A generalized scaling form of diffusivity is identified that satisfactorily explains such crossover behaviour.

Chapter 4

Dissipative and nondissipative avalanches on small-world networks

Sandpile dynamics is inherently dissipative in the sense that, during relaxation an avalanche dissipates sand grain which minimizes the potential energy to find a (meta-)stable configuration of the sand distribution in the system. However, in the case of boundary dissipation, the toppling activities can be treated as "locally conserved" in the bulk as the number of sand gains truly conserved in the system when a bulk site topples once. But such conservation does not hold when a boundary site topples and looses one (or more) sand grain(s) from the system. In view of such a situation, an avalanche is called a dissipative avalanche if it dissipates at least one sand grain from the system during its lifetime, otherwise it is called a nondissipative avalanche. Classification of the avalanches into dissipative and nondissipative avalanches is expected to provide more insight into the statistical properties of the sandpile dynamics. Drossel[207] demonstrated that the size distribution of dissipative avalanches of BTW sandpile in 2d follows power-law scaling with definite exponents that do not obey finite-size scaling (FSS). Later, Dickman and Campelo[156] showed both in one and two dimensions that the dissipative and nondissipative avalanches of stochastic sandpile model (SSM) on regular lattice obey different FSS behaviour with certain logarithmic correction beside the power-law scaling with different exponents for different types of avalanches. In the previous chapters, both the deterministic and stochastic sandpile models with bulk dissipation are considered where the number of sand grains do not truly conserved in a toppling activity as there is always a possibility of dissipation of a sand grain at each attempt of redistribution of sand grains.

This chapter is based on the Ref. [201]; H. Bhaumik and S. B. Santra, Phys. Rev. E. 94, 062138 (2016).

It is then intriguing to study avalanche properties of dissipative and nondissipative avalanches of the dissipative models separately on small world network (SWN) in which if shortcut density ϕ is varied, the SWN would interpolate regular lattice and random network. It is therefore important to explore the various scaling forms of the dissipative and nondissipative avalanches varying ϕ under bulk dissipation mode. In this chapter, the deterministic dissipative sandpile model (DDSM) on two dimensional SWN and dissipative stochastic sandpile model (DSSM) on both one and two dimensional SWN are studied.

4.1 Numerical simulation

Extensive computer simulations are performed to study the critical properties of nondissipative and dissipative avalanches of DDSM on 2d-SWN and DSSM on SWN in both 1d and 2d. Recall that in DDSM (defined in chapter 2) the toppling rule of ith node is given by, $h_i \to h_i - h_c$ and $h_j = h_j + 1$, where the critical height h_c is taken as the degree k_i of ith node and $j = 1, 2, ..., k_i$. Whereas for DSSM (defined in chapter 3), $h_c = 2$ and $j = j_1, j_2$ are the two randomly and independently selected nodes from k_i adjacent nodes. Both the models are simulated with an additional flag with values 0 or 1. Before starting of each avalanche the flag is kept at 0, and during the avalanche evolution if at least one sand grain lost from the system the flag is on to 1 such that at the end of the processes, an avalanche can be identified as dissipative (flag = 1) or nondissipative (flag = 0). Starting from an empty configuration the models invariably reach the steady state. The steady-state critical properties are characterized studying various avalanche properties in the steady state at different values of ϕ and system size L. The maximum lattice size used for 1d is $L = 8192$ and that for 2d is $L = 1024$. Data are averaged over 32×10^6 avalanches collected on 32 different SWN configurations for a given ϕ and L. First, the result of the DSSM will be described and then that of the DDSM will be presented and compared.

4.2 Results and discussion: stochastic sandpile model

For each avalanche, the number of toppling of every node is stored in an array $S_\phi[i], i = 1, \cdots, L^d$. Various geometrical properties of an avalanche such as avalanche

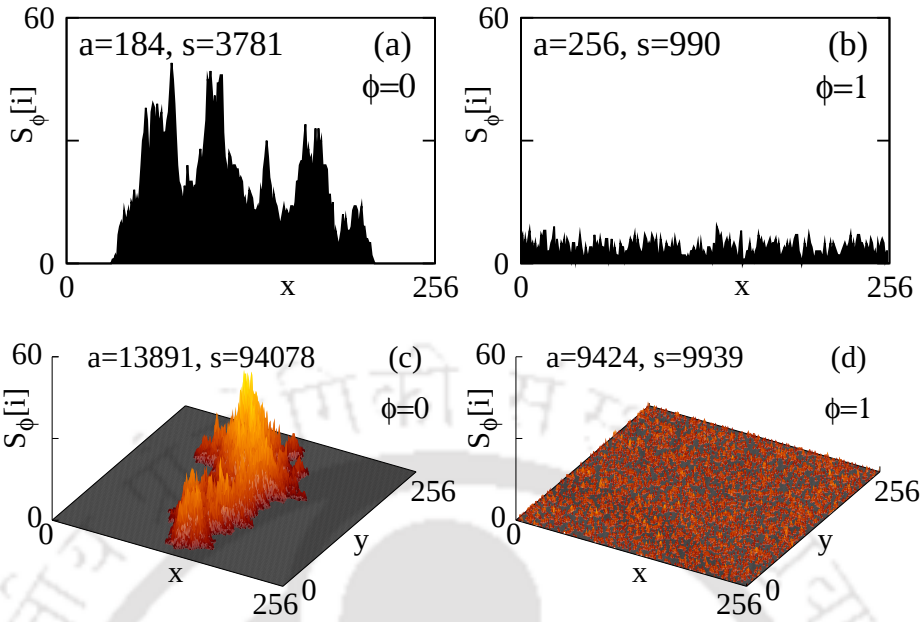

Figure 4.1: The toppling surfaces of typical large avalanches of DSSM on SWN are shown. The toppling surface of an avalanche generated on a 1d lattice of size $L = 256$ is shown in (a) for $\phi = 0$ and in (b) for $\phi = 1$. The surface generated on a 2d square lattice of size $L = 256$ for $\phi = 0$ is shown in (c) and for $\phi = 1$ is shown in (d). The size (s) and area (a) of the corresponding avalanches are mentioned in the respective plots.

size s, avalanche area a, etc., is then estimated from $S_\phi[i]$ as

$$s = \sum_{i=1}^{L^d} S_\phi[i], \quad a = \sum_{i=1}^{L^d} 1 \quad \forall \quad S_\phi[i] \neq 0. \tag{4.1}$$

Before discussing the scaling behaviour of nondissipative and dissipative avalanches of DSSM on small-world regime, the avalanche properties of all the avalanches as well as those of nondissipative and dissipative avalanches on regular lattice ($\phi = 0$) and random network ($\phi = 1$) are analyzed following the moment analysis technique.

4.2.1 Toppling surfaces

The toppling surface can be defined by mapping the values of the toppling number $S_\phi[i]$ at different node of an avalanche into the height profile of a surface[83]. In order to visualize the avalanche, the toppling surfaces for typical large avalanches in the steady state, generated on a 1d lattice of size $L = 256$, are presented for $\phi = 0$ and $\phi = 1$ respectively in Figs. 4.1(a) and 4.1(b). Toppling surfaces generated on a 2d square lattice of size $L = 256$ are presented in Fig. 4.1(c) for $\phi = 0$ and for $\phi = 1$ in Fig. 4.1(d). It could be noticed that the toppling surface at $\phi = 0$ are

highly fluctuating and rough in both the dimensions. Large toppling numbers that represent peaks of the surface appear at random positions. In both the dimensions, the maximum height of the surfaces on regular lattice ($\phi = 0$) is much higher than that on random network ($\phi = 1$). Though the maximum height is much smaller in 1d for $\phi = 1$, all the lattice site toppled more than once, whereas in 2d, the toppling surface on random network consists of mostly singly toppled sites, only and 0.06% of the sites toppled more than once. The toppling surfaces differ considerably on regular lattice and random network in different dimensions. It is expected that the scaling behaviour of avalanche properties would be different for different dimensions and different values of ϕ.

4.2.2 Moment analysis at $\phi = 0$ & 1

The critical steady state of the sandpile model is mostly characterized by power-law scaling of the probability distributions of avalanche size (s) occurring in the steady state. For a given ϕ and L, the probability to have an avalanche of size s is given by $N_{s,\phi}/N_{\rm tot}$, where $N_{s,\phi}$ is the number of avalanches of size s out of the total number of avalanches $N_{\rm tot}$ generated at the steady state. The distribution of s follows a power-law scaling with a well-defined exponent τ and obeys FSS[64,175]. The FSS form of the probability distribution of s in DSSM is given by

$$P_\phi(s, L) = s^{-\tau} f_\phi \left[\frac{s}{L^D}\right] \tag{4.2}$$

where f_ϕ is a ϕ-dependent scaling function and D is the capacity dimension. Very often the power-law scaling is found to sustain over a short range of avalanche sizes and hinders precise extraction of the exponent τ from the slope of the plot of $P_\phi(s, L)$ against s in double logarithmic scale. A more reliable estimate of the exponent can be made employing moment analysis[65,82]. For a given ϕ, the qth moment of s is defined as

$$\langle s^q(L)\rangle_\phi = \int_0^\infty s^q P_\phi(s, L) ds \sim L^{\sigma_\phi(q)} \tag{4.3}$$

where,

$$\sigma_\phi(q) = D(q - \tau + 1) \tag{4.4}$$

is the moment scaling function for $q > \tau - 1$ [for $q < \tau - 1$, $\sigma_\phi(q) = 0$]. Values of $\sigma_\phi(q)$ are estimated from the slope of the plots of $\langle s^q(L)\rangle_\phi$ versus L in double logarithmic scale for 400 equidistant values of q between 0 and 4. The value of D can be measured from the saturated value of $\partial\sigma_\phi(q)/\partial q$ in the large-q limit.

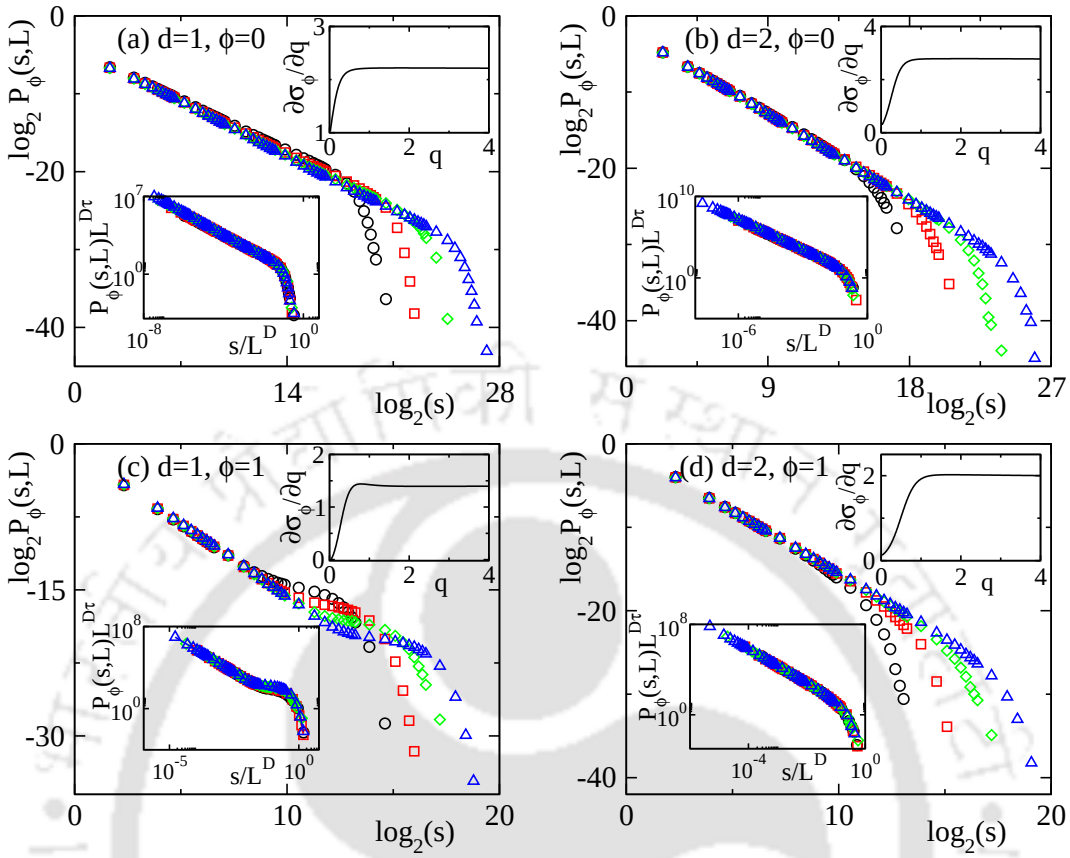

Figure 4.2: Plot of $P_\phi(s, L)$ of all the avalanches for $\phi = 0$ (a) for 1d and (b) for 2d. $P_\phi(s, L)$ for $\phi = 1$ are plotted in (c) and (d) for 1d and 2d respectively. Different curves corresponds to different system size L as, for 1d, $L = 2^{10}$ (○), $L = 2^{11}$ (□), $L = 2^{12}$ (◇), and $L = 2^{13}$ (△), whereas for 2d they are $L = 2^7$ (○), $L = 2^8$ (□), $L = 2^9$ (◇), and $L = 2^{10}$ (△). Upper inset in each figure shows the plot of $\partial\sigma_\phi(q)/\partial q$ against q whereas, the lower inset shows the corresponding FSS data collapse.

The derivative $\partial\sigma_\phi(q)/\partial q$ is determined numerically by the finite-difference method. Once D is known the exponent τ can be estimated from Eq. (4.4) using the value of $\sigma_\phi(1)$.

4.2.2.1 All avalanches

$P_\phi(s, L)$ of all the avalanches for various values of L are presented in Fig. 4.2 for 1d and 2d for $\phi = 0$ and 1. Reasonable power-law scaling is observed for these extreme values of ϕ in both the dimensions. The flat tail in $P_\phi(s, L)$ for $\phi = 1$ in 1d is due to large dissipative avalanches, which will be discussed later separately. Employing moment analysis, values of D and τ are estimated for all four situations. For $\phi = 0$, estimates of D are found to be 2.21 ± 0.02 and 2.76 ± 0.02 for 1d and 2d respectively. Since for $\phi = 0$, $\sigma_\phi(1) \approx 2$ in both the dimensions, the values of τ

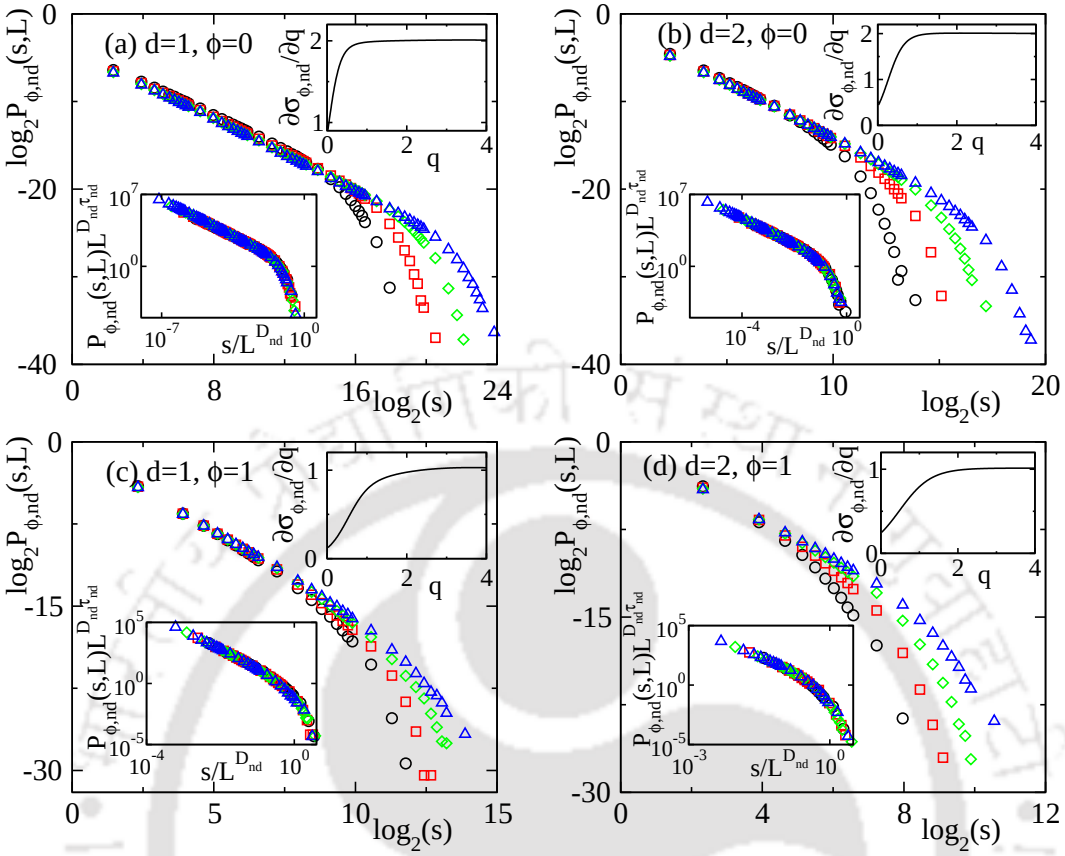

Figure 4.3: Plot of $P_{\phi,\mathrm{nd}}(s,L)$ for different L (with same symbol as in Fig. 4.2) for $\phi = 0$ in (a) for 1d and in (b) for 2d. For $\phi = 1$ the same has been plotted in (c) and (d) for 1d and 2d respectively. Insets in each figure are same as that of Fig. 4.2 but for nondissipative avalanches.

estimated from Eq. (4.4) are 1.09 ± 0.02 in 1d and 1.28 ± 0.01 in 2d. As expected, the exponents are found very close to the reported values for SSM on regular lattice in respective dimensions, for instance, $\tau = 1.112 \pm 0.006$, $D = 2.253 \pm 0.014$ in 1d and $\tau = 1.273 \pm 0.002$, $D = 2.750 \pm 0.006$ in 2d[67,74], whereas for $\phi = 1$, the values of D are found to be 1.39 ± 0.02 and ≈ 2 in 1d and 2d, respectively. In 2d, the avalanches on random network ($\phi = 1$) consist mostly single toppled nodes, hence $D \approx 2$ is expected whereas the value of $D > 1$ in 1d suggests that the avalanches consist of multiple toppled nodes. In both the dimensions, the value of τ for $\phi = 1$ is ≈ 1.50, the mean-field value as obtained in branching processes[68,153,161]. The values of the exponents are listed in Table 4.1. The FSS form of $P_\phi(s,L)$ is verified by plotting the scaled distribution $P_\phi(s,L)L^{D\tau}$ against the scaled variable s/L^D in the respective lower inset of Fig. 4.2 using the respective values of the critical exponents obtained.

4.2.2.2 Nondissipative and dissipative avalanches

Avalanches are now classified into nondissipative and dissipative avalanches. During the evolution, a dissipative avalanche must dissipate at least a sand grain once whereas no sand grain be dissipated in a nondissipative avalanche. The avalanche size distribution $P_\phi(s, L)$ can be written in terms of $P_{\phi,\mathrm{nd}}(s, L)$ and $P_{\phi,d}(s, L)$, the distributions of nondissipative and dissipative avalanches, as

$$P_\phi(s, L) = P_{\phi,\mathrm{nd}}(s, L) + P_{\phi,d}(s, L) \tag{4.5}$$

with

$$P_{\phi,\mathrm{nd}}(s, L) = \frac{n_{s,\mathrm{nd}}}{N_{\mathrm{tot}}} \quad \text{and} \quad P_{\phi,d}(s, L) = \frac{n_{s,d}}{N_{\mathrm{tot}}}, \tag{4.6}$$

where $n_{s,\mathrm{nd}}$ and $n_{s,d}$ are number of nondissipative and dissipative avalanches of size s out of a total of N_{tot} avalanches. First, the analysis of nondissipative avalanches is given and then that of dissipative avalanches is presented.

The FSS form of the distribution $P_{\phi,\mathrm{nd}}(s, L)$ is assumed to be

$$P_{\phi,\mathrm{nd}}(s, L) = s^{-\tau_{\mathrm{nd}}} f_{\phi,\mathrm{nd}}\left[\frac{s}{L^{D_{\mathrm{nd}}}}\right] \tag{4.7}$$

where $f_{\phi,\mathrm{nd}}$ is a scaling function, τ_{nd} and D_{nd} are the respective exponents. $P_{\phi,\mathrm{nd}}(s, L)$ for $\phi = 0$ and 1 are plotted in Fig. 4.3 for several values of L for both 1d and 2d. Performing moment analysis, the values of D_{nd} are found as $D_{\mathrm{nd}} \approx 2$ for $\phi = 0$ and $D_{\mathrm{nd}} \approx 1$ for $\phi = 1$ in both 1d and 2d. It could be recalled here that the dissipation factor is chosen from the inverse of $\langle n_\phi \rangle$. On an average the avalanche of size $s > \langle n_\phi \rangle/2$ must dissipate at least one sand grain (the factor 2 is for one toppling consists transfer of two sand grains). Since $\langle n_\phi \rangle \sim L^2$ as $\phi \to 0$ due to diffusive behaviour of random walker on regular lattice and $\langle n_\phi \rangle \sim L$ as $\phi \to 1$ for superdiffusive behaviour of random walker on random network[169], the cutoff of $P_{\phi,\mathrm{nd}}(s, L)$ must scale with L in the same way as $\langle n_\phi \rangle$ scales with L. Knowing the values of D_{nd} and $\sigma_{\phi,\mathrm{nd}}(1)$, the values of τ_{nd} are estimated. The values of $\sigma_{\phi,\mathrm{nd}}(1)$ are found as 1.78 for $\phi = 0$ and 0.48 for $\phi = 1$ in 1d. Accordingly, $\tau_{\mathrm{nd}} = 1.11(2)$ for $\phi = 0$ and $\tau_{\mathrm{nd}} = 1.52(2)$ for $\phi = 1$ in 1d. The power-law scaling of $P_{\phi,\mathrm{nd}}(s, L)$ is found similar to that of $P_\phi(s, L)$ as the values of τ and τ_{nd} are found more or less same for both the distributions for $\phi = 0$ and 1, whereas, in 2d, the values of the exponents are found as $\tau_{\mathrm{nd}} = 1.29 \pm 0.01$ for $\phi = 0$ [since $\sigma_{\phi,\mathrm{nd}}(1) = 1.4$] and $\tau_{\mathrm{nd}} = 1.54 \pm 0.05$ for $\phi = 1$ as $\sigma_{\phi,\mathrm{nd}}(1) = 0.5$. On regular lattice it is the SSM result, whereas on random network it is the mean-field result. The values of D_{nd} and τ_{nd} for nondissipative

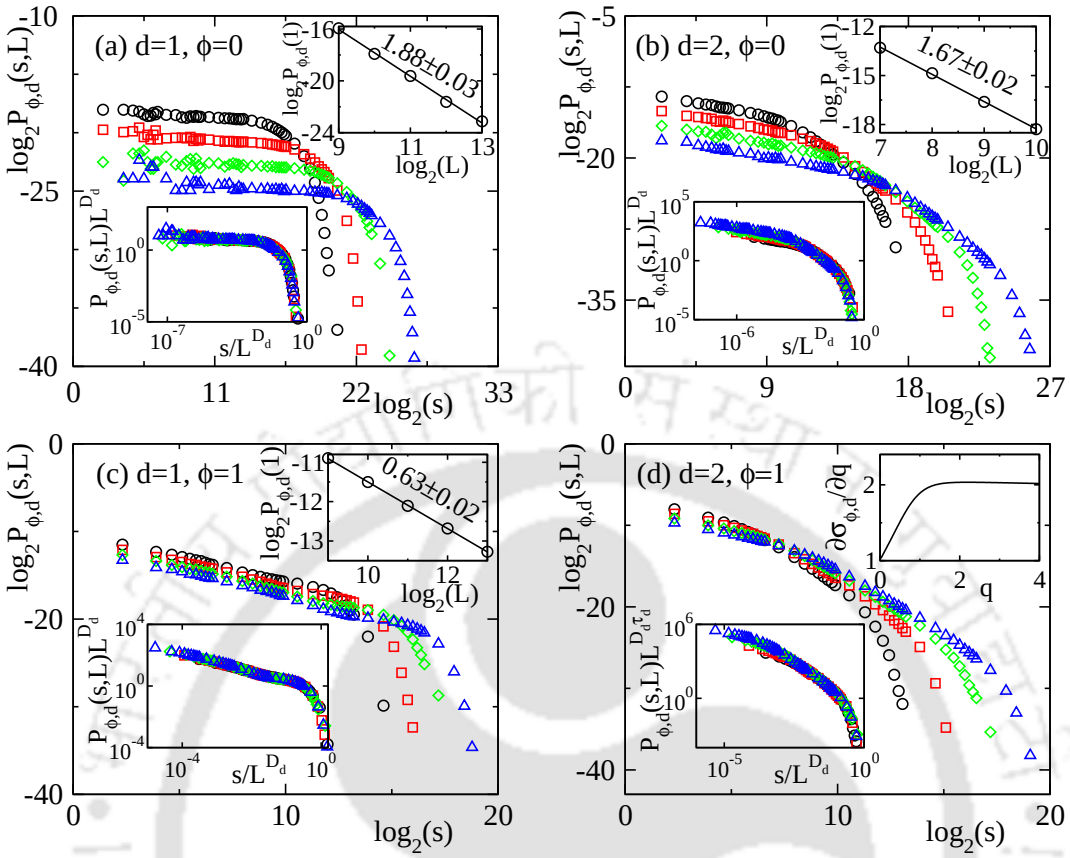

Figure 4.4: Plot of $P_{\phi,d}(s,L)$ for various L (with same symbol as in Fig. 4.2) for $\phi = 0$ in (a) for 1d and in (b) for 2d. For $\phi = 1$ the same has been plotted in (c) and (d) for 1d and 2d, respectively. Upper insets: (a)-(c) shows the plot of $P_{\phi,d}(1,L)$ against L, and (d) shows variation of $\partial\sigma_{\phi,d}(q)/\partial q$ against q. Lower insets shows the corresponding FSS data collapse (see text).

avalanches are listed in Table 4.1. Using the values of $\tau_{\rm nd}$ and $D_{\rm nd}$, a reasonable data collapse is obtained for $P_{\phi,{\rm nd}}(s,L)$ as shown in the lower insets of Fig. 4.3.

The size distribution of dissipative avalanches $P_{\phi,d}(s,L)$ for several values of L are presented in Fig. 4.4 for $\phi = 0$ and 1 in both the dimensions. Interestingly, the distributions $P_{\phi,d}(s,L)$ are very different in nature than the corresponding $P_{\phi,{\rm nd}}(s,L)$. Preliminary estimate of the size distribution exponent τ_d by linear least-squares fit to the data points in double-logarithmic scale reveals that $\tau_d < 1$ except for $\phi = 1$ in 2d. Following Christensen and coworkers[208,209], a new scaling form of $P_{\phi,d}(s,L)$ is proposed as

$$P_{\phi,d}(s,L) = s^{-\tau_d} L^{D_d(\tau_d-1)} f_{\phi,d}\left[\frac{s}{L^{D_d}}\right] \tag{4.8}$$

where $f_{\phi,d}$ is a new scaling function and τ_d and D_d are exponents for dissipative avalanches. The moment of such a distribution is obtained as $\langle s^q(L)\rangle_{\phi,d} \sim L^{\sigma_{\phi,d}(q)}$,

		nondissipative	dissipative	all
1d	$\phi = 0$	$D_{\rm nd} = 2.009$	$D_d = 2.214$	$D = 2.215$
		$\tau_{\rm nd} = 1.11(2)$	$\tau_d = 0.14(1)$	$\tau = 1.09(2)$
	$\phi = 1$	$D_{\rm nd} = 1.022$	$D_d = 1.402$	$D = 1.395$
		$\tau_{\rm nd} = 1.52(2)$	$\tau_d = 0.54(2)$	$\tau = 1.50(1)$
2d	$\phi = 0$	$D_{\rm nd} = 2.004$	$D_d = 2.791$	$D = 2.764$
		$\tau_{\rm nd} = 1.29(1)$	$\tau_d = 0.40(2)$	$\tau = 1.28(1)$
	$\phi = 1$	$D_{\rm nd} = 1.013$	$D_d = 2.023$	$D = 2.008$
		$\tau_{\rm nd} = 1.54(5)$	$\tau_d = 1.45(3)$	$\tau = 1.51(2)$

Table 4.1: Best estimated values of D and τ for DSSM in 1d and 2d at $\phi = 0$ and at $\phi = 1$ for nondissipative avalanches, dissipative avalanches, and all avalanches. As the values of D is estimated from $\partial\sigma_\phi(q)/\partial q$ the error in determination of D is $2\Delta q$ i.e., ± 0.020. The number in the parentheses is the uncertainty of last digit of the value τ determined from the scaling relations.

where $\sigma_{\phi,d}(q) = qD_d$. Noticeably, the moment exponent $\sigma_{\phi,d}(q)$ becomes independent of the size distribution exponent τ_d. Performing moment analysis for both 1d and 2d, the values of D_d for dissipative avalanches are found close to that of the all avalanches as presented in Table 4.1. In the limit $s/L^{D_d} \to 0$, the scaling function $f_{\phi,d}[s/L^{D_d}]$ becomes a constant and the distribution is given by $P_{\phi,d}(s, L) \approx s^{-\tau_d} L^{D_d(\tau_d-1)}$. Consequently, $P_{\phi,d}(1, L) \sim L^{D_d(\tau_d-1)}$ for $s = 1$. The exponent τ_d is then estimated from the slope of the plot of $P_{\phi,d}(1, L)$ vs L in double logarithmic scale as presented in the upper insets of Figs. 4.4 (a), 4.4(b), and 4.4(c). The values of τ_d are estimated as 0.14 ± 0.01 for $\phi = 0$ and 0.54 ± 0.01 for $\phi = 1$ in 1d. It is interesting to note that such a flat distribution (i.e., $\tau_d \to 0$ for $\phi = 0$ in 1d) is also reported by Amaral and Lauritsen[210] for the dissipative avalanches of a 1d rice pile model. In contrary to the present observation, Dickman and Campelo[156] found a power-law scaling of $P_d(s, L)$ with exponent $\tau_d = 0.637$ for SSM with boundary dissipation on 1d regular lattice. In 2d, the exponent τ_d is obtained here as 0.40 ± 0.02 for $\phi = 0$ whereas Dickman and Campelo[156] reported $\tau_d = 0.98$ for SSM on a 2d regular lattice with boundary dissipation. Thus the scaling behaviour of dissipative avalanches of DSSM differs substantially from that of dissipative avalanches of SSM with boundary dissipation in both the dimensions at $\phi = 0$. Such difference in the scaling behaviour for dissipative avalanches with different modes of dissipation is probably due to different topological properties of network in the bulk and at the boundary because the degree of a node at the boundary differs from that of a node in the bulk. Moreover, it should be noted that for the model of boundary dissipation, Dickman and Campelo introduced a logarith-

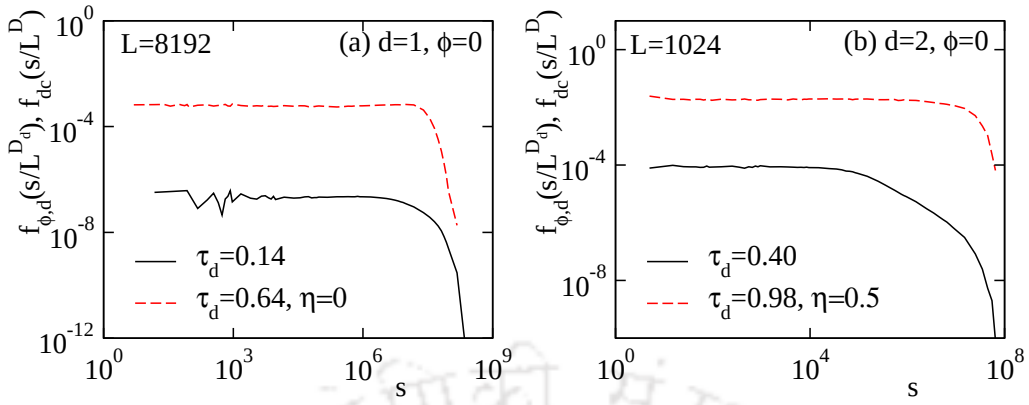

Figure 4.5: Plot of $f_{\phi,d}(= P_{\phi,d}(s)s^{\tau_d})$ (in solid black line) and $f_{dc}(= P_{\phi,d}(s)s^{\tau_d}[\ln(s)]^{-\eta})$ (in dashed red line) against s for 1d, $L = 8192$, in (a) and for 2d, $L = 1024$, in (b). The values of the τ_d and η for f_{dc} are taken from Ref. [156]. Since the plots are for a given L, the L dependency of the argument is dropped.

mic correction in the distribution of dissipative avalanches and the distribution was given by

$$P_{dc}(s, L) = s^{-\tau_d}[\ln(s)]^{\eta} f_{dc}\left[\frac{s}{L^D}\right] \tag{4.9}$$

where η is an another exponent. In order to verify whether such a correction to scaling is present in the present model with bulk dissipation, the scaling function $f_{\phi,d}$ given in Eq. (4.8) for $\phi = 0$ is plotted in Figs. 4.5(a) and 4.5(b) for 1d and 2d, respectively. For comparison, the scaling function f_{dc} that of the model with boundary dissipation given in Eq. (4.9) is also plotted in the respective plots. It can be seen that without any correction, the scaling function $f_{\phi,d}$ is reasonably constant over a wide range of s in double logarithmic scale in the case of bulk dissipation, whereas it requires a correction to scaling, $[\ln(s)]^{\eta}$, in the case of boundary dissipation for $d = 2$ ($\eta = 0.5$), as observed by Dickman and Campelo[156]. Hence the scaling forms considered here for the model with bulk dissipation are not subject to any logarithmic correction. However, the scaling behaviour of all avalanches are found to be same for both the models as reported in Ref. [176]. This is because the leading singularity is provided by nondissipative avalanches. In order to verify the form of the scaling function given the Eq. (4.8), data collapse has been performed by plotting $P_{\phi,d}(s, L)L^{D_d}$ against s/L^{D_d} for different values of L. Reasonable data collapse for different $P_{\phi,d}(s, L)$ are obtained as shown in the respective lower insets of Figs. 4.4. For $\phi = 1$ in 2d, the FSS form of the distribution $P_{\phi,d}(s, L)$ is expected to follow the usual distribution as given in Eq. (4.2). From the plot of $\partial\sigma_{\phi,d}(q)/\partial q$ vs q as given in upper inset of Fig. 4.4(d), D_d is found to be 2.023 ± 0.020, again close to the value of all avalanches. The value of τ_d is estimated from Eq. (4.4)

as 1.45 ± 0.03, which is a little less than mean-field result as obtained for the all avalanches. However, taking $\tau_d = 3/2$ and $D_d = 2.023$ the best data collapse is obtained, given in the lower inset of Fig. 4.4(d), which confirms the respective form of the scaling function.

It should be noted here that the fraction of dissipative avalanches decays with system size L as it was also reported by Dickman and Campelo[156]. Though in the thermodynamic limit the percentage of dissipative avalanches are negligible, they have an important contribution in determining the capacity dimension that appears in the FSS scaling form. With close observation of Table 4.1 it can be noted that value of $\tau_{\rm nd}$ for nondissipative avalanches are very close that of τ of the all avalanches whereas, the value of D_d for dissipative avalanches are very close to the value of D of all the avalanches for both the extreme values of ϕ in both the dimensions. Note that, the large avalanches which are responsible for the cutoff of the distribution of all avalanches are mostly dissipative, and in the moment analysis the leading contribution comes from those large dissipative avalanches. Hence, the scaling behaviour of such large dissipative avalanches is expected to play a significant role in the catastrophic cascading effect.

4.2.3 The small-world regime: scaling and coexistence

Since SWN preserves both the characteristic of regular lattice and random network, it is important to study the critical properties of the avalanche size distribution in the SWN regime, $2^{-12} < \phi < 0.1$. It has already been shown in chapter 3 that the size distribution $P_\phi(s)$ of all the avalanches exhibit coexistence of two scaling forms in the small-world regime. The size distribution $P_{\phi,\rm nd}(s)$ of the nondissipative avalanches are plotted in Fig. 4.6(a) for 1d and in Fig. 4.6(b) for 2d. In Fig. 4.6(c) and (d), $P_{\phi,d}(s)$ are plotted for 1d and 2d respectively. For 1d and 2d, the values of ϕ used are 2^{-6} and 2^{-8}, respectively, for both the distributions. Since the dissipation occurs in an annealed manner, the maximum size of an avalanche could not be large without dissipating a sand, so the distributions $P_{\phi,\rm nd}(s)$ shrink quickly. Hence the MF scaling form is not prominent enough. However, as $P_\phi(s)$ and $P_{\phi,\rm nd}(s)$ show similar scaling behaviour, it is expected that $P_{\phi,\rm nd}(s)$ also exhibits coexistence of two scaling forms corresponds to $\phi = 0$ and $\phi = 1$, when the system size L is large enough. Interestingly, $P_{\phi,d}(s)$ exhibits its respective scaling forms on regular lattice ($\phi = 0$) and random network ($\phi = 1$) in the same distribution. The straight lines with respective slopes in these plots are guides to the eye. The crossover from one

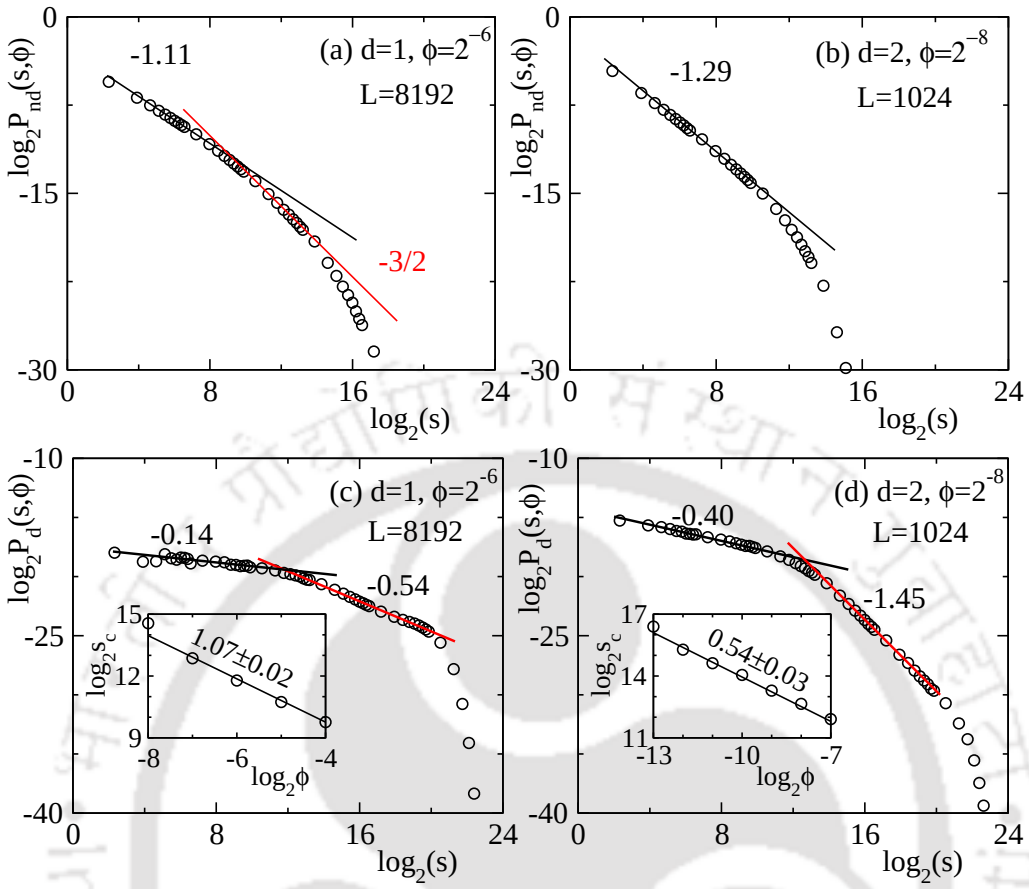

Figure 4.6: Plot of $P_{\phi,\mathrm{nd}}(s)$ against s in (a) for 1d with $\phi = 2^{-6}$ for $L = 8192$ and in (b) for 2d with 2^{-8} for $L = 1024$. The corresponding $P_d(s,\phi)$ is shown in (c) for 1d and in (d) for 2d. The solid lines with the required slope through the data points are guides to the eye. The variation of s_c of dissipative avalanche with ϕ is shown in the respective inset of (c) and (d). The error in estimation of s_c is of the order of the symbol size.

scaling form to other occurs at their respective crossover avalanche size s_c for $P_{\phi,d}(s)$. For $s < s_c$, the avalanches are small, compact, and mostly confined on a regular lattice, whereas for $s > s_c$, they are large, sparse, and mostly exposed to random network. Since $P_{\phi,\mathrm{nd}}(s)$ and $P_\phi(s)$ have similar scaling behaviour, it is expected that $P_{\phi,\mathrm{nd}}(s)$ display a similar crossover scaling as that of $P_\phi(s)$. The coexistence of more than one scaling form in the same distribution of avalanche properties for different sandpile model has been already reported in the literature[154,169,181,211,212]. As one expects the scaling form of regular lattice as $\phi \to 0$ and that of random network as $\phi \to 1$, the value of s_c is found to depend on ϕ. The dependence of s_c on ϕ is assumed as

$$s_c \sim \phi^{-\alpha} \tag{4.10}$$

where α is an exponent. The value of α for all avalanches has already been obtained in chapter 3. Similarly the value of α can also be obtained for nondissipative avalanches. From the conditional expectation of avalanche size for a fixed avalanche area, one expects $s_c \sim a_c^{\gamma_{sa}} \approx \xi^{d\gamma_{sa}}$, where a_c is the average avalanche area for the avalanches of size s_c, γ_{sa} is an exponent[68], and ξ is the crossover length scale below which SWN behaves as regular lattice[138–140]. As $\xi \sim \phi^{-1/d}$, one obtains $s_c \sim \phi^{-\gamma_{sa}}$ and has $\alpha = \gamma_{sa}$. However, a dissipative avalanche occurs only after a required number of toppling equivalently $\langle n_\phi \rangle$. As $\langle n_\phi \rangle \sim \phi^{-1/d}$ in the large-ϕ limit corresponding to random network, one expects $s_c \sim \phi^{-1/d}$ with $\alpha = 1/d$. For a given ϕ the value of s_c of dissipative avalanche is estimated from the intersection point of the straight lines with required slope in the respective regions. The estimated values of s_c is then plotted against ϕ in double logarithmic scale in the respective insets of Figs. 4.6(c) and 4.6(d). It can be seen that for both the cases s_c shows a reasonable power-law scaling with ϕ. By linear least-squares fit through the data points the values of α for dissipative avalanches are found to be 1.07 ± 0.02 for 1d and $\alpha = 0.54 \pm 0.03$ for 2d which are close to the inverse of respective dimensions.

It has already been observed in chapter 3 that, due to the coexistence of two scaling forms, $P_\phi(s, L)$ of DSSM does not satisfy FSS in SWN regime. It is then expected that scaling forms of $P_{\phi,\mathrm{nd}}(s, L)$ and $P_{\phi,d}(s, L)$ also do not obey the FSS on SWN. Instead of FSS form, the ϕ dependence of these distributions are then verified on SWN for a fixed L. A generalized scaling form for nondissipative avalanches on SWN is proposed as

$$P_{\mathrm{nd}}(s,\phi) = \begin{cases} s^{-\tau_{\mathrm{nd1}}} \mathsf{f}\left(\frac{s}{s_c(\phi)}\right) & \text{for } s \leqslant s_c \\ s^{-\tau_{\mathrm{nd2}}} \mathsf{g}\left(\frac{s}{s_c(\phi)}\right) & \text{for } s \geqslant s_c \end{cases} \tag{4.11}$$

where f and g are the respective scaling functions and τ_{nd1}, τ_{nd2} are the corresponding critical exponents for nondissipative avalanches in the $s < s_c$ and $s > s_c$ regions, respectively. At $s = s_c$ for a given ϕ, the limiting values of $P_{\mathrm{nd}}(s, \phi)$ from both the regions must be the same. As $s_c \sim \phi^{-\alpha}$, then one should have $\phi^{\alpha\tau_{\mathrm{nd1}}} \mathsf{f}(1) = \phi^{\alpha\tau_{\mathrm{nd2}}} \mathsf{g}(1)$. Hence, the ϕ-independent scaled distribution can be obtained as

$$P_{\mathrm{nd}}(s,\phi)\phi^{-\alpha\tau_1} = \begin{cases} (s\phi^\alpha)^{-\tau_{\mathrm{nd1}}} \mathsf{f}(s\phi^\alpha) & \text{for } s \leqslant s_c \\ (s\phi^\alpha)^{-\tau_{\mathrm{nd2}}} \mathsf{f}(s\phi^\alpha) & \text{for } s \geqslant s_c \end{cases} \tag{4.12}$$

in terms of a single scaling function f[169]. Such a scaling form is also found to exist in the dynamic scaling of roughness of fractured surfaces[182,183]. To verify

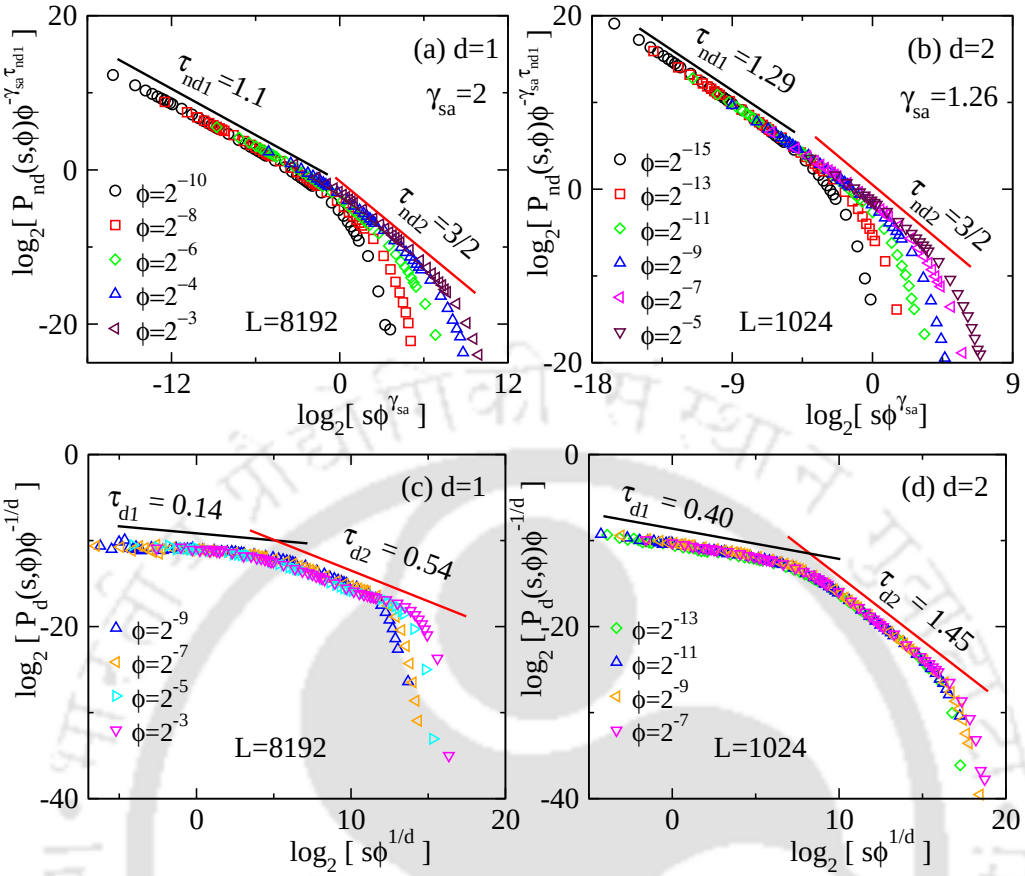

Figure 4.7: Scaled probability distribution (for nondissipative avalanches) against scaled variable is plotted for selected values of ϕ in (a) for 1d with $L = 8192$ and in (b) for 2d with $L = 1024$ to verify the scaling forms given in Eq. (4.12). The same has been verified for dissipative avalanches in (c) for 1d and in (d) for 2d.

the scaling forms given in Eq. (4.12), the scaled probabilities for nondissipative avalanches are plotted against the scaled variable in Figs. 4.7(a) and 4.7(b) for 1d and 2d, respectively, taking $\alpha = \gamma_{sa}$. It can be seen that a good data collapse is obtained using $\gamma_{sa} = 2$, $\tau_{\rm nd1} = 1.1$ for 1d and using $\gamma_{sa} = 1.26$, $\tau_{\rm nd2} = 1.28$ for 2d. The straight lines with required slopes in the respective regions are guides to the eye. It confirms the validity of the proposed scaling function form given in Eq. (4.11). Similarly, a generalized size distribution function can be written for dissipative avalanches around its crossover size s_c taking $\alpha = 1/d$. The scaled probabilities for $P_d(s,\phi)\phi^{-1/d}$ for dissipative avalanches are plotted against the scaled variable $s\phi^{1/d}$ in Figs. 4.7(c) and 4.7(d) for 1d and 2d respectively. Reasonable data collapse is obtained as expected. It is then important to notice that if a dynamical model like sandpile is studied on SWN, multiple scaling forms of an event size will coexist in the distribution of the same.

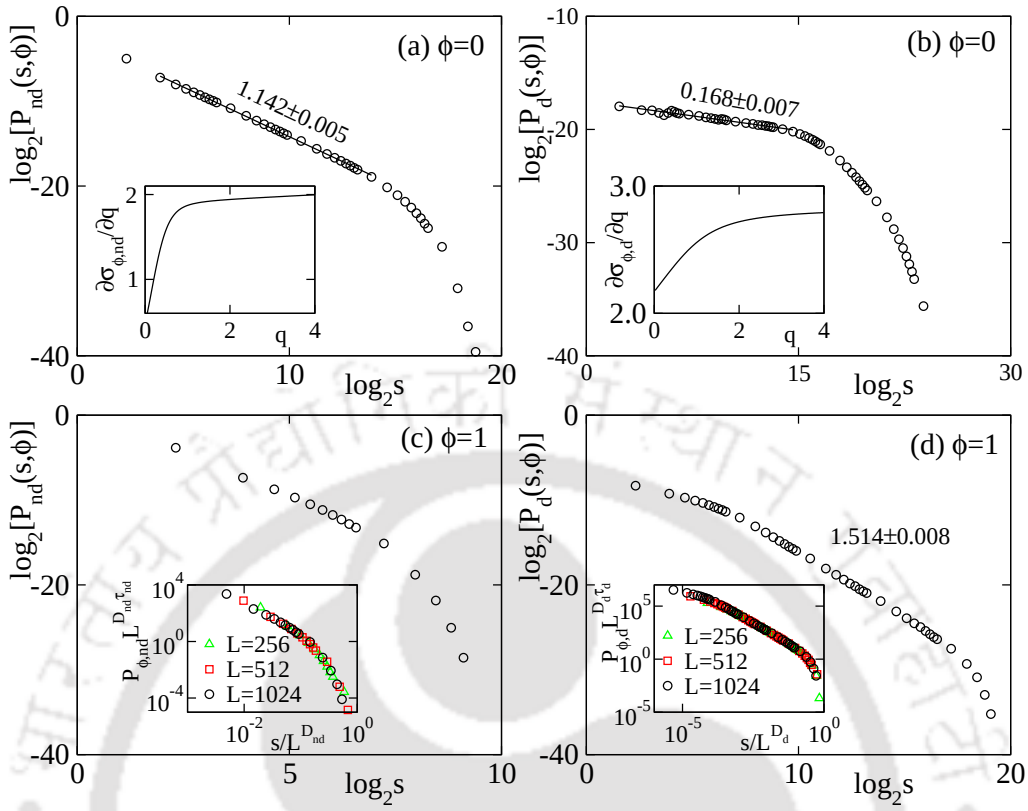

Figure 4.8: Plot of (a) $P_{\rm nd}(s,\phi)$ and (b) $P_d(s,\phi)$ for $\phi = 0$ with system size $L = 1024$. $\partial\sigma_{\phi,\rm nd}/\partial q$ and $\partial\sigma_{\phi,d}/\partial q$ are plotted in the respective insets. Plot of (c) $P_{\rm nd}(s,\phi)$ and (d) $P_d(s,\phi)$ for $\phi = 1$. Insets of (c) and (d) show the FSS data collapse for different system sizes $L = 256(\triangle), 512(\square), 1024(\bigcirc)$.

4.3 DDSM: nondissipative and dissipative avalanches

In order to investigate the FSS behaviour of deterministic BTW model with boundary dissipation, Drossel[207] in 2000 reported that nondissipative and dissipative avalanches of deterministic BTW model with boundary dissipation not only follow a new scaling behaviour but also do not follow FSS. Since the dissipative deterministic sandpile model does not follow FSS on regular lattice but it follows FSS on random network (as seen in chapter 2), it is intriguing to study the scaling behaviour of nondissipative and dissipative avalanches separately on SWNs. The size distribution of nondissipative and dissipative avalanches for two extreme values of ϕ are presented in Fig. 4.8. It should be noted that the distribution of all avalanches of DDSM do not obey FSS on regular lattice ($\phi = 0$), which has been shown in chapter 2. It has also been verified by Drossel[207] that the nondissipative and dissipative avalanches of deterministic model do not follow FSS when studied on regular lattice with boundary dissipation. Such violation of FSS for nondissipative and dissipa-

	DDSM(2d)		
	nondissipative	dissipative	all
$\phi = 0$	$\tau_{\rm nd} = 1.142(5)$	$\tau_d = 0.168(7)$	$\tau = 1.11(1)$
$\phi = 1$	$D_{\rm nd} = 1.01(1)$	$D_d = 2.01(2)$	$D = 2$
	$\tau_{\rm nd} = 1.50(3)$	$\tau_d = 1.50(1)$	$\tau = 1.50(1)$

Table 4.2: Values of D and τ for DDSM in 2d at $\phi = 0$ and at $\phi = 1$ for nondissipative avalanches, dissipative avalanches, and all avalanches.

tive avalanches are also observed in the present study with bulk dissipation. The derivative of the moment scaling function $\partial\sigma_{\phi,nd}/\partial q$ and $\partial\sigma_{\phi,d}/\partial q$ do not converge in large q limit which are shown in the insets of Figs. 4.8(a) and Figs. 4.8(b), respectively. Hence, instead of estimating the exponents τ_d and $\tau_{\rm nd}$ for $\phi = 0$ from moment analysis, those are estimated by fitting the straight lines through the data points of the distributions in double logarithmic scale. In this method the exponents for $\phi = 0$ are found to be $\tau_{\rm nd} = 1.142 \pm 0.005$ and $\tau_d = 0.168 \pm 0.007$ for a system of size $L = 1024$. The distribution exponent $\tau_{\rm nd}$ is found to be very close to the distribution exponent τ of all the avalanches as found in chapter 2. Contrary to the present observation, the value of τ_d of BTW model on a regular lattice with boundary dissipation was reported as 7/9 by Drossel[207]. Hence the distribution exponent of dissipative avalanches significantly depends on the mode of dissipation. It could also be noted here that, the value of the exponent τ_d of DDSM differs considerably from that of DSSM ($\tau_{d,\rm DSSM} = 0.40$) for $\phi = 0$. On the other hand, the size distributions of nondissipative and dissipative avalanches for $\phi = 1$ are presented in Figs. 4.8(c) and 4.8(d), respectively. Since all the avalanches of DDSM follow FSS in random network regime ($\phi \to 1$) it is expected that nondissipative and dissipative avalanches should also follow FSS. Performing moment analysis the values of the exponents are found to be $\tau_d = 3/2$ and $D_d = 2.01 \pm 0.02$ for the dissipative avalanches, and $\tau_{\rm nd} = 3/2$ and $D_{\rm nd} \approx 1$ for nondissipative avalanches. Taking the respective values of the exponents of nondissipative and dissipative avalanches, the collapse of data are obtained for various system sizes which are shown in respective inset of Figs. 4.8(c) and 4.8(d). The values of all the critical exponents of nondissipative and dissipative avalanches of DDSM at extreme values of ϕ are summarized in Table 4.2. It could be observed that, though the values of various critical exponents $\tau_d, \tau_{\rm nd}, D_d$, and $D_{\rm nd}$ for the deterministic and stochastic models are found to differ considerably on regular lattice ($\phi = 0$) they are same for both the models on random network ($\phi = 1$). On an infinite dimensional random network the avalanche properties are always found to follow MF scaling, irrespective of toppling rules of the

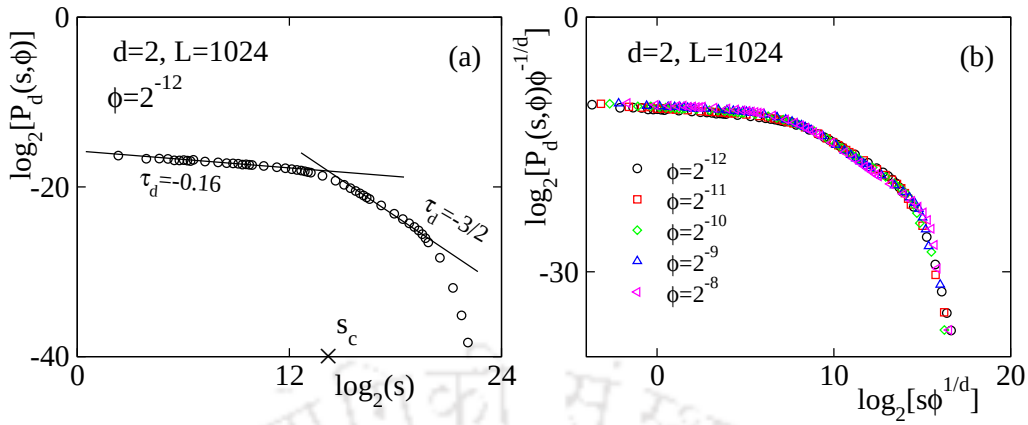

Figure 4.9: Plot of (a) $P_d(s,\phi)$ for $\phi = 2^{-12}$ with $L = 1024$. Lines are with respective slopes as marked. (b) Scaled distributions are plotted for selected values of ϕ for the dissipative avalanches.

model (deterministic or stochastic) or the types of the avalanches, nondissipative, dissipative. Since the dimension of the random network is much higher than the upper critical dimension $d_c = 4$ of both the models[66,67], it is expected that both the models should exhibit MF scaling.

Knowing the scaling behaviour of the distribution functions for nondissipative and dissipative avalanches at extreme values of ϕ, it is now important to check the scaling behaviour of the same in the SWN regime. It is intriguing to see whether the dissipative avalanches of DDSM obey similar crossover scaling behaviour as that of the DSSM or not. Since distributions of all avalanches and nondissipative avalanches exhibit similar scaling behaviour it is expected that nondissipative avalanches also exhibit coexistence scaling similar to that of all avalanche as discussed in chapter 2. In the following results of dissipative avalanches are presented. The distribution of dissipative avalanches $P_d(s,\phi)$ is shown in Fig. 4.9(a) for a suitable value of ϕ. It can be seen that different scaling forms depending of the size of the avalanches are prominent and it is possible to identify the crossover size (s_c) which separates the two regimes. The dissipative avalanches of size $s < s_c$ obey the power-law scaling with exponent $\tau_d = 0.16$ that corresponds to the scaling behaviour of dissipative avalanches at $\phi = 0$. The dissipative avalanches of size $s > s_c$ shows the mean-field scaling ($\tau_d = 3/2$). Such two scaling behaviours are shown by the straight lines. Following the previous scaling arguments a similar coexistence scaling for dissipative avalanches can also be obtained taking $s_c \sim \phi^{-1/d}$, d being the space dimension. The scaled distribution is plotted against the scaled variable for different values of ϕ in Fig. 4.9(b) where a reasonable collapse of data is obtained. Hence it can be infer

that the coexistence scaling theory not only valid for different types of models but can be applied also for different types of avalanches when the correct scaling form of the crossover size is incorporated.

4.4 Conclusion

The effect of network topology and specific dissipation mode (bulk or boundary) on the steady-state critical properties of nondissipative and dissipative avalanches of both the deterministic and stochastic models are studied. For the stochastic version of dissipative model, the nondissipative avalanches display usual stochastic scaling of SSM on regular lattice ($\phi = 0$) and mean-field scaling on random network ($\phi = 1$) as that of all avalanches. However, the dissipative avalanches represent a number of novel scaling properties on regular lattice as well as on random network in both 1d and 2d. The scaling behaviour of these avalanches on regular lattice is found to differ considerably from the Dickman-Campelo scaling as observed with the open boundary in both dimensions. The bulk dissipation is found to have a nontrivial effect on dissipative avalanches over the boundary dissipation. No logarithmic correction to scaling is found to occur as it was required for these avalanches on regular lattice with boundary dissipation. A set of new scaling exponents are found to describe the scaling of dissipative avalanches on regular lattice and random network. On SWN, in the intermediate range of ϕ, the model exhibits coexistence of more than one scaling form in both 1d and 2d around a crossover size $s_c(\phi)$. For nondissipative and dissipative avalanches, however, the crossover size s_c scales with ϕ with two different exponents. On the other hand, for deterministic models, nondissipative and dissipative avalanches do not obey FSS at $\phi = 0$ as it was observed by Drossel[207], whereas both the types of avalanches follow FSS at $\phi = 1$ as BTW-type correlation in toppling wave does not exist on random network. The scaling exponents that describe the power-law behaviour of dissipative avalanches are estimated at extreme values of ϕ. Similar to stochastic model, the deterministic model also exhibits coexistence of more than one scaling form in small world regime and it is possible to identify the crossover size s_c for such avalanches. For both the models the coexistence scaling form of the avalanche size distribution function around s_c is proposed and numerically verified. SWN can not only segregates of several scaling forms that appear in the event size distribution of a dynamical system but also found to have profound effect on the critical behaviour that self-organized on networks.

Chapter 5

Preferential sandpile model on scale-free networks

Though the concept of self-organized criticality (SOC) found to have a wide range of applications, self-organizing systems as such do not have any control parameter. Any attempt to control such systems by external means may initiate unwanted devastating effects because of its complex feedback mechanism. Carefully designed techniques are attempted in the recent past to control the critical dynamics of sandpile avalanches on Euclidean space as well as on complex networks. A few examples are: suppression of the avalanches in a local region of a lattice[166,167] or triggering the avalanches at highest degree nodes that are about to become critical[214], dropping of sands on the nodes nearer to the nodes which are expected to be critical[168], modification of inter-connectivity of the interdependent networks[215], etc. The outcome of these control processes on self-organizing systems are found to be unexpected and novel. At the same time, the difficulty in implementing such control processes in these systems makes controlling SOC a challenging problem[168].

On the other hand, it has already been described in chapter 1 that, topological features of many infrastructural facilities of modern society like power transmission grid, internet, World Wide Web etc., can be well described by complex networks[9,12,14]. In many cases the degree of nodes of such networks are distributed in a power-law fashion,

$$P_k \sim k^{-\alpha} \tag{5.1}$$

α being the characteristic degree exponent. Such networks are known as scale-free network (SFN)[9]. Due to strong heterogeneity in the degree distribution of

This chapter is based on the Ref. [213]; H. Bhaumik and S. B. Santra, arXiv, cond-mat.stat-mech/1705.10646.

SFN the translational symmetry, nodes with similar neighbourhood, is found to be absent for $\alpha < 4$ and it is identified as scale-free regime whereas the regime corresponding to $\alpha > 4$ is known to be random regime[216]. Such networks very often suffer from cascading failure. Black out of electric power grid in an entire country[29,217], breakdown of internet[120] or financial market[218] etc are a few classic examples of such devastating cascading failure. Study of SOC on these networks took the central stage in recent times[11,219] because such failure phenomena can be described by avalanche dynamics of a sandpile model. The avalanches dynamics of both the BTW sandpile model and the stochastic sandpile model (SSM) have been studied on SFN by Goh *et al.*[161,220,221]. Controlled SOC of the BTW model on complex network has also been studied by allowing certain degree of failure tolerance for the nodes[222]. A heterogeneous load distribution scheme developed by Hou *et al.*[223] shows that weak heterogeneity in the load distribution diminish the avalanche size whereas strong heterogeneity leads to large failure.

It this chapter, controlling of SOC on SFN has been performed developing a two-state sandpile model with preferential sand distribution, namely preferential sandpile model (PSM). In the previous chapters, SOC has been explored and controlled varying the substrate topology from regular lattice to small world network to random network by tuning the shortcut density from 0 to 1. However, defining PSM on SFN would provides much wider scope of tuning system parameters to control SOC. Different mechanisms of controlling of SOC on SFN can be adopted. First, the heterogeneity in the degree distribution of the network can be modified by tuning α, the degree exponent. Second, the rate of bulk dissipation as sand flowing from a node to another node can be varied. Third and most vital, the flow of sand to the nodes of specific degrees rather than to random ones as in the SSM can be controlled. The effect of all these variations of the parameters on SOC of PSM is studied here.

5.1 The model

Scale-free networks of N nodes are generated employing uncorrelated configurational model[224]. In order to get a scale-free degree distribution, a random number r, uniformly distributed between $[0, 1]$, is drawn for each node and degree $k = \mathrm{INT}[k_{\min}/r^{1/(\alpha-1)}]$ where $k_{\min} = 2$, is assigned. The natural upper cutoff of the degree for a SFN is $k_{\max} = N^{\beta}$ where $\beta = 1/(\alpha - 1)$. However, for $\alpha \leq 3$ the upper cutoff is set to $\sqrt{N}$ instead of the natural cutoff which eventually would

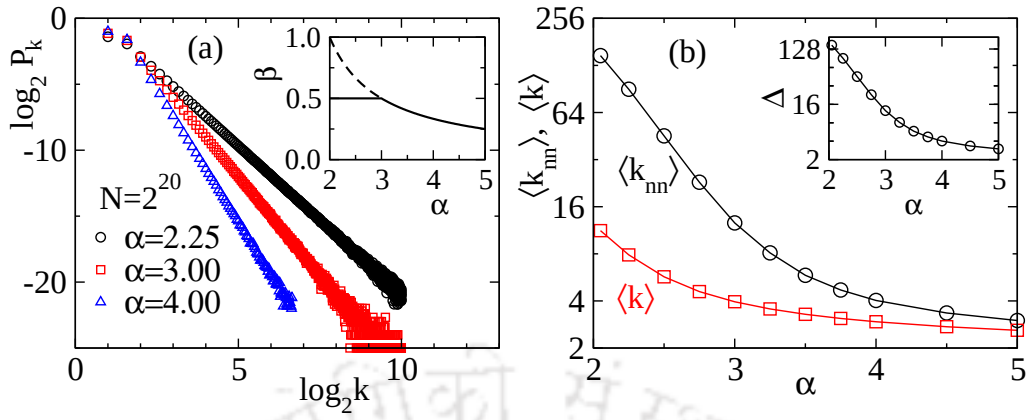

Figure 5.1: (a) Plot of P_k against k for different values of α for a network of size $N = 2^{20}$. The distribution is sampled over 32 configurations. Inset: Plot of $\beta = \ln k_{\max}/\ln N$ *vs* α shown in solid line. The dashed line shows the natural cutoff $\beta = 1/(\alpha - 1)$ for $\alpha < 3$. (b) Plot of $\langle k_{nn}\rangle$ ($\bigcirc$) and $\langle k\rangle$ ($\square$) against α. Inset shows how their difference $\Delta = \langle k_{nn}\rangle - \langle k\rangle$ changes with α.

satisfy the conditions of no multiple edge or self-edge of the nodes in an uncorrelated random SFN. The degree distributions of some of the networks considered are shown in Fig. 5.1(a) for different values of α. The values of β used to fix $k_{\max}$ for different values of α are shown in the inset of Fig. 5.1(a). The likely neighbourhood of nodes is identified by comparing the average nearest neighbour degree $\langle k_{nn}\rangle$ with the average degree $\langle k\rangle$ of a network as shown in Fig. 5.1(b). The difference between the two averages $\Delta = \langle k_{nn}\rangle - \langle k\rangle$ is shown in the inset of Fig. 5.1(b) and found to be quite large for small α, scale-free regime and decreases to $k_{\min}$ as $\alpha \to \infty$, random regime.

For a given α, the SFN with N nodes is driven by adding sand grains, one at a time, to a randomly chosen node i. If the height h of the sand column at the ith node is greater than or equal to the threshold value $h_c = 2$, the sand column becomes unstable or critical and collapses by distributing two sand grains to two neighbouring nodes, n_1 and n_2. For a systematic study, the degree $k(n_1)$ of the node n_1 is fixed to the lowest possible value and the choice of $k(n_2)$ the degree of the other node n_2 will be varied from a lower value to the maximum possible value among the available adjacent nodes of the critical node. The toppling rule of the ith critical node is then given by

$$h_i \to h_i - h_c,$$
$$\text{and} \quad h_j = \begin{cases} h_j & \text{if } r \le \epsilon, \\ h_j + 1 & \text{otherwise} \end{cases} \tag{5.2}$$

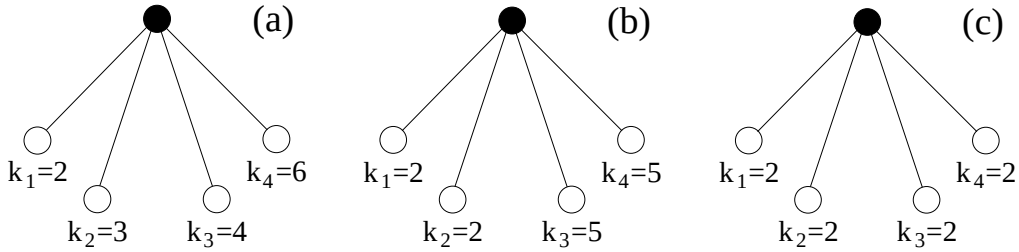

Figure 5.2: Toppling rules for PSM on a node of degree $k = 4$ are demonstrated. The black filled circle represents the critical node which has 4 adjacent nodes (open circle) with degree, say, k_1, k_2, k_3, and k_4. In (a) $k_1 < k_2 < k_3 < k_4$, the nodes with degree k_1 and k_4 receive one sand grain each. In (b) $k_1 = k_2 < k_3 = k_4$, two sand grains are distributed among one of the randomly chosen node from $\{k_1, k_2\}$ and another from $\{k_3, k_4\}$. In (c) $k_1 = k_2 = k_3 = k_4$, two sand grains are randomly given to any two distinct nodes.

where r is a random number, ϵ is the dissipation factor by which a sand grain is removed from the system at each sand transfer, and $j = \{n1, n2\}$ corresponds to two adjacent nodes of specific degrees. The toppling rule for a critical node is demonstrated in Fig. 5.2 taking $k(n_1)$ be the lowest degree ($k_{\mathrm{nn,min}}$) and $k(n_2)$ be the highest degree ($k_{\mathrm{nn,max}}$) among its neighbouring nodes. If more than one node has the same degree for selecting n_1 and n_2, one of them is chosen randomly. If the toppling of a critical node causes the adjacent nodes critical, subsequent toppling follows on these nodes in parallel until all the nodes in the network become under critical. These toppling activities lead to an avalanche. As the avalanche seized, another sand grain is added to the system.

The model is studied varying α from 2 to 5 for a given ϵ. Since on the random network, $\epsilon \sim 1/\sqrt{N}$ [169] for a network of N nodes, for most of the values of α the value of ϵ is taken to be $1/\sqrt{N}$. However, the effect of ϵ on the sandpile dynamics in this model is verified for a few specific values of α. For a given α and ϵ, the model is mostly studied taking n_1 as the lowest degree node and n_2 as the highest degree node among the neighbouring nodes of the critical node. However, the effect of the choice of $k(n_2)$ on SOC in this model is verified for a few intermediate values of degree k. If the degree of n_2 is taken to be close to that of the lowest degree node n_1 one expects MF behaviour as most of nodes will be having intermediate to low degrees whereas it is expected to deviate from the MF as k of n_2 chosen to be high that of a few nodes in the network.

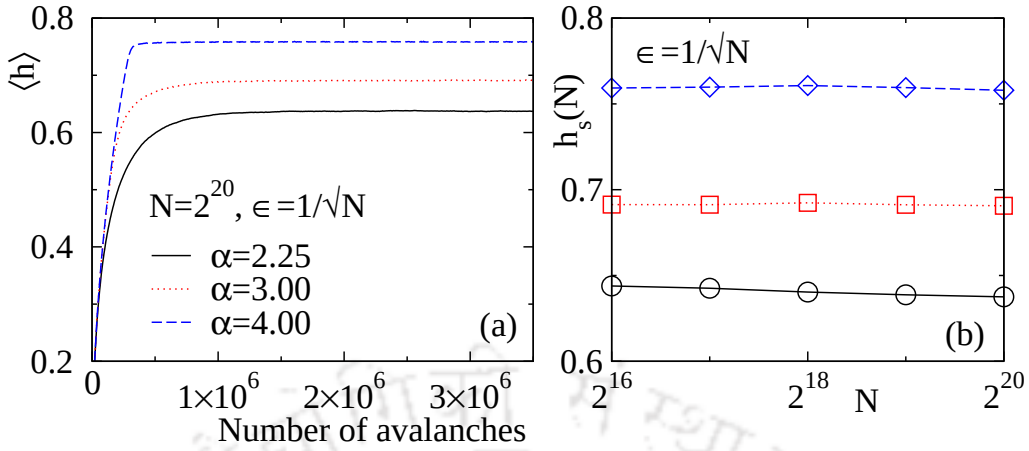

Figure 5.3: (a) Plot of $\langle h \rangle$ against number of avalanches on SFN of size $N = 2^{20}$ for $\alpha = 2.25$ (black solid line), 3 (red dotted line), and 4 (blue dashed line) taking $\epsilon = 1/\sqrt{N}$. (b) The variation of h_s with network size N for $\alpha = 2.25$ (○), 3 (□), and 4 (◇) for the same value of ϵ.

5.2 Numerical simulation and steady state

An extensive computer simulation is performed varying α from 2 to 5. For a given α, the size of the networks N varied from $N = 2^{16}$ to $N = 2^{20}$ in multiple of 2. In order to estimate the avalanche properties, the following statistical averages are made. For a given α and N, thirty two different SFN configurations are considered. On each SFN, 10^6 avalanches are collected neglecting the first 3×10^6 avalanches during which steady state has been achieved in all networks. Therefore, for a given α and N, a total of 32×10^6 avalanches is taken for data averaging. The critical behaviour of different avalanche properties like the avalanche size s (total number of toppling in an avalanche), area a (the number of distinct nodes toppled in an avalanche), and lifetime t (the number of parallel updates to make all the nodes under critical) of an avalanche are measured in the steady state to characterize the PSM on SFN. Data presented below for various values of α taking $\epsilon = 1/\sqrt{N}$ and n_2 as the largest degree neighbour of the critical node if it is not mentioned otherwise.

The steady state corresponding to the balance of incoming and outgoing fluxes of sand grains leads to time independent average height of the sand columns in the network. The average height $\langle h \rangle$ is calculated as

$$\langle h \rangle = \frac{1}{N} \sum_{i=1}^{N} h_i \tag{5.3}$$

where h_i is the height of the sand column at the ith node. In Fig. 5.3(a), $\langle h \rangle$ is

plotted against the number of avalanches for different values of α on a network of size $N = 2^{20}$. Starting from an empty configuration, the steady state of PSM is achieved after more than 10^6 avalanches for all values of α. It can be seen that the values of $\langle h \rangle$ at the steady state increases as α increases. Since the critical height $h_c = 2$ in this model, at the end of an avalanche, the nodes either will have a sand or they will remain empty. Thus for $\alpha = 4$, nearly 75% of the nodes are having sands whereas for $\alpha = 2.25$, nearly 60% of the nodes are having sands. For a given value of α, the saturated average height h_s of the sand columns in the steady state is estimated taking average over last 10^5 avalanches of every 32 different configurations. For a given value of α, h_s is found to be independent of network size N as shown in the Fig. 5.3(b) for three different values of α. It has also been verified that h_s increases if the dissipation factor ϵ decreases and vice verse for a given α as expected.

In order to compare the results of PSM with that of the SSM, the above numerical computation has also been repeated for SSM on the similar networks. In the case of SSM, similar variations of h_s with α, N and ϵ are observed.

5.3 Avalanche evolution

Time evolution of a few typical avalanches of PSM generated on a network of size $N = 2^{14}$ are shown in the upper row of Fig. 5.4 for different values of α. For comparison, time evolved morphology of the avalanches of SSM on the same networks are given in the lower row of Fig. 5.4. The degree k of the nodes is presented along the horizontal axis and time (the parallel updates) is presented along the downward vertical axis. The black dots represent the toppled nodes, the gray colour corresponds to the nodes of certain degree with no toppling and white space represents no node of that degree. The avalanches presented here have a common size $s = 800$ for both the models, the area a are mentioned at the bottom of each configuration and their lifetime t (maximum number of parallel updates) can be seen from the vertical axis. The time evolution of an avalanche of PSM differs considerably from that of the SSM on the given network. As α increases, a increases but t decreases in the case of PSM whereas both t and a decrease slightly for the SSM. For PSM, an avalanche of a fixed size is found to have large lifetime (t) as well as small avalanche area (a) in the scale-free regime ($2 \leq \alpha \leq 3$) that indicates multiple toppling of the nodes whereas in the random regime with $\alpha \geq 4$, the avalanche of same size has small lifetime and large avalanche area a which indicates single toppling of the nodes. On the other hand, for SSM, both t and a are the largest in the scale-free

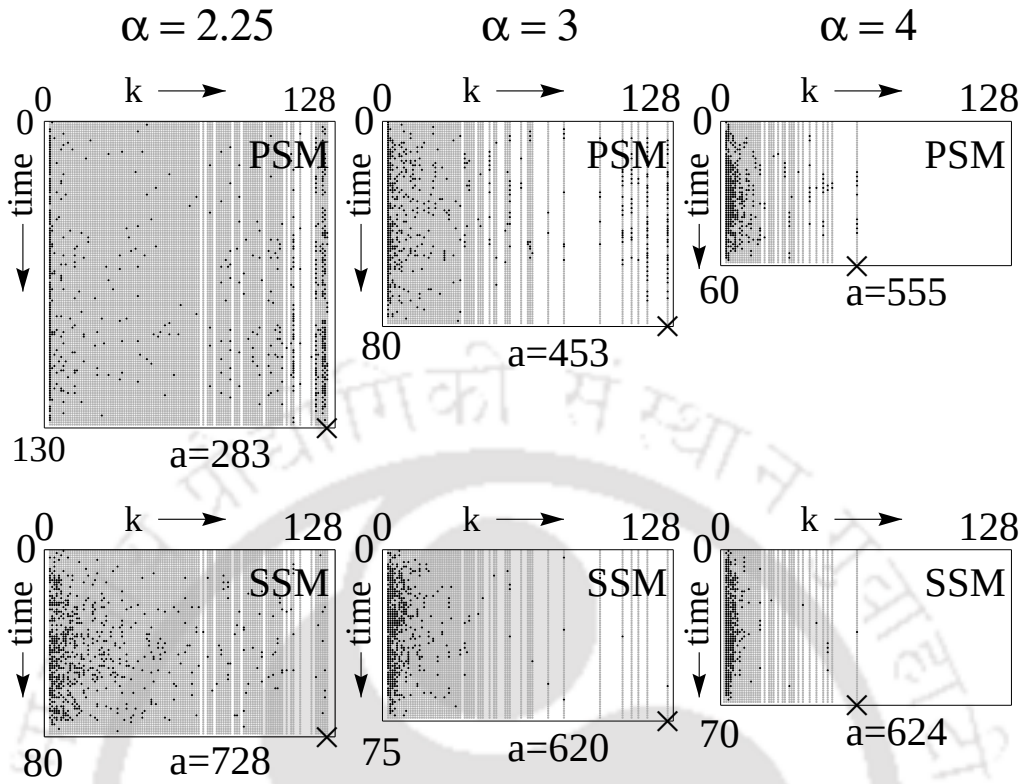

Figure 5.4: Time evolution of typical avalanches of PSM (upper row) and those of SSM (lower row) in degree space are shown for $\alpha = 2.25$ (left column), $\alpha = 3$ (middle column), and, $\alpha = 4$ (right column) on a network of size $N = 2^{14}$ taking $\epsilon = 1/\sqrt{N}$. The black dots represent the toppled nodes and the gray colour represents the nodes with no toppling. The white space corresponds to no nodes of such degree. The crosses represent the maximum degree present in the network.

regime. It can be noted that the density of toppled nodes in PSM is high at the lower as well as the higher degree nodes of the network in scale-free regime whereas most of the lower degree nodes are involved in an avalanche in the random regime. On the other hand, in SSM, the density of toppled nodes decreases with increasing k at all values of α. Such degree dependence of the toppling number density ρ_k can be quantified by toppling number density-density correlation $C_\rho(\Delta k)$ function in the degree space. It is defined as

$$C_\rho(\Delta k) = \frac{\langle \rho_{k+\Delta k}\rho_k \rangle - \langle \rho_k \rangle^2}{\langle \rho_k^2 \rangle - \langle \rho_k \rangle^2} \tag{5.4}$$

where the toppling number density for a given α is $\rho_k = \langle s_k/s \rangle_\alpha$ with s_k being the number of toppling occurring at the nodes of degree k in an avalanche of size s, $\Delta k = 1, 2, \cdots$, and $\langle \cdots \rangle$ denotes an average over the number of Δks occurring

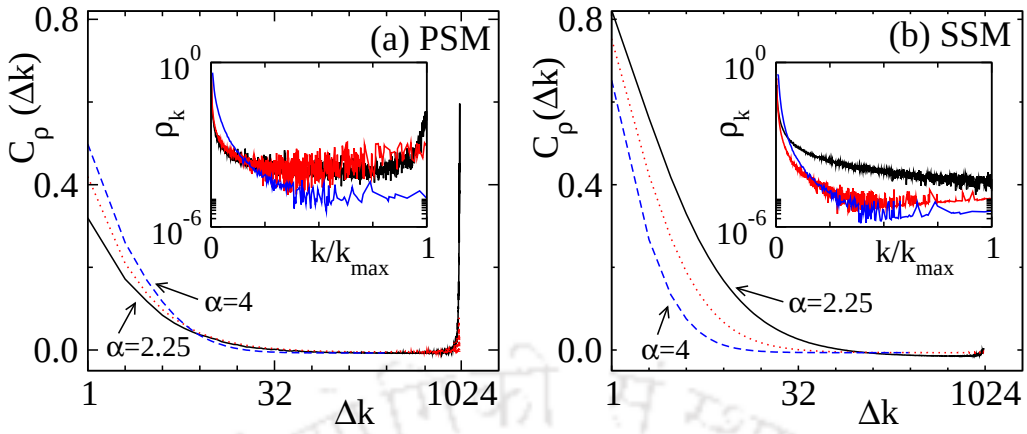

Figure 5.5: Plot of $C_\rho(\Delta k)$ against Δk for (a) PSM and (b) SSM for different values of $\alpha : 2.25$ (solid line), 3 (dotted line) and 4 (dashed line) with network size $N = 2^{20}$. ρ_k are plotted against $k/k_{\max}$ in the respective insets for $\alpha = 2.25$ (black), 3 (red) and 4 (blue).

between $k_{\max}$ and $k_{\min}$ of a network. $C_\rho(\Delta k)$ is calculated on a network of size $N = 2^{20}$ for three different values of $\alpha = 2.25, 3, 4$ and plotted against Δk in Fig. 5.5(a) for PSM and in Fig. 5.5(b) for SSM. The variation of toppling number density ρ_k against the normalized degree $k/k_{\max}$ are shown in the respective insets which rightly depict the final morphology of an avalanche in the k-space (Fig. 5.4). A few conclusions can be made from the plot of $C_\rho(\Delta k)$. First, there is a drastic change in the behaviour at $\alpha = 4$ (random regime) than at $\alpha = 2.25$ (scale-free regime) in PSM (Fig. 5.4(a)). In the random regime, most of the contributions to the correlation function $C_\rho(\Delta k)$ come from small Δk ($\Delta k < 32$) that corresponds to sand transfer between nearest degrees whereas in the scale-free regime it is dominated by both small and high Δk that correspond to sand transfer between extreme degree nodes beside that between nearest degree nodes. Second, in the case of SSM (Fig. 5.4(b)), most of the contributions to the correlation function $C_\rho(\Delta k)$ come from small Δk irrespective of the values of α, i.e., random or scale-free regime. Third, as α decreases the contribution from small Δk decreases in PSM whereas in SSM the effect is just reverse. Thus on the scale-free network, the sand transfer mechanism is completely different on the PSM than on the SSM. In PSM the nodes of extreme degrees are mostly involved during an avalanche whereas in SSM the avalanche needs to explore the whole network through sand transfer between nodes of nearest degrees. Such a behaviour is due to the targeted sand distribution to the nodes of specific degrees rather than random sand distribution as in SSM. It is then important to characterize the critical properties of PSM as a function of the controlled parameters such as α, ϵ, and $k(n_2)$ and study their consequences on the cascading effect in this model.

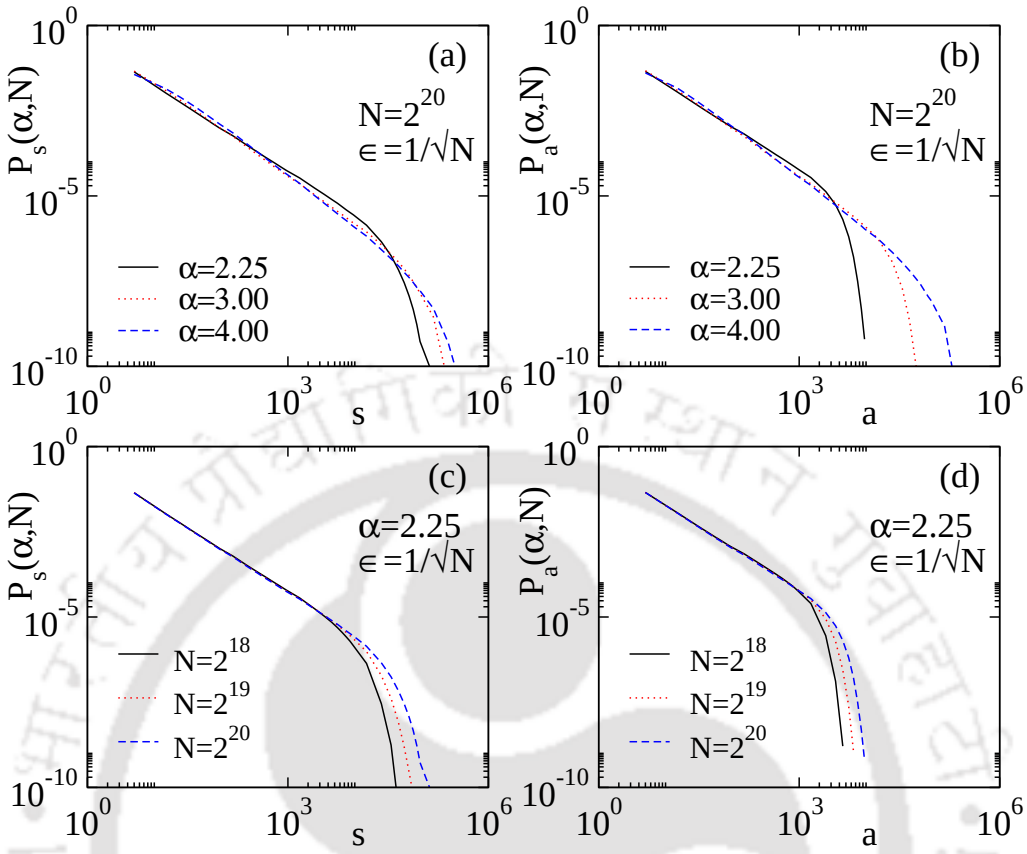

Figure 5.6: Plot of $P_s(\alpha, N)$ against s and $P_a(\alpha, N)$ against a in (a) and (b) respectively for $\alpha = 2.25$ (solid line), $\alpha = 3$ (dotted line), $\alpha = 4$ (dashed line) for a network of size $N = 2^{20}$. For a given α, the distributions for different network sizes $N = 2^{18}$ (solid line), $N = 2^{19}$ (dotted line), and $N = 2^{20}$ (dashed line) are shown in (c) for $P_s(\alpha, N)$ and in (d) for $P_a(\alpha, N)$. All distributions are estimated taking $\epsilon = 1/\sqrt{N}$.

5.4 Probability distribution, moment analysis, and FSS

To characterize the properties of PSM with $k(n_1) = k_{\text{nn,min}}$ and $k(n_2) = k_{\text{nn,max}}$, the probability distributions $P_x(\alpha, N)$ of avalanche properties $x \in \{s, a\}$ at the critical steady state are determined for various values of degree exponent α, keeping the dissipation factor $\epsilon = 1/\sqrt{N}$ where N is the network size. For $N = 2^{20}$, the distributions $P_s(\alpha, N)$ and $P_a(\alpha, N)$ are plotted in Figs. 5.6(a) and 5.6(b) respectively for several values of α. Keeping α fixed at 2.25, the same distributions $P_s(\alpha, N)$ and $P_a(\alpha, N)$ for different values of N are plotted in Figs. 5.6(c) and 5.6(d) respectively. Though the cutoffs depend on both N and α for a given ϵ, the scaling exponents seem to be independent of the network size N for a given α but it depends on α for a given N. Hence, for given α and N, a finite-size scaling (FSS) form of $P_x(\alpha, N)$ is

assumed as

$$P_x(\alpha, N) = x^{-\tau_x(\alpha)} f_{x,\alpha}\left[\frac{x}{N^{D_x(\alpha)}}\right], \tag{5.5}$$

where $\tau_x(\alpha)$ is the scaling exponent, $D_x(\alpha)$ is the capacity dimension, and $f_{x,\alpha}$ is a α dependent scaling function of an avalanche property x for a given ϵ. Estimating the critical exponents, the FSS form of the distribution function will be verified in the following. Though the two-state models like SSM[55,56] follow FSS on regular lattice, the BTW model does not. It is then intriguing to verify whether FSS of PSM when defined on SFN is valid or not.

In order to estimate the values of the exponents $\tau_x(\alpha)$ and $D_x(\alpha)$, [Eq. (5.5)], the concept of moment analysis[65] has been used. For a given α, the qth moment of x as function of N can be obtained as

$$\langle x^q(\alpha, N)\rangle \;=\; \int_0^\infty x^q P_x(\alpha, N) dx \sim N^{\sigma_x(\alpha,q)}, \tag{5.6}$$

where the qth moment scaling exponent

$$\sigma_x(\alpha, q) = D_x(\alpha)q + D_x(\alpha)[1 - \tau_x(\alpha)] \tag{5.7}$$

for $q > \tau_x(\alpha) - 1$ and it is zero for $q < \tau_x(\alpha) - 1$. For each value of α, a sequence of values of $\sigma_x(\alpha, q)$ as a function of q is determined by estimating the slope of the plots of $\log\langle x^q(\alpha, N)\rangle$ versus $\log(N)$ for 400 equidistant values of q between 0 and 4. $\sigma_s(\alpha, q)$ and $\sigma_a(\alpha, q)$ are plotted against q for $\alpha = 2.25$, 3, and 4 in Figs. 5.7(a) and 5.7(b) respectively. First, it can be seen that for $q = 1$, the value of $\sigma_s(\alpha, 1)$ is found to be $\approx 1/2$ (indicated by arrows in Fig. 5.7(a)) irrespective of the values of α. Since the dissipation factor is taken as $\epsilon = 1/\sqrt{N}$ for all values of α, to maintain the steady state, the average number of toppling required for an avalanche to dissipate one sand grain is $\sqrt{N}$. Hence, $\langle s\rangle \sim N^{1/2}$, i.e., $\sigma_s(\alpha, 1) = 1/2$ for all α. In order to estimate the values of the exponents, the direct method developed by Lübeck[65] is employed. Following such method, straight lines are fitted through the data points $\{\sigma_x(\alpha, q), q\}$ in the range of $2 \leq q \leq 4$ and the exponents $\tau_x(\alpha)$ and $D_x(\alpha)$ are obtained from the intercepts on the q-axis and $\sigma_x(\alpha, q)$ axis respectively for a given α. Following Eq. (5.7), the q intercept provides $\tau_x(\alpha) - 1$, the $\sigma_x(\alpha, q)$ intercept provides $D_x(\alpha)[1 - \tau_x(\alpha)]$. The estimated values of the exponents are: $\tau_s = 1.296(7)$, $\tau_a = 1.407(6)$, $D_s = 0.720(6)$, $D_a = 0.534(5)$ for $\alpha = 2.25$; $\tau_s = 1.403(6)$, $\tau_a = 1.478(6)$, $D_s = 0.852(5)$, $D_a = 0.837(6)$ for $\alpha = 3$; $\tau_s = 1.491(5)$, $\tau_a = 1.503(4)$,$D_s = 0.975(6)$,$D_a = 0.994(5)$ for $\alpha = 4$.

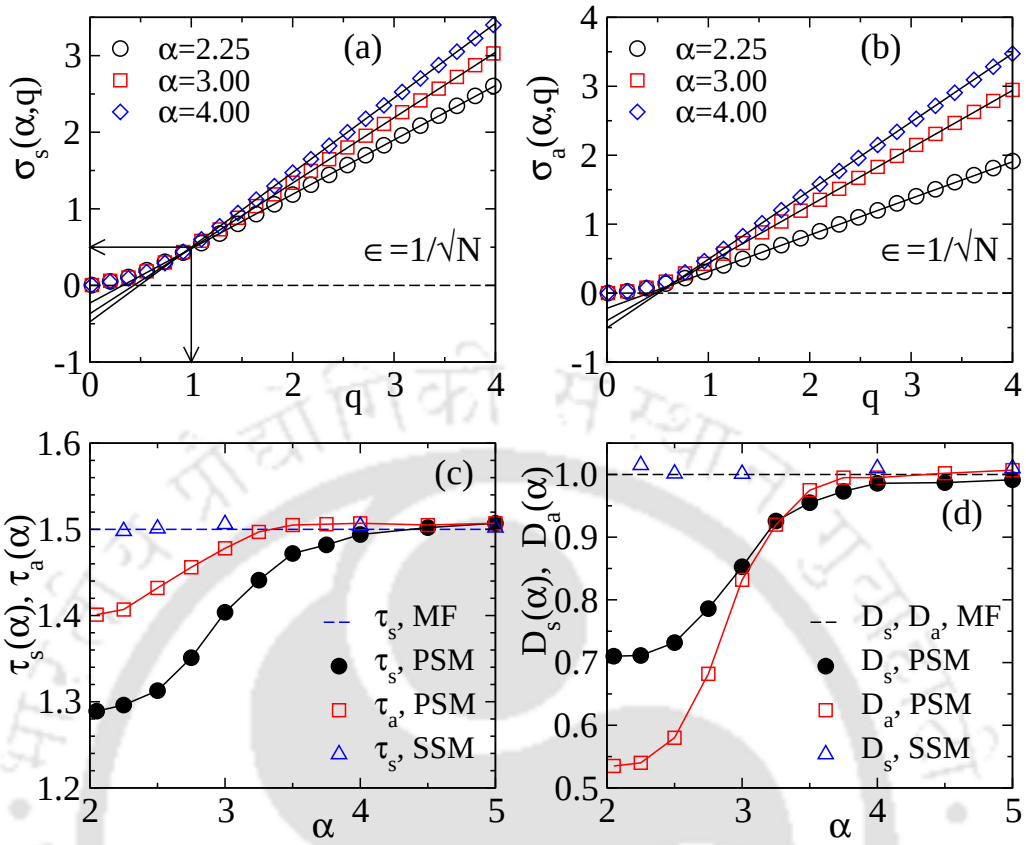

Figure 5.7: Plot of (a) $\sigma_s(\alpha, q)$ and (b) $\sigma_a(\alpha, q)$ against q for $\alpha = 2.25$ (●), $\alpha = 3$ (□), and $\alpha = 4$ (◇). For clarity only 25 points out of 400 points are shown. The solid lines represent the linear least square fit through the data points. (c) Plot of $\tau_s(\alpha)$ (black filled circle) and $\tau_a(\alpha)$ (red open square) against α. For comparison, $\tau_s(\alpha) = \tau_a(\alpha)$ for SSM are given in blue triangles. (d) Plot of $D_s(\alpha)$ (black filled circle) and $D_a(\alpha)$ (red open square) against α. The values of $D_s(\alpha) = D_a(\alpha)$ for SSM are shown in blue triangles. The dashed lines in (c) and (d) represents the MF value. The error in the values of the exponents are of the order of symbol size.

The number in the parentheses is the uncertainty of last digit in the numerical value of the respective exponents. The values of $\tau_x(\alpha)$ and $D_x(\alpha)$ are estimated at various different values of α and presented as a function of α in Figs. 5.7(c) and 5.7(d) respectively. In order to compare the values of the exponents of PSM with those of the SSM, the estimates of the values of these exponents for the SSM are also presented in the same figures. The numerical values are listed in Table 5.1 and compared with those of the SSM. Throughout the range of α, scale-free as well as random, the exponents of SSM are found to follow MF values[68,153] as also reported in[161]. In MF analysis, the exponents are found to be $\tau_s = \tau_a = 3/2$ and $D_s = D_a = 1$ as loop less structures (nodes without multiple toppling) are assumed in the branching process. However, SSM has a different scaling behaviour

α	PSM				SSM			
	τ_s	τ_a	D_s	D_a	τ_s	τ_a	D_s	D_a
2.25	1.296	1.407	0.71	0.54	1.498	1.516	1.01	0.99
3.00	1.403	1.478	0.85	0.83	1.506	1.513	1.03	0.98
4.00	1.494	1.507	0.98	0.99	1.504	1.493	1.03	1.03
5.00	1.507	1.507	0.99	1.00	1.502	1.501	1.02	1.04

Table 5.1: Estimated values of exponents for PSM and SSM for different values of α. For both the models the dissipation factor is taken as $\epsilon = 1/\sqrt{N}$. Maximum error in estimation of τ_x is 0.008, whereas that for the D_x is 0.01.

than MF on small world networks[201] in contrary to the present observation. In PSM, on the other hand, all four exponents, τ_s, τ_a, D_s, D_a, have MF values in the random regime ($\alpha \geq 4$) but they vary continuously with α and become lower than the MF values in the scale-free regime ($\alpha \leq 4$) as observed in the epidemic spreading model on complex networks[225]. Smaller values of τ_s and τ_a indicate that in the thermodynamic limit, the probability to have an avalanche of larger size is higher in the PSM than in a stochastic model. Therefore in the preferential model, the cascading effect will sustain for a longer period of time than on a stochastic model. Thus the network structure played a crucial role in determining the critical behaviour of PSM in contrary to SSM. It is worth mentioning here that for BTW type deterministic sandpile model on SFN, the exponent $\tau_s(\alpha)$ also has a continuous dependence on α as $\tau_s(\alpha) = \alpha/(\alpha - 1) > 3/2$ in the range $2 < \alpha < 3$ and $\tau_s(\alpha)$ remains to be $3/2$ for $\alpha > 3$[161]. In BTW, the nodes with higher degree sustain large number of sand grains and play a role of reservoirs whereas in PSM no nodes of any degree can sustain large number of sand grains, hence, such reservoirs do not exist. In contrary, in PSM, the higher degree nodes of fixed critical height ($h_c = 2$) topple frequently due to constant supply of sand grains to such nodes owing to the preferential rule.

Knowing the values of the exponents τ_x and D_x, the scaling function form of $P_x(\alpha, N)$ given in Eq. (5.5) is verified for both s and a. The scaled avalanche size distributions are plotted against their respective scaled variables in double logarithmic scales for three different network sizes $N = 2^{16}$, 2^{18} and 2^{20} for $\alpha = 2.25$ (in black) and $\alpha = 4$ (in red) in Fig. 5.8(a) and Fig. 5.8(b) for P_s and P_a respectively taking $\epsilon = 1/\sqrt{N}$. Using the respective values of the exponents, good collapse of data are found to occur for both s and a irrespective of the values of α. Hence, the FSS forms for s and a assumed in Eq. (5.5) are correct over the wide range of α for a given ϵ. Since the model obeys FSS there is no complete toppling balance[82]

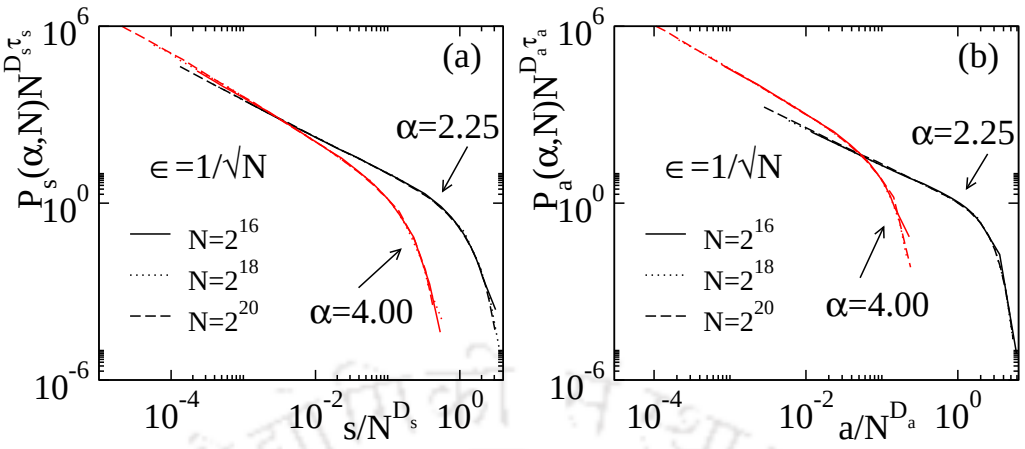

Figure 5.8: Plot of $P_x(\alpha, N)N^{D_x(\alpha)\tau_x(\alpha)}$ *vs* $x/N^{D_x(\alpha)}$ for $N = 2^{16}$ (solid line), $N = 2^{18}$ (dotted line), $N = 2^{20}$ (dashed line) for $x = s$ in (a) and for $x = a$ in (b) taking corresponding values of exponents. Distributions for $\alpha = 2.25$ and for $\alpha = 4$ are marked by arrows.

in PSM where in toppling of a node sands are distributed to its neighbouring nodes of highest and lowest degree and there is no guarantee that two sand grains will be received back in toppling of those lowest and highest degree neighbouring nodes. As a consequence, the toppling waves[76,78] generated from a fixed critical node are found to be uncorrelated. As the values of the critical exponents are found very different from those of the SSM in the scale-free regime ($\alpha < 4$), PSM then belongs to a new universality class than SSM in this regime of SFN. The results of the above model remain unchanged even if the two sand grains of a critical node goes randomly and independently to any of the highest and the lowest degree neighbouring nodes instead of giving one sand grain each to the highest and the lowest degree neighbouring nodes.

5.5 Effect of dissipation rate

Another way of controlling SOC on the network is to control the value of ϵ, the dissipation rate[168,222]. On a scale-free network with $\alpha = 2.25$ the distributions $P_s(\alpha, N)$ and $P_a(\alpha, N)$ for two other values of dissipation factor $\epsilon = 1/N^{0.4}$, and $\epsilon = 1/N^{0.6}$ are obtained and shown in Figs. 5.9(a) and 5.9(b), respectively. The cutoff of the distributions are found to depend on ϵ as expected. Estimates of $\sigma_s(\alpha, q)$ and $\sigma_a(\alpha, q)$ are made for all three values of ϵ at $\alpha = 2.25$. Variation of $\sigma_s(\alpha, q)$ and $\sigma_a(\alpha, q)$ against q are shown in Figs. 5.9(c) and 5.9(d) respectively. First of all the value of $\sigma_s(1)$ for $q = 1$ are found to increases as the value of ϵ

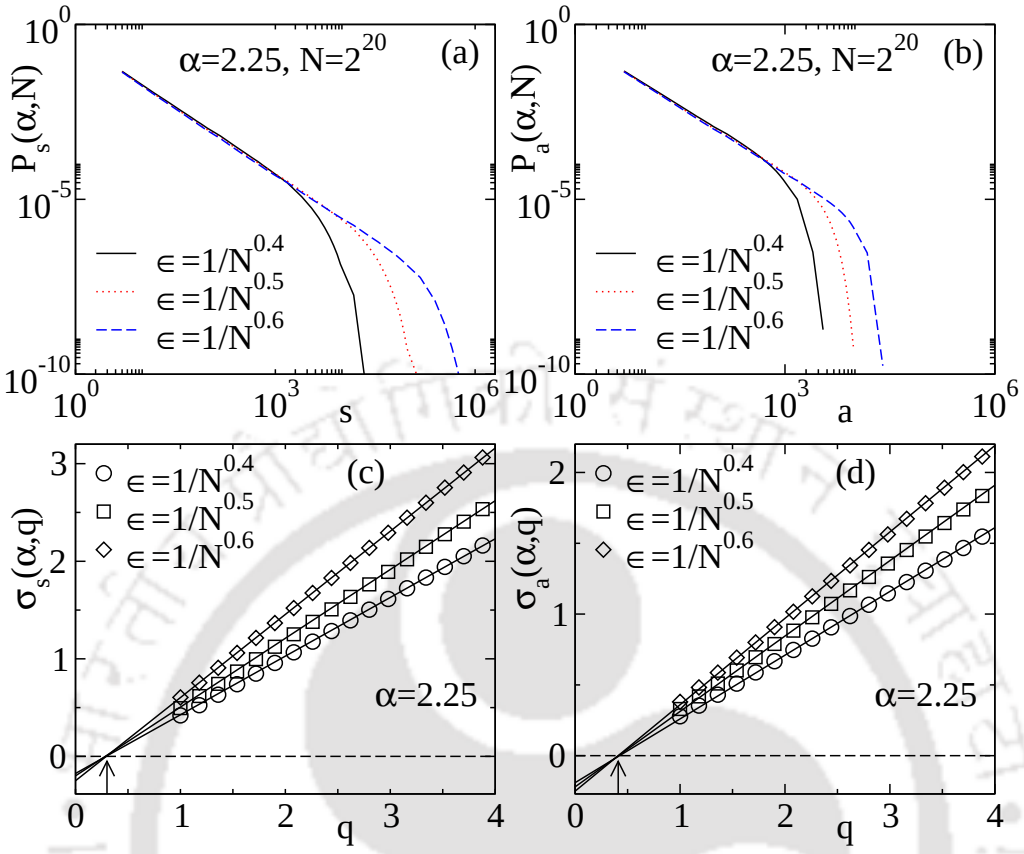

Figure 5.9: Plot of (a) $P_s(\alpha, N)$ and (b) $P_a(\alpha, N)$ for $\epsilon = 1/N^{0.4}$ (black solid line), $\epsilon = 1/N^{0.5}$ (red dotted line), and $\epsilon = 1/N^{0.6}$ (blue dashed line) for a fixed value of $\alpha = 2.25$ and $N = 2^{20}$. Plot of (c) $\sigma_s(\alpha, q)$ and (d) $\sigma_a(\alpha, q)$ against q for $\epsilon = 1/N^{0.4}$ ($\bigcirc$), $\epsilon = 1/N^{0.5}$ ($\square$), and $\epsilon = 1/N^{0.6}$ ($\diamond$). The solid lines represent the linear least square fit through the data points. The intersection points of the fitted lines are marked by the arrow heads. The dashed lines correspond to $\sigma_x = 0$. For clarity points for $q < 1$ are dropped.

decreases as expected. Secondly, the plots intersect the q-axis at a single point. Since the q intercepts are $\tau_s - 1$ or $\tau_a - 1$, the scaling exponents τ_s or τ_a remain independent of the choice of ϵ. For $\alpha = 2.25$, the estimated values of τ_s and τ_a for $\epsilon = 1/N^{0.4}$ and $1/N^{0.6}$ are found to be within the error bar of the corresponding value of τ_s and τ_a for $\epsilon = 1/N^{0.5}$. However, the slope of the plots are found strongly dependent on ϵ. Since the slope determines the capacity dimension D_x, it should depend on ϵ for a given α. For $\alpha = 2.25$, the values of D_s are found to be 0.610(5) and 0.857(4) for $\epsilon = 1/N^{0.4}$ and $1/N^{0.6}$ respectively and are out of the error bars of the corresponding value of $D_s = 0.720(6)$ for $\epsilon = 1/N^{0.5}$. A similar result is also observed for D_a. Not only in the scale-free regime, the observation is found to be valid in random regime too. Such dependence of the capacity dimension on the

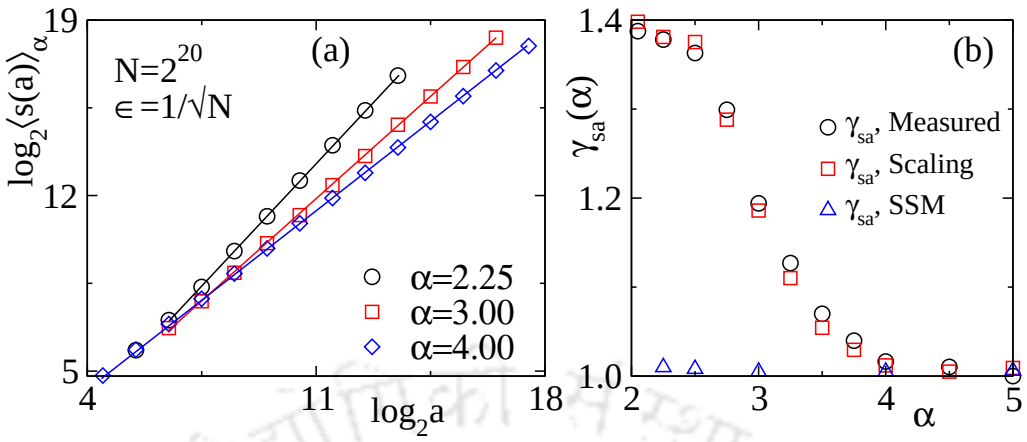

Figure 5.10: (a) Plot of $\langle s(a)\rangle_\alpha$ against a on a network of size $N = 2^{20}$ with $\epsilon = 1/\sqrt{N}$ for $\alpha = 2.25$ (○), $\alpha = 3$ (□), and $\alpha = 4$ (◇). (b) Plot of $\gamma_{sa}(\alpha)$ versus α; Circles represent the measured values of γ_{sa} and squares represent the same obtained from Eq. (5.9). Blue triangles in (b) represent γ_{sa} for the SSM.

choice of the dissipation factor at a fixed slow driving is also reported in few other studies of sandpile models on complex networks[161,163]. In context of absorbing state phase transition it is also observed that the critical exponent of sandpile models can be tuned varying the dissipation rate and driving mechanism of the system defined on regular lattice[226–228].

5.6 Conditional and other expectations

Further insight can be obtained by studying the conditional expectation $\langle s(a)\rangle_\alpha$ for the avalanches of size s with a fixed area a. For a given α, $\langle s(a)\rangle_\alpha$ expected to scale as

$$\langle s(a)\rangle_\alpha = \int sP(s|a)ds \sim a^{\gamma_{sa}(\alpha)}, \tag{5.8}$$

where $P(s|a)$ is the conditional probability distribution and $\gamma_{sa}(\alpha)$ is an exponent. The exponent $\gamma_{sa}(\alpha)$ is expected to satisfy a scaling relation

$$\gamma_{sa}(\alpha) = \frac{\tau_a(\alpha) - 1}{\tau_s(\alpha) - 1} \tag{5.9}$$

with the exponents $\tau_s(\alpha)$ and $\tau_a(\alpha)$ as in usual sandpile models[6]. The values of $\langle s(a)\rangle_\alpha$ are plotted against a in double logarithmic scale for three different values of $\alpha = 2.25$, 3 and 4 keeping $\epsilon = 1/\sqrt{N}$ in Fig. 5.10(a). The values of γ_{sa} are measured by linear least square method through the data points. The variation of γ_{sa} with α

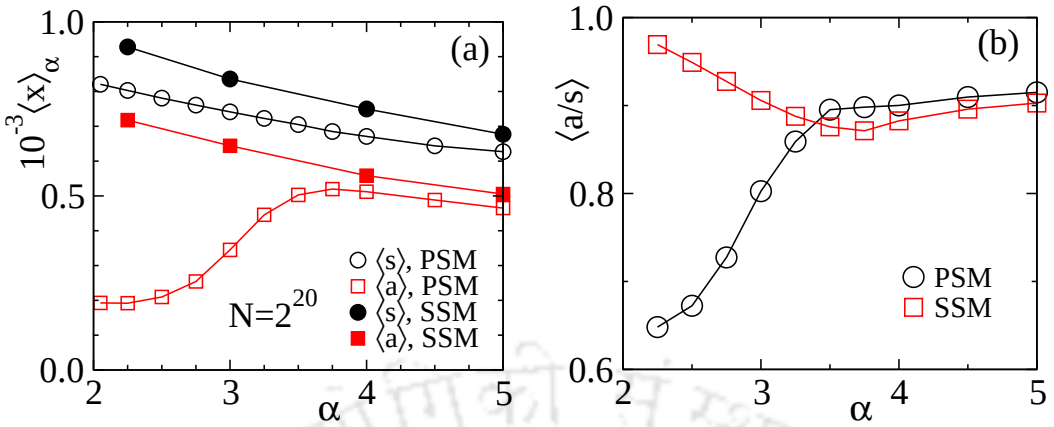

Figure 5.11: (a) Plot of $\langle s\rangle_\alpha$ (circle) and average area $\langle a\rangle_\alpha$ (square) against α for PSM (open symbol) and for SSM (filled symbol). (b) Plot of $\langle a/s\rangle$ against α for PSM (○) and SSM (□). Data are collected on networks of size $N = 2^{20}$ with $\epsilon = 1/\sqrt{N}$.

is shown in Fig. 5.10(b). In order to verify the scaling relation given in Eq. (5.9), the estimates of $(\tau_a(\alpha)-1)/(\tau_s(\alpha)-1)$ are also plotted in Fig. 5.10(b) and compared with the directly measured value of γ_{sa}. It can be seen that the scaling holds within the error bars. As the exponents τ_s and τ_a are independent of dissipation factor ϵ, the exponent γ_{sa} is also independent of ϵ. For $\alpha \geq 4$, $\gamma_{sa} \approx 1$ whereas for $\alpha < 4$, the value of γ_{sa} is more than one and found to be ≈ 1.4 as $\alpha \to 2$. Thus, for $\alpha \geq 4$ the avalanche size s proportional to the area a and for $\alpha < 4$ the total number of toppling becomes higher than the numbers of nodes involved in an avalanche.

Apart from the critical exponents and the scaling relations, the nature of the avalanches, confined or sparse, can be studied by estimating the expectation of a property $x \in \{s, a\}$ as a function of degree exponent α. For a given α, the distribution of a property x is assumed as

$$P_\alpha(x) = x^{-\tau(\alpha)} g\left[\frac{x}{x_c(\alpha)}\right], \tag{5.10}$$

where $\tau_x(\alpha)$ is an α dependent exponent, $x_c(\alpha)$ is the upper cut off of the property x and g is a scaling function. For a given α, the expectation

$$\langle x\rangle_\alpha = \int_0^{x_c(\alpha)} x P_\alpha(x) dx \tag{5.11}$$

depends on both $\tau_x(\alpha)$ and $x_c(\alpha)$. Estimated values of $\langle x\rangle_\alpha$ for a network of size $N = 2^{20}$ are plotted against α in Fig. 5.11(a) both for PSM and SSM. It can be seen that for SSM, both $\langle s\rangle_\alpha$ and $\langle a\rangle_\alpha$ increase proportionately while α decrease.

In case of PSM, though $\langle s \rangle_\alpha$ increases, $\langle a \rangle_\alpha$ decreases as α decreases. A large drop in $\langle a \rangle_\alpha$ in the scale-free regime indicates confinement of the avalanches in smaller and smaller areas. Note that, even if the values of $\tau_a(\alpha)$ decreases, $\langle a \rangle_\alpha$ decreases in the scale free regime due to the fact that $a_c(\alpha)$ decreases rapidly with α (see Fig. 5.6(b)). Thus preferential sand distribution has much control on confining an avalanche over a limited number of nodes than in SSM.

Beside studying the global average of the avalanche properties, the confinement can also be studied by estimating the ratio of avalanche area to the avalanche size a/s[168] of an individual avalanche. As a/s tends to 1, the avalanche would have equal size and area and hence loop less structure whereas if it tends to smaller value ($\ll 1$), an avalanche of large size will be confined on a small area leading to multiple toppling. An average of a/s can be obtained as

$$\langle a/s \rangle = \int (a/s) P_{a/s}(\alpha, N) d(a/s) \tag{5.12}$$

where $P_{a/s}(\alpha, N)$ is the distribution of the ratio a/s. The estimated values of $\langle a/s \rangle$ are presented against α in Fig. 5.11(b) for both PSM and SSM. It can be seen that the value of $\langle a/s \rangle$ remains almost constant around 0.9 for $\alpha > 3.5$ and then decreases to 0.65 continuously as α decreases to 2.25 in the case of PSM. Whereas in the case of SSM, though it remains almost constant around 0.9 for $\alpha > 3.5$, but it increases to ≈ 1.0 as α decreases to 2.25. Thus in the scale-free regime, the random sand distribution in SSM makes the avalanche, the cascading effect, to access more and more nodes of the network whereas preferential sand distribution to extreme degrees in PSM makes the avalanche restricted to lesser and lesser number of nodes in the network. Such an observation is consistent with the avalanche evolution morphology shown in Fig. 5.4 as well as with that of the toppling number density-density correlation in Fig. 5.4. On the other hand, in the random regime the difference between sandpile models disappear and all the models produce the MF result. Hence, varying the network structure, one can control the avalanche area, the number of affected nodes in a cascading process, in a self-organizing system. Such controlling effect has also been reported in the study of controlling self-organizing dynamics on networks[215,222,223].

5.7 Controlling of preference in sand distribution

SOC in this model can be efficiently controlled by selecting the preferred nodes to which the sand grains will be distributed. Keeping n_1 fixed to the lowest degree ($k_{\rm nn,min}$) node among the neighbouring nodes, the degree of n_2, $k(n_2)$ is varied from $k_{\rm nn,min}+1$ to the highest degree $k_{\rm nn,max}$ of the available neighbouring nodes. The model is studied for four different choices of the degree $k(n_2)$ as $k_{\rm nn,max}$, $k_{\rm nn,max}/2$, $k_{\rm nn,max}/4$ and $k_{\rm nn,min}+1$. In case of fractional values of $k_{\rm nn,max}/2$ or $k_{\rm nn,max}/4$, nearest integer values have been taken. If the node of the desired degree is absent in the set of the neighbouring nodes, the nearest possible value of the desired degree is considered. The avalanche size distribution for various different choices of $k(n_2)$ are shown in Fig. 5.12(a). It can be seen that as the values $k(n_2)$ increases from $k_{\rm nn,min}+1$ to $k_{\rm nn,max}$ not only the cutoff but also the slope of the distributions are changed. The moment scaling functions of avalanche size $\sigma_s(\alpha,q)$ are calculated and shown in Fig. 5.12(b). Note that the slope of $\sigma_s(\alpha,q)$, and hence the capacity dimension D_s changes for different choice of $k(n_2)$. However, since the dissipation factor is set to $\epsilon=1/\sqrt{N}$, $\sigma_s(\alpha,q)$ has the value $1/2$ at $q=1$ for all $k(n_2)$. Consequently, in order to hold the relation $D_s(2-\tau_s)=\sigma_s(\alpha,1)=1/2$, τ_s has to vary accordingly. Following the similar method, as stated earlier in Sec. 5.4, τ_s and D_s are estimated for different values of α and $k(n_2)$. Variation of the avalanche size distribution exponent τ_s and the capacity dimension D_s as a function of α for such different choices of $k(n_2)$ are shown in Figs. 5.12(c) and 5.12(d), respectively. It can be seen that as the difference between $k(n_1)$ and $k(n_2)$ increases the deviation in the value of τ_s from the MF value $(3/2)$ becomes more prominent in the scale-free regime and maximum possible deviation occurs for $k(n_2)=k_{\rm nn,max}$. However, in the random regime, all such preferential choices lead to the MF result. Such a variation in the values of the avalanche area exponent τ_a is also observed. There are two important observations. First, as the two sand grains are given to two nodes of lower degrees the system follow MF scaling in the scale-free as well as in the random regimes of the network. The MF scaling seems to be associated with the randomness of the system. In the random network regime, the network structure itself is randomizing the system whereas in the scale-free regime randomization occurs due to the sand distribution among the lower degree nodes which are large in number. Second, as the two sand grains are sent to two nodes of extreme degrees the system exhibits a drastically different scaling behaviour in the scale-free regime but the random network still displays MF scaling. Once again, the effect of random network is strong enough to randomize the system irrespective

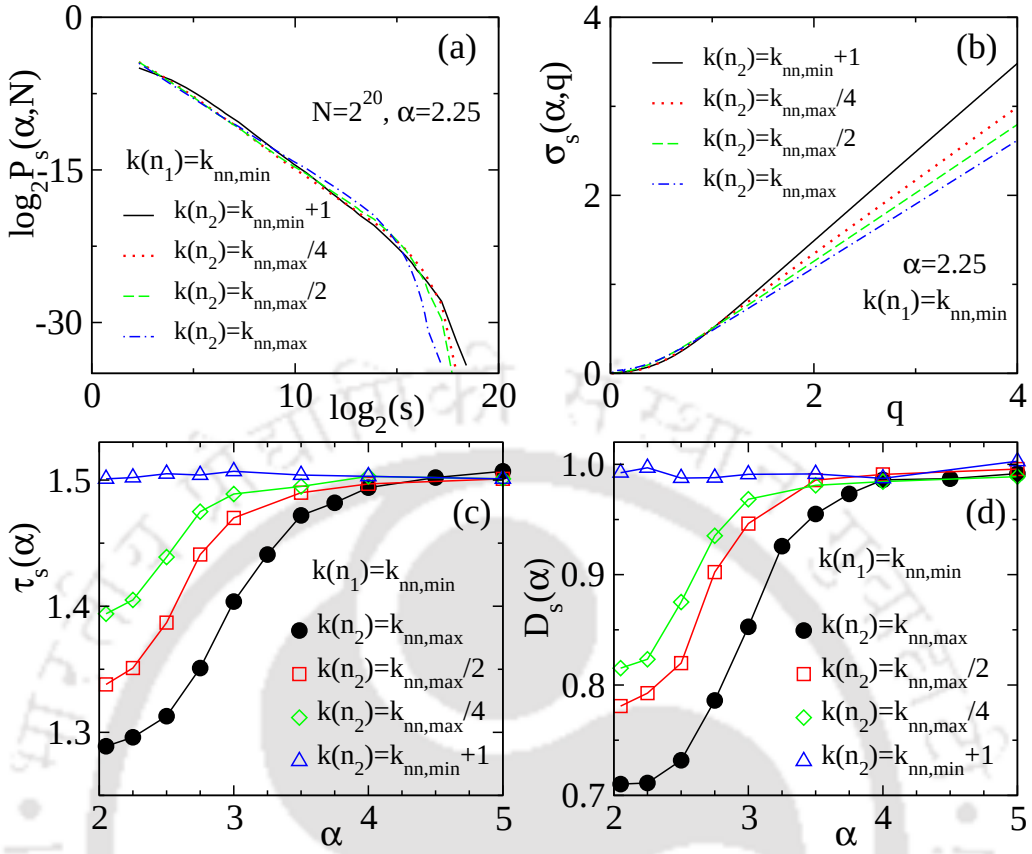

Figure 5.12: (a) For fixed $\alpha = 2.25$ and $N = 2^{20}$, $P_s(\alpha, N)$ are plotted for different values of $k(n_2)$: $k_{\mathrm{nn,min}} + 1$ (black solid line), $k_{\mathrm{nn,max}}/4$ (red dotted line), $k_{\mathrm{nn,max}}/2$ (green dashed line), and $k_{\mathrm{nn,max}}$ (blue dotted dashed line). (b) Variation of $\sigma_s(\alpha, q)$ for $\alpha = 2.25$ shown for different choice of $k(n_2)$ (same line style as in (a)). Plot of (c) $\tau_s(\alpha)$ and (d) $D_s(\alpha)$ against α for various preferential rules: $k(n_2) = k_{\mathrm{nn,min}} + 1$ ($\triangle$), $k_{\mathrm{nn,max}}/4$ ($\diamond$), $k_{\mathrm{nn,max}}/2$ ($\square$), and $k_{\mathrm{nn,max}}$ ($\bullet$). For all the cases $k(n_1)$ is taken as $k_{\mathrm{nn,min}}$.

of preferential sand distribution. On the other hand, when the sands are directed toward fewer nodes of highest degrees the avalanche gets confined within lesser number of nodes leading to multiple toppling and hence a new critical behaviour emerges. It is worth mentioning here that if the preferential sand distribution is performed by fixing the degree $k(n_1) = k_{\mathrm{nn,max}}$ and $k(n_2)$ is varied from $k_{\mathrm{nn,max}}$ to $k_{\mathrm{nn,min}}$ noncritical behaviour appeared until $k(n_2)$ becomes close to $k_{\mathrm{nn,min}}$. It should be noted that sand distribution to nodes of specific degrees is not equivalent to the driving mechanism adopted in the studies of absorbing state phase transition [226–228].

It is now important to have cost analysis of the controlling mechanism for different preferential rules. Following [168,222], the cost per avalanche is defined considering

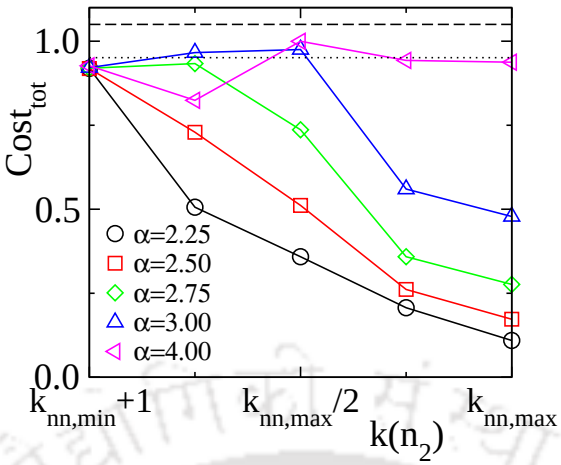

Figure 5.13: Plot of cost function against $k(n_2)$ for different α: 2.25 (○), 2.50 (□), 2.75 (◇), 3 (△), and 4 (◁). The dashed line represents the value of cost function for SSM with $\alpha = 2.25$, and the dotted line represents that for SSM with $\alpha = 4$.

two concave function of avalanche size and area, and is given by,

$$\text{Cost}_{\text{tot}} = \text{c}[\text{s}]^{\gamma_s} + \text{c}[\text{a}]^{\gamma_a}, \tag{5.13}$$

with $\text{Cost}_{\text{tot}} = -2$ for $s = 0$ (or, $a = 0$) and $\gamma_a > \gamma_s > 0$. As the present model has a fixed dissipation rate, cost of dissipation is not included. The above definition ensures the fact that more the avalanche more the cost will be and for zero avalanche size there will be benefit 1 from each term. Setting $\gamma_a > \gamma_s$, the cost for one node damage (area) is greater than the cost of toppling of one node (size). Taking $c = 0.0008$, $\gamma_s = 1.05$, and $\gamma_s = 1.1$, the cost function is evaluated and plotted in Fig. 5.13. Though for $\alpha = 4$ the cost function remains almost constant with $k(n_2)$, it decreases rapidly with $k(n_2)$ for $\alpha < 4$. The cost function is found to have the minimum value for $\alpha = 2.25$ and $k(n_2) = k_{\text{nn,max}}$. For the sake of comparison the cost function of SSM is also estimated for two extreme values of α, the dashed line for $\alpha = 2.25$ and the dotted line for $\alpha = 4$. For both the αs, the value of cost function of SSM is higher than that of PSM with $k(n_2) = k_{\text{nn,max}}$. Hence, the cost of preferential sand distribution to the extreme degrees which eventually lead to the confinement of large avalanches to a lesser number of nodes is much less than that of the stochastic sand distribution.

It can be noted here that the results of PSM obtained here on the uncorrelated SFNs. The results have also been verified for correlated Barabási-Albert SFN with $\alpha = 3$, generated by preferential attachment method[144,145]. The distributions P_s and P_a are found similar to those of PSM on the corresponding uncorrelated SFN

with $\alpha = 3$ for a fixed choice of $\epsilon, k(n_1)$, and $k(n_2)$. However, the SSM on optimized Barabási-Albert SFN imposed on two dimensional square lattice with degree exponent $\alpha = 3$ exhibits a different scaling behaviour with exponent $\tau_s = 1.30$[163]. A similar result is also obtained in the study of BTW type sandpile model on geographically embedded SFNs[164]. This is because of the fact that the optimization process destroys the small-world behaviour though the degree distribution remains scale-free. The scaling behaviour of $P_x(\alpha, N)$ are found to be independent on the cutoff degree of the network as it is also reported in the study of explosive percolation on SFN[229].

5.8 Conclusion

Self-organized criticality in a two-state preferential sandpile model studied tuning three parameters such as the degree distribution exponent α of the network, bulk dissipation rate ϵ and the degrees of the nodes to which sands will be distributed. Such preferential sand distribution leads to an entirely different avalanche evolution, toppling number density-density correlation in the degree space and scaling behaviour than that of the SSM on the same network in the scale-free regime ($\alpha < 4$). The effect becomes most prominent when the degree of the nodes that receive sands are fixed to the lowest and the highest possible values of the neighbouring nodes. New sets of critical exponents are found to characterize the universality class of the model at different values of α and the choice of specific nodes for a given ϵ. In the random regime ($\alpha > 4$) of the network the model boils down to MF model and becomes independent of the choice of specific nodes. It has been found that the values of the distribution exponents (τ_x) is robust against the values of dissipation factor ϵ, whereas the capacity dimensions (D_x) depend on ϵ strongly. If the sands are distributed to the extreme degree nodes, the large avalanches are found to be confined in a smaller number of nodes in contrary to random sand distribution which leads to exposition to the whole network in the scale-free regime. Such an observation leads to an important conclusion that the catastrophic cascading effect on a scale-free network can be confined by directing the loads to extreme degree nodes.

Chapter 6

Summary and Conclusion

The effect of heterogeneity, compactness and clustering of a network on the critical properties of different sandpile models are thoroughly studied varying network structure and topology. Beside regular lattice and random network, different topologies of small world network (SWN) and scale-free network (SFN) are considered. Bulk dissipative versions of the deterministic BTW and the stochastic sandpile model (SSM) have been developed as no boundary exists on a network where the system could dissipate. Several different parameters such as shortcut density ϕ in SWN, degree exponent α in SFN, dissipation factor ϵ, selection of nodes of specific degree k are tuned to characterize specific effects on self-organizing criticality (SOC) in these sandpile models. The network topology and other parameters are found to have a profound role in determining the critical behaviour of sandpile models. A number of new scaling forms are invented to explain the unexpected novel critical behaviour of the models when studied on network. Below we summarize the effect of network structure and topology on the critical properties of different sandpile models as discussed in previous chapters.

The effect of SWN topology on the dissipative deterministic sandpile model (DDSM) is studied in chapter 2. The BTW-type correlated scaling and mean-field (MF) scaling are found to appear on regular lattice for $\phi \lesssim 2^{-12}$ and on random network for $\phi > 0.1$ respectively. On SWN ($2^{-12} < \phi < 0.1$), the model exhibits both the scaling behaviors simultaneously. A characteristic value of every avalanche property are identified around which the crossover occurs. New coexistence scaling forms for the probability distribution functions are developed and numerically verified. The avalanche clusters following BTW scaling are found to be compact whereas those following MF scaling are found to be sparse and scattered all over the network. Though DDSM does not follow finite-size scaling (FSS) on regular lattice

or on SWN, the model obeys FSS on random network. On random network, the avalanches are consisting of nodes that toppled only once. Hence, the probability of appearance of a node that toppled more than once on random network is vanishingly small. Consequently, precise toppling balance becomes ineffective, toppling waves become uncorrelated that ensures the system to follow FSS. BTW-type correlated sandpile models will then follow FSS if they are defined on substrates without a spatial structure and having long-distance connections. Because of the presence of long-distance connections, sand transport becomes superdiffusive on random network though it is diffusive on regular lattice. Different scaling forms for diffusion are identified and verified. Therefore, as the shortcut density ϕ is tuned from 0 (regular lattice) to 1 (random network) through a series of SWN structures, the DDSM exhibits a varying self-organizing critical behaviour.

In chapter 3, a dissipative stochastic sandpile model (DSSM) is constructed and studied on SWN both in 1d and 2d varying the shortcut density ϕ. In this chapter, emphasis is given in analyzing the critical properties of the stochastic model on the SWN regime ($2^{-13} < \phi < 0.1$). Several new geometrical quantities such as toppling surface and its fragmentation, compactness, and fluctuation in fragment size are defined and characterized as a function of avalanche size s for a given ϕ, within the SWN regime. The average height $\langle S_s \rangle$ and area $\langle a_s \rangle$ of the toppling surface are studied as a function of avalanche size s. It is found that there exists three regimes of avalanche size s, separated by two crossover sizes s_1 and s_2 ($s_1 < s_2$). Below s_1, the avalanches are found to be compact as those are on regular lattice. For $s_1 < s < s_2$, the avalanches are fragmented into many sub-clusters those are connected by the long-ranged links of the network. Novel scaling forms of s_1 and s_2 as well as that of $\langle S_s \rangle$ and $\langle a_s \rangle$ are developed and numerically verified. Distributions of avalanche size s and area a are also found to exhibit two scaling forms about a crossover size $s_c = s_1$. Manna scaling on regular lattice below s_c and MF scaling on the random network above s_c are found to coexists. Since two scaling forms appear simultaneously in the SWN regime, the probability distributions of various avalanche properties of DSSM do not follow the usual FSS in contrary to the fact that stochastic sandpile model follow FSS on the regular lattice. Around s_c, a coexistence scaling form of the distributions and the expectation value are developed and numerically verified. The sand transport behaviour in DSSM is found to change from diffusive to superdiffusive nature as SWN evolve from regular lattice to random network, similar to the deterministic model. A generalized scaling form of diffusivity is identified that satisfactorily explains such crossover behaviour.

The effect of network topology on the steady-state critical properties of nondissipative and dissipative avalanches of both the deterministic and stochastic models under bulk dissipation are studied in chapter 4. The nondissipative avalanches of both the models display their usual scaling behaviour on the regular lattice ($\phi = 0$) and MF scaling on the random network ($\phi = 1$). However, the dissipative avalanches represent a number of novel scaling properties on the regular lattice as well as on the random network in both 1d and 2d. Drossel in 2000 and Dickman-Campelo in 2003 reported new scaling forms for the dissipative clusters with dissipation at the open boundary in both dimensions for the deterministic and stochastic models respectively. The bulk dissipation is found to have a nontrivial effect on dissipative avalanches over the boundary dissipation as a set of new scaling exponents are found to describe the scaling of dissipative avalanches on regular lattice and random network in the case of bulk dissipation. A. On SWN, in the intermediate range of ϕ, the model exhibits coexistence of more than one scaling forms in both 1d and 2d around a crossover size $s_c(\phi)$. For nondissipative and dissipative avalanches, however, the crossover size s_c scales with ϕ with two different exponents. Similar to stochastic model, the deterministic model also exhibits coexistence of more than one scaling forms in small world regime and it is possible to identify the crossover size s_c for such avalanches. For both the models the coexistence scaling form of the avalanche size distribution function around s_c is proposed and numerically verified. SWN can not only segregate of several scaling forms that appear in the event size distribution of a dynamical system but also found to have profound effect on the self-organizing critical behaviour on networks.

In chapter 5, a new two-state stochastic model with preferential sand distribution is developed on scale-free network. Self-organized criticality in such a sandpile model on scale-free network is studied tuning three parameters such as the degree distribution exponent α of the network, bulk dissipation rate ϵ and the degrees of the nodes to which sands will be distributed. Such preferential distribution of sand leads to an entirely different avalanche evolution in the degree space in comparison to stochastic sand distribution. The toppling number density-density correlation function reveals that the sand transport mechanism in the preferential model is drastically different from that of the stochastic model and is the sole reason to have an entirely new critical behaviour in this model in the scale-free regime ($\alpha < 4$). To characterize the universality class of the model at different values of α and the choice of specific nodes for a given ϵ, a new set of critical exponents are found. In the random regime ($\alpha > 4$) of the network the model reproduces the MF result and be-

comes independent of the choice of specific nodes. It has been found that the values of the distribution exponents (τ_x) is robust against the values of dissipation factor ϵ, whereas the capacity dimensions (D_x) depend on ϵ strongly. Beside having a new critical behaviour than MF in the scale-free regime, the large avalanches are found to be confined in a smaller number of nodes in contrary to random sand distribution which leads to exposition to the whole network. Moreover, in this preferential model such confinement of the catastrophic cascades on a scale-free network is achieved with minimum cost. Thus, sand distribution to the extreme degree nodes on a scale free network is an efficient and cost effective mechanism to control self-organizing criticality.

To conclude, deterministic and stochastic sandpile models on SWN and a preferential sandpile model on SFN are constructed and studied using extensive numerical simulations. A number of new scaling forms are invented to explain the novel and unusual critical behaviour that appear in these systems. Different aspects of these models are explored varying both the network parameter and the parameters of the sandpile models. A set of new results, new critical exponents, new scaling forms, new universality, etc are found to occur. Different mechanisms are developed to facilitate the controlling of catastrophic cascades on the complex networks. In one hand, SWN behaves like a segregator of different scaling forms, on the other hand, preferential sand distribution on SFN leads to explore a new universality class as well as makes the catastrophe to be confined.

In closing, the models developed here are generic in nature however could be extended to various real-world problems by modifying the parameters of the model suitably. It is worth mentioning that the methodologies used and results obtained in this thesis may be beneficial from both theoretical and experimental points of view. For example, the developed theory of coexistence scaling can be applied for other dynamical processes occurring on the small-world network where the resulting events have scale invariance character. The techniques developed for identifying the crossover values of event properties can also be useful for such systems. The correlation function that describes the correlation between the degree of a node and the number of toppling, could be applicable to extract more in-depth information about the underlying transport mechanism of the dynamical systems happening on complex networks. The developed control schemes to confine the avalanche as well as to minimize the probability of large cascading failure are definitely useful from engineering and economical perspectives.

Bibliography

[1] H. E. Stanley, *Introduction to Phase Transitions and Critical Phenomena*, Oxford University Press, New York, 1971.

[2] J. J. Binney, N. J. Dowrick, A. J. Fisher, and M. E. J. Newman, *The Theory of Critical Phenomena*, Oxford University Press, Oxford, 1992.

[3] J. M. Yeomans, *Statistical Mechanics of Phase Transitions*, Clarendon Press, Oxford, 1992.

[4] P. Bak, C. Tang, and K. Wiesenfeld, Phys. Rev. Lett. **59**, 381 (1987).

[5] P. Bak, C. Tang, and K. Wiesenfeld, Phys. Rev. A **38**, 364 (1988).

[6] H. J. Jensen, *Self-Organized Criticality*, Cambridge University Press, Cambridge, 1998.

[7] K. Christensen and N. R. Moloney, *Complexity and Criticality*, Imperial College Press, London, 2005.

[8] G. Pruessner, *Self- Organized Criticality: Theory, Models and Characterization*, Cambridge University Press, Cambridge, 2012.

[9] R. Albert and A.-L. Barabási, Rev. Mod. Phys. **74**, 47 (2002).

[10] M. E. J. Newman, SIAM Review **45**, 167 (2003).

[11] S. N. Dorogovtsev, A. V. Goltsev, and J. F. F. Mendes, Rev. Mod. Phys. **80**, 1275 (2008).

[12] M. E. J. Newman, *Networks: An Introduction*, Oxford University Press, Oxford, 2010.

[13] M. E. J. Newman, A.-L. Barabási, and D. J. Watts, *The Structure and Dynamics of Networks: (Princeton Studies in Complexity)*, Princeton University Press, Princeton, NJ, USA, 2006.

[14] E. Ben-Naim, H. Frauenfelder, and Z. Toroczkai, *Complex Networks*, Springer-Verlag, Berlin, Heidelberg, Germany, 2004.

[15] A.-L. Barabási, *Network science*, Cambridge University Press, 2016.

[16] A. Arenas, A. Díaz-Guilera, and R. Guimerà, Phys. Rev. Lett. **86**, 3196 (2001).

[17] M. A. de Menezes and A.-L. Barabási, Phys. Rev. Lett. **92**, 028701 (2004).

[18] E. Almaas, B. Kovacs, T. Vicsek, Z. N. Oltvai, and A.-L. Barabási, Nature **427**, 839 (2004).

[19] R. Albert and A.-L. Barabási, Phys. Rev. Lett. **84**, 5660 (2000).

[20] V. Kaufman, T. Mihaljev, and B. Drossel, Phys. Rev. E **72**, 046124 (2005).

[21] R. Pastor-Satorras, C. Castellano, P. Van Mieghem, and A. Vespignani, Rev. Mod. Phys. **87**, 925 (2015).
[22] Y. Moreno and A. Vazquez, EPL (Europhysics Letters) **57**, 765 (2002).
[23] Y. Moreno, R. Pastor-Satorras, A. Vzquez, and A. Vespignani, EPL (Europhysics Letters) **62**, 292 (2003).
[24] D.-H. Kim, B. J. Kim, and H. Jeong, Phys. Rev. Lett. **94**, 025501 (2005).
[25] L. de Arcangelis, C. Perrone-Capano, and H. J. Herrmann, Phys. Rev. Lett. **96**, 028107 (2006).
[26] J. Hesse and T. Gross, Frontiers in Systems Neuroscience **8**, 166 (2014).
[27] S. Lise and M. Paczuski, Phys. Rev. Lett. **88**, 228301 (2002).
[28] D. Hughes, M. Paczuski, R. O. Dendy, P. Helander, and K. G. McClements, Phys. Rev. Lett. **90**, 131101 (2003).
[29] A. E. Motter and Y.-C. Lai, Phys. Rev. E **66**, 065102 (2002).
[30] K. Chen, P. Bak, and S. P. Obukhov, Phys. Rev. A **43**, 625 (1991).
[31] O. Peters, C. Hertlein, and K. Christensen, Phys. Rev. Lett. **88**, 018701 (2001).
[32] O. Peters and K. Christensen, Phys. Rev. E **66**, 036120 (2002).
[33] O. Peters, A. Deluca, A. Corral, J. D. Neelin, and C. E. Holloway, Journal of Statistical Mechanics: Theory and Experiment **2013**, P06019 (2013).
[34] H. Takayasu and H. Inaoka, Phys. Rev. Lett. **68**, 966 (1992).
[35] S. Hergarten and H. J. Neugebauer, Phys. Rev. Lett. **86**, 2689 (2001).
[36] M. Paczuski and D. Hughes, Physica A **342**, 158 (2004).
[37] M. Paczuski, S. Boettcher, and M. Baiesi, Phys. Rev. Lett. **95**, 181102 (2005).
[38] M. Baiesi, M. Paczuski, and A. L. Stella, Phys. Rev. Lett. **96**, 051103 (2006).
[39] P. Bak and K. Sneppen, Phys. Rev. Lett. **71**, 4083 (1993).
[40] N.-N. Pang, EPL (Europhysics Letters) **35**, 79 (1996).
[41] J. M. Beggs and D. Plenz, J. Neuroscience **23**, 11167 (2003).
[42] J. M. Beggs and D. Plenz, J. Neuroscience **24**, 5216 (2004).
[43] B. Carreras, D. Newman, I. Dobson, and A. Poole, Circuits and Systems I: Regular Papers, IEEE Transactions on **51**, 1733 (2004).
[44] S. Field, J. Witt, F. Nori, and X. Ling, Phys. Rev. Lett. **74**, 1206 (1995).
[45] P. J. Cote and L. V. Meisel, Phys. Rev. Lett. **67**, 1334 (1991).
[46] J. S. Urbach, R. C. Madison, and J. T. Markert, Phys. Rev. Lett. **75**, 276 (1995).
[47] G. DURIN, G. BERTOTTI, and A. MAGNI, Fractals **03**, 351 (1995).
[48] P. Cizeau, S. Zapperi, G. Durin, and H. E. Stanley, Phys. Rev. Lett. **79**, 4669 (1997).
[49] G. Durin and S. Zapperi, Phys. Rev. Lett. **84**, 4705 (2000).
[50] D. Kim, S. Choe, and S. Shin, Phys. Rev. Lett. **90**, 087203 (2003).
[51] G. A. Held, D. H. Solina, H. Solina, D. T. Keane, W. J. Haag, P. M. Horn, and G. Grinstein, Phys. Rev. Lett. **65**, 1120 (1990).
[52] V. Frette, K. Christensen, A. Malthe-Sørenssen, J. Feder, T. Jøssang, and P. Meakin, Nature **379**, 49 (1996).
[53] B. Plourde, F. Nori, and M. Bretz, Phys. Rev. Lett. **71**, 2749 (1993).

[54] D. V. Denisov, Y. Y. Villanueva, K. A. Lőrincz, S. May, and R. J. Wijngaarden, Phys. Rev. E **85**, 051309 (2012).
[55] S. S. Manna, J. Phys. A **24**, L363 (1991).
[56] D. Dhar, Physica A **263**, 4 (1999).
[57] D. Dhar and R. Ramaswamy, Phys. Rev. Lett. **63**, 1659 (1989).
[58] Y. C. Zhang, Phys. Rev. Lett. **63**, 470 (1989).
[59] O. Biham, E. Milshtein, and O. Malcai, Phys. Rev. E **63**, 061309 (2001).
[60] R. P. Satorras and A. Vespignani, J. Phys. A **33**, L33 (2000).
[61] M. Kloster, S. Maslov, and C. Tang, Phys. Rev. E **63**, 026111 (2001).
[62] S. B. Santra, S. R. Chanu, and D. Deb, Phys. Rev. E **75**, 041122 (2007).
[63] K. Christensen, H. C. Fogedby, and H. J. Jensen, J. Stat. Phys. **63**, 653 (1991).
[64] M. DeMenech, A. L. Stella, and C. Tebaldi, Phys. Rev. E **58**, R2677 (1998).
[65] S. Lübeck, Phys. Rev. E **61**, 204 (2000).
[66] S. Lübeck and K. D. Usadel, Phys. Rev. E **55**, 4095 (1997).
[67] H. N. Huynh and G. Pruessner, Phys. Rev. E **85**, 061133 (2012).
[68] K. Christensen and Z. Olami, Phys. Rev. E **48**, 3361 (1993).
[69] S. Lübeck, International Journal of Modern Physics B **18**, 3977 (2004).
[70] P. Ruelle and S. Sen, Journal of Physics A: Mathematical and General **25**, L1257 (1992).
[71] A. Ben-Hur and O. Biham, Phys. Rev. E **53**, R1317 (1996).
[72] A. Chessa, H. E. Stanley, A. Vespignani, and S. Zapperi, Phys. Rev. E **59**, R12 (1999).
[73] H. Nakanishi and K. Sneppen, Phys. Rev. E **55**, 4012 (1997).
[74] H. Huynh, G. Pruessner, and L. Chew, J. Stat. Mech **2011**, P09024 (2011).
[75] P. Alstrøm, Phys. Rev. A **38**, 4905 (1988).
[76] V. B. Priezzhev, D. V. Ktitarev, and E. V. Ivashkevich, Phys. Rev. Lett. **76**, 2093 (1996).
[77] M. Paczuski and S. Boettcher, Phys. Rev. E **56**, R3745 (1997).
[78] D. V. Ktitarev, S. Lübeck, P. Grassberger, and V. B. Priezzhev, Phys. Rev. E **61**, 81 (2000).
[79] M. DeMenech and A. L. Stella, Phys. Rev. E **62**, R4528 (2000).
[80] M. DeMenech and A. L. Stella, Physica A **309**, 289 (2002).
[81] A. L. Stella and M. DeMenech, Physica A **295**, 101 (2001).
[82] R. Karmakar, S. S. Manna, and A. L. Stella, Phys. Rev. Lett. **94**, 088002 (2005).
[83] J. A. Ahmed and S. B. Santra, Europhys. Lett. **90**, 50006 (2010).
[84] J. A. Ahmed and S. B. Santra, Phys. Rev. E **85**, 031111 (2012).
[85] H. Bhaumik, J. A. Ahmed, and S. B. Santra, Phys. Rev. E **90**, 062136 (2014).
[86] M. Henkel, H. Hinrichsen, and S. Lubeck, *Nonequilibrium Phase Transitions*, volume 1, Springer, Berlin, 2008.
[87] R. Dickman, M. A. Muñoz, A. Vespignani, and S. Zapperi, Brazilian Journal of Physics **30**, 27 (2000).
[88] R. Dickman, A. Vespignani, and S. Zapperi, Phys. Rev. E **57**, 5095 (1998).
[89] A. Vespignani, R. Dickman, M. A. Muñoz, and S. Zapperi, Phys. Rev. Lett. **81**,

5676 (1998).
[90] A. Vespignani, R. Dickman, M. A. Muñoz, and S. Zapperi, Phys. Rev. E **62**, 4564 (2000).
[91] M. Basu, U. Basu, S. Bondyopadhyay, P. K. Mohanty, and H. Hinrichsen, Phys. Rev. Lett. **109**, 015702 (2012).
[92] S. B. Lee, Phys. Rev. Lett. **110**, 159601 (2013).
[93] S. B. Lee, Phys. Rev. E **89**, 062133 (2014).
[94] S. B. Lee, Phys. Rev. E **89**, 060101 (2014).
[95] M. A. Muñoz, R. Dickman, A. Vespignani, and S. Zapperi, Phys. Rev. E **59**, 6175 (1999).
[96] H. R. Bernard, P. D. Kilworth, M. J. Evans, C. McCarty, and G. A. Selley, Ethnology **27**, 155179 (1988).
[97] L. A. Adamic and A. B. Hubermann, Science **287**, 2115 (2000).
[98] L. A. Amaral, A. Scala, M. Barthelemy, and H. E. Stanley, Proc Natl Acad Sci U S A **97**, 11149 (2000).
[99] V. Batagelj and A. Mrvar, Social Networks **22**, 173 (2000).
[100] M. E. J. Newman, Phys. Rev. E **64**, 016131 (2001).
[101] M. E. J. Newman, Phys. Rev. E **64**, 016132 (2001).
[102] M. E. J. Newman, Proceedings of the National Academy of Sciences **98**, 404 (2001).
[103] S. Milgram, Psychology To-day **2**, 6067 (1967).
[104] J. Travers and S. Milgram, Sociometry **32**, 425443 (1969).
[105] H. Jeong, B. Tombor, R. Albert, Z. N. Oltvai, and A.-L. Barabási, Nature **407**, 651654 (2000).
[106] D. A. Fell and A. Wagner, Nature Biotechnology **18**, 1121 (2000).
[107] J. Stelling, S. Klamt, K. Bettenbrock, S. Schuster, and E. D. Gilles, Nature **420**, 190193 (2002).
[108] H. Jeong, S. Mason, A.-L. Barabási, and Z. N. Oltvai, Nature **411**, 4142 (2001).
[109] S. Maslov and K. Sneppen, Science **296**, 910913 (2002).
[110] P. Uetz et al., Nature **403**, 623627 (2000).
[111] N. Guelzim, S. Bottani, P. Bourgine, and F. Kepes, Nature Genetics **31**, 6063 (2002).
[112] S. Shen-Orr, R. Milo, S. Mangan, and U. Alon, Nature Genetics **31**, 6468 (2002).
[113] O. Sporns, Complexity **8**, 5660 (2002).
[114] O. Sporns, G. Tononi, and G. M. Edelman, Cerebral Cortex **10**, 127141 (2000).
[115] D. J. Watts, *Small Worlds*, Princeton University Press, 1999.
[116] D. Watts and S. Strogatz, Nature **393**, 440 (1998).
[117] V. Kalapala, V. Sanwalani, A. Clauset, and C. Moore, Phys. Rev. E **73**, 026130 (2006).
[118] V. Latora and M. Marchiori, Physica A **314**, 109 (2002).
[119] P. Sen, S. Dasgupta, A. Chatterjee, P. A. Sreeram, G. Mukherjee, and S. S. Manna, Phys. Rev. E **67**, 036106 (2003).
[120] R. Pastor-Satorras and A. Vespignani, *Evolution and Structure of Internet: A Sta-*

tistical Physics Approach, Cambridge University Press, 2004.
[121] G. Caldarelli, R. Marchetti, and L. Pietronero, EPL (Europhysics Letters) **52**, 386 (2000).
[122] S. Maslov, K. Sneppen, and A. Zaliznyak, Physica A **333**, 529 (2004).
[123] J. C. Doyle et al., Proceedings of the National Academy of Sciences of the United States of America **102**, 14497 (2005).
[124] S. Redner, European Physical Journal B **4**, 131 (1998).
[125] A. Vazquez, arXiv, cond-mat/0105031 (2001).
[126] R. Albert, H. Jeong, and A. L. Barabási, Nature (London) **401**, 130 (1999).
[127] A. L. Barabási, R. Albert, and H. Jeong, Physica A **281**, 69 (2000).
[128] A. Broder et al., Comput. Netw. **33**, 309 (2000).
[129] S. N. Dorogovtsev and J. F. F. Mendes, Proceedings of the Royal Society of London B: Biological Sciences **268**, 2603 (2001).
[130] R. F. i. Cancho and R. V. Solé, Proceedings of the Royal Society of London B: Biological Sciences **268**, 2261 (2001).
[131] J. P. K. Doye, Phys. Rev. Lett. **88**, 238701 (2002).
[132] A. Scala, L. A. N. Amaral, and M. Barthelemy, EPL (Europhysics Letters) **55**, 594 (2001).
[133] R. Cohen and S. Havlin, *Complex Networks*, Cambridge university Press, Cambridge, 2010.
[134] M. E. J. Newman, Journal of Statistical Physics **101**, 819 (2000).
[135] P. Erdös and A. Rényi, Publ. Math. Inst. Hun. Acad. Sci **5**, 17 (1960).
[136] B. Bollobás, *Random Graphs*, Academic Press, London, 1985.
[137] B. Bollobás, Transactions of the American Mathematical Society **267**, 41 (1981).
[138] M. E. J. Newman and D. J. Watts, Phys. Rev. E **60**, 7332 (1999).
[139] M. E. J. Newman and D. J. Watts, Physics Letters A **263**, 341 (1999).
[140] M. A. de Mendes, C. F. Moukarzel, and T. J. P. Penna, Europhys. Lett. **50**, 574 (2000).
[141] M. Barthélémy and L. A. N. Amaral, Phys. Rev. Lett. **82**, 3180 (1999).
[142] M. Barthélémy and L. A. N. Amaral, Phys. Rev. Lett. **82**, 5180 (1999).
[143] G. Caldarelli, R. Pastor-Satorras, and A. Vespignani, The European Physical Journal B **38**, 183 (2004).
[144] A.-L. Barabási and R. Albert, Science **286**, 509 (1999).
[145] A. L. Barabási, R. Albert, and H. Jeong, Physica A **272**, 173 (1999).
[146] B. Bollobás and O. Riordan, Cominatorica **24**, 5 (2004).
[147] R. Cohen and S. Havlin, Phys. Rev. Lett. **90**, 058701 (2003).
[148] S. N. Dorogovtsev, J. F. F. Mendes, and A. N. Samukhin, Phys. Rev. Lett. **85**, 4633 (2000).
[149] P. L. Krapivsky and S. Redner, Phys. Rev. E **63**, 066123 (2001).
[150] M. Molloy and B. A. Reed, Random Structures & Algorithms **6**, 161 (1995).
[151] K.-I. Goh, D.-S. Lee, B. Kahng, and D. Kim, Phys. Rev. Lett. **91**, 148701 (2003).
[152] A. Barrat, M. Barthlemy, and A. Vespignani, *Dynamical Processes on Complex*

Networks, Cambridge University Press, New York, NY, USA, 1st edition, 2008.
[153] E. Bonabeau, Journal of the Physical Society of Japan **64**, 327 (1995).
[154] J. Lahtinen, J. Kertsz, and K. Kaski, Physica A **349**, 535 (2005).
[155] L. de Arcangelis and H. Herrmann, Physica A **308**, 545 (2002).
[156] R. Dickman and J. M. M. Campelo, Phys. Rev. E **67**, 066111 (2003).
[157] A. P. Vieira, J. S. Andrade, H. J. Herrmann, and R. F. S. Andrade, Phys. Rev. E **76**, 026111 (2007).
[158] K.-M. Lee, K. I. Goh, and I. M. Kim, Journal of the Korean Physical Society **60**, 641 (2012).
[159] N. Zachariou, P. Expert, M. Takayasu, and K. Christensen, PloS one **10**, e0142685 (2015).
[160] P. Fronczak, A. Fronczak, and J. A. Hołyst, Phys. Rev. E **73**, 046117 (2006).
[161] K.-I. Goh, D.-S. Lee, B. Kahng, and D. Kim, Phys. Rev. Lett. **91**, 148701 (2003).
[162] P.-A. Noël, C. D. Brummitt, and R. M. D'Souza, Phys. Rev. E **89**, 012807 (2014).
[163] R. Karmakar and S. S. Manna, J. Phys. A. **38**, L87 (2005).
[164] L. Huang, L. Yang, and K. Yang, Phys. Rev. E **73**, 036102 (2006).
[165] H. Bhaumik, The European Physical Journal B **91**, 21 (2018).
[166] D. O. Cajueiro and R. F. S. Andrade, Phys. Rev. E **81**, 015102 (2010).
[167] D. O. Cajueiro and R. F. S. Andrade, Phys. Rev. E **82**, 031108 (2010).
[168] P.-A. Noël, C. D. Brummitt, and R. M. D'Souza, Phys. Rev. Lett. **111**, 078701 (2013).
[169] H. Bhaumik and S. B. Santra, Phys. Rev. E **88**, 062817 (2013).
[170] B. Bollobás, editor, *Phase Transitions and Critical Phenomena*, Academic Press, London, 1985.
[171] M. E. J. Newman, C. Moore, and D. J. Watts, Phys. Rev. Lett. **84**, 3201 (2000).
[172] B. B. Mandelbrot, *The fractal Geometry of Nature*, Freeman, New York, 1992.
[173] I. Graham and C. C. Matthai, Phys. Rev. E **68**, 036109 (2003).
[174] G. Bianconi and M. Marsili, Phys. Rev. E **70**, 035105(R) (2004).
[175] C. Tebaldi, M. DeMenech, and A. L. Stella, Phys. Rev. Lett. **83**, 3952 (1999).
[176] O. Malcai, Y. Shilo, and O. Biham, Phys. Rev. E **73**, 056125 (2006).
[177] Y. Shilo and O. Biham, Phys. Rev. E **67**, 066102 (2003).
[178] D. Dhar, Physica A **369**, 29 (2006).
[179] E. Milshtein, O. Biham, and S. Solomon, Phys. Rev. E **58**, 303 (1998).
[180] H. Bhaumik and S. B. Santra, AIP Conf. Proc. **1447**, 209 (2012).
[181] M. Hoore and S. Moghimi-Araghi, J. Phys. A: Math. Theor. **46**, 195001 (2013).
[182] J. M. López and J. Schmittbuhl, Phys. Rev. E **57**, 6405 (1998).
[183] S. Morel, J. Schmittbuhl, J. M. López, and G. Valentin, Phys. Rev. E **58**, 6999 (1998).
[184] D. Dhar, Physica A **270**, 69 (1999).
[185] P. Grassberger and S. S. Manna, J. Phys (France) **51**, 1077 (1990).
[186] S. S. Manna, J. Stat. Phys. **59**, 509 (1990).
[187] D. Dhar and S. S. Manna, Phys. Rev. E **49**, 2684 (1994).
[188] S. Banerjee, S. B. Santra, and I. Bose, Z. Phys. B **96**, 571 (1995).

[189] G.-J. Pan, D.-M. Zhang, Y.-P. Yin, and M.-H. He, Physica A **383**, 435 (2007).
[190] S. S. Manna and A. L. Stella, Physica A **316**, 135 (2002).
[191] F. Jasch and A. Blumen, Phys. Rev. E **63**, 041108 (2001).
[192] J. Lahtinen, J. Kertész, and K. Kaski, Phys. Rev. E **64**, 057105 (2001).
[193] E. Almaas, R. V. Kulkarni, and D. Stroud, Phys. Rev. E **68**, 056105 (2003).
[194] H. Bhaumik and S. Santra, Physica A **511**, 358 (2018).
[195] R. Pastor-Satorras and A. Vespignani, The European Physical Journal B - Condensed Matter and Complex Systems **18**, 197 (2000).
[196] H. N. Huynh, L. Y. Chew, and G. Pruessner, Phys. Rev. E **82**, 042103 (2010).
[197] S. A. Moosavi and A. Montakhab, Phys. Rev. E **89**, 052139 (2014).
[198] J. A. Ahmed and S. Santra, Physica A **391**, 5332 (2012).
[199] The positions of the peaks and dips are found slightly shifted from the origin in the logarithmic scale. The amount of shifts represent the respective metric factors. Evaluation of s_1 performed estimating the matric factors.
[200] J. A. Bonachela and M. A. Muñoz, Phys. Rev. E **78**, 041102 (2008).
[201] H. Bhaumik and S. B. Santra, Phys. Rev. E **94**, 062138 (2016).
[202] S. Benella, G. Consolini, F. Giannattasio, T. T. Chang, and M. Echim, Entropy **19**, 383 (2017).
[203] B. Tadić, U. Nowak, K. D. Usadel, R. Ramaswamy, and S. Padlewski, Phys. Rev. A **45**, 8536 (1992).
[204] C.-Y. Lin, C.-F. Chen, C.-N. Chen, C.-S. Yang, and I.-M. Jiang, Phys. Rev. E **74**, 031304 (2006).
[205] C.-F. Chen, A.-C. Cheng, Y.-D. Wang, and C.-Y. Lin, Computer Physics Communications **182**, 226 (2011), Computer Physics Communications Special Edition for Conference on Computational Physics Kaohsiung, Taiwan, Dec 15-19, 2009.
[206] B. Tadi and S. Thurner, Physica A **332**, 566 (2004).
[207] B. Drossel, Phys. Rev. E **61**, R2168 (2000).
[208] N. Farid and K. Christensen, New Journal of Physics **8**, 212 (2006).
[209] K. Christensen, N. Farid, G. Pruessner, and M. Stapleton, The European Physical Journal B **62**, 331 (2008).
[210] L. A. N. Amaral and K. B. Lauritsen, Phys. Rev. E **54**, R4512 (1996).
[211] S. Moghimi-Araghi and M. Sebtosheikh, Phys. Rev. E **92**, 022116 (2015).
[212] S. A. Moosavi and A. Montakhab, Phys. Rev. E **92**, 052804 (2015).
[213] H. Bhaumik and S. B. Santra, arXiv, cond-mat.stat-mech/1705.10646 (2017).
[214] D. O. Cajueiro and R. Andrade, The European Physical Journal B **77**, 291 (2010).
[215] C. D. Brummitt, R. M. D'Souza, and E. A. Leicht, Proceedings of the National Academy of Sciences of the United States of America **109**, E680 (2012).
[216] Z. Wu, C. Lagorio, L. A. Braunstein, R. Cohen, S. Havlin, and H. E. Stanley, Phys. Rev. E **75**, 066110 (2007).
[217] M. L. Sachtjen, B. A. Carreras, and V. E. Lynch, Phys. Rev. E **61**, 4877 (2000).
[218] C. D. Brummitt and T. Kobayashi, Phys. Rev. E **91**, 062813 (2015).
[219] Y. Wang, H. Fan, W. Lin, Y.-C. Lai, and X. Wang, Scientific Reports **6**, 24445

(2016).
[220] D.-S. Lee, K.-I. Goh, B. Kahng, and D. Kim, Physica A **338**, 84 (2004).
[221] K.-I. Goh, D.-S. Lee, B. Kahng, and D. Kim, Physica A **346**, 93 (2005).
[222] J. Qi and S. Pfenninger, EPL (Europhysics Letters) **111**, 38006 (2015).
[223] Y. Hou, X. Xing, M. Li, A. Zeng, and Y. Wang, Physica A **481**, 160 (2017).
[224] M. Catanzaro, M. Boguñá, and R. Pastor-Satorras, Phys. Rev. E **71**, 027103 (2005).
[225] W. Wang, M. Tang, H. E. Stanley, and L. A. Braunstein, Reports on Progress in Physics **80**, 036603 (2017).
[226] G. Pruessner and O. Peters, Phys. Rev. E **73**, 025106 (2006).
[227] M. J. Alava, L. Laurson, A. Vespignani, and S. Zapperi, Phys. Rev. E **77**, 048101 (2008).
[228] G. Pruessner and O. Peters, Phys. Rev. E **77**, 048102 (2008).
[229] F. Radicchi and S. Fortunato, Phys. Rev. Lett. **103**, 168701 (2009).

List of publications

A. Journals

1. *Critical properties of sandpile on small-world network*, Himangsu Bhaumik and S. B. Santra, Phys. Rev. E **88**, 062817 (2013).

2. *Crossover from rotational to stochastic sandpile universality in the random rotational sandpile model*, Himangsu Bhaumik, J. A. Ahmed and S. B. Santra, Phys. Rev. E. **90**, 062136 (2014).

3. *Dissipative stochastic sandpile model on small-world network : properties of non-dissipative and dissipative avalanches*, Himangsu Bhaumik and S. B. Santra, Phys. Rev. E. **94**, 062138 (2016).

4. *Conserved Manna model on Barabasi–Albert scale-free network*, Himangsu Bhaumik, The European Physical Journal B **91**, 21 (2018).

5. *Stochastic sandpile on small-world networks: scaling and crossover*, Himangsu Bhaumik and S. B. Santra, Physica A **511**, 0358 (2018).

6. *Controlling self-organized criticality of a preferential sandpile model on scale-free networks*, Himangsu Bhaumik and S. B. Santra, Submitted.

7. *Sandpile dynamics on percolation backbone*, Himangsu Bhaumik and S. B. Santra, Manuscript under preparation.

B. Conferences

1. *Crossover from rotational to stochastic sandpile*, Himangsu Bhaumik, Jahir Abbas Ahmed and S. B. Santra, AIP Conf. Proc. **1349**, 198-199 (2011).

2. *Dissipative Sandpile On Growing Random Graph*, Himangsu Bhaumik and S. B. Santra, AIP Conf. Proc. **1447**, 209-210 (2012).

3. *Dissipative Sandpile on random network*, Himangsu Bhaumik and S. B. Santra, CMDAYS 2011, Gauhati University, Guwahati.

4. *Anti-percolation in the etching of a random solid*, Bappaditya Roy, Himangsu Bhaumik and S.B.Santra, CMDAYS 2011, Gauhati University, Guwahati.

5. *Directed Sandpile on random and scale-free network*, Himangsu Bhaumik and S.B.Santra, Conference on Computational Physics (CCP2012), Kobe, Japan.

6. *Dissipative sandpile on Small-world network: coexistence of two scaling forms*, Himangsu Bhaumik and S.B.Santra, CMDAYS 2013,NIT Rourkela, Rourkela, Odisha.

7. *Sandpile dynamics on percolation backbone*, Himangsu Bhaumik and S.B.Santra, CMDAYS 2015, Visva-Bharati, Santiniketan, West Bengal.

8. *Study of stochastic dissipative sandpile on small-world networks*, Himangsu Bhaumik and S.B.Santra, Conference on Computational Physics (CCP2015), IIT Guwahati, India.

9. *Sandpile model with preferential sand distribution on scale-free Networks*, Himangsu Bhaumik and S. B. Santra, FRAC-MEET 2017, IMSc, Chennai, India.